Supplementary Information updated
and replaced on 26th October 2018

Supplementary Information

Synthetic biology approaches and combinatorial biosynthesis towards heterologous lipopeptide production

Fu Yan,[a]‡ Christian Burgard,[a]‡ Alexander Popoff,[a] Nestor Zaburannyi,[a] Gregor Zipf,[b] Josef Maier,[c] Hubert S. Bernauer,[b] Silke C. Wenzel,[a] Rolf Müller[a]*

a. Helmholtz Institute for Pharmaceutical Research Saarland (HIPS), Helmholtz Centre for Infection Research and Department of Pharmacy at Saarland University, Saarland University Campus, Building E8.1, 66123 Saarbrücken, Germany. *E-mail: rom@helmholtz-hzi.de*

b. ATG:biosynthetics GmbH, Weberstraße 40, 79249 Merzhausen, Germany

c. IStLS − Information Services to Life Sciences, Härlestraße 24/1, 78727 Oberndorf am Neckar/Boll, Germany

‡ These authors contributed equally

Contents

1. Strains and culture conditions

Escherichia coli strains (HS996 or DH10B) were routinely grown in LB medium (1% tryptone, 0.5% yeast extract, 0.5% NaCl) at 37 °C. For myxochromide production analysis, *Myxococcus xanthus* DK1622 wild type strain,[1] the myxochromide A-deficient mutant strain *M. xanthus* DK1622 *ΔmchA-tet*[2] and its heterologous expression mutants (harboring artificial *mch* clusters) were routinely grown in 300 mL shaking flasks on a 50 mL scale in CTT medium (casitone 1%, Tris-HCl 10 mM, K_2HPO_4/KH_2PO_4 1 mM, $MgSO_4 \times 7\ H_2O$ 8 mM, pH adjusted to 7.6) at 30 °C and 180 rpm for 4-5 days. For the isolation of hybrid myxochromides, fermentations on a 1 L scale were performed under the same conditions in 5 L shaking flasks. Cultures were amended with antibiotics if necessary in the following final concentrations: ampicillin 100 µg/mL, kanamycin 50 µg/mL and oxytetracycline 10 µg/mL.

2. Design and assembly of artificial gene clusters

2.1 Design of artificial gene clusters

Biosynthetic gene cluster (BGC) sequences for the production of myxochromides in *M. xanthus* were designed based on the native BGCs listed in Table S1.[3] During the design and *de novo* synthesis, the BGCs were separated into seven fragments – *promoter*, *mchA'*, *3mchA-5mchB* linker, *mchB'*, *3mchB-5mchC* linker, *mchC'* and *3mchC-mchD-terminator*. To facilitate subcloning and assembly, unique restriction sites were introduced into each fragment (Table S2). To allow for versatile engineering of the myxochromide PKS/NRPS megasynthetase, splitter elements (SE) were introduced between each catalytic domain-encoding fragment (except $mchC_B$') of the biosynthesis genes *mchA-C* (Table S3). SEs are composed of a type II endonuclease restriction enzyme recognition site (R-site) flanked by type IIS endonuclease recognition sequences (*Aar*I or *Bsa*I) that are extended with 5 bp (for *Bsa*I) or 8 bp (for *Aar*I) sequences to include their variable R-site (Fig. S1). The type II endonuclease R-sites are unique in each synthetic gene construct and enable the exchange, deletion or insertion of domain and module fragments via conventional restriction/ligation methods. The variable 4 bp *Aar*I or *Bsa*I R-sites are designed to be unique for the domain-linker fragments along the entire BGC sequence, and thus can be used as unique fusion sites for the directed reassembly of the *mchA'-C'* genes after the "desplitting" process (see Fig. 2). Sequences of the designed SEs and the position at which they were introduced into the respective *mch* gene are shown in Table S2. Recognition sites of endonucleases selected for the constructional design (e.g. including the design of SEs, fragment subcloning and assembly, and synthetic vectors), in total 19 different R-sites (see Table S2), were eliminated from the BGC sequences by silent point mutations. DNA synthesis was commissioned by ATG:biosynthetics GmbH (Merzhausen, Germany). Since DNA synthesis is restricted by the length of a gene, the large genes *mchA*, *mchB* and *mchC* were split into seven synthetic fragments (*mchA_fragA*, *mchA_fragB*, *mchB_fragA*, *mchB_fragB*, *mchC_fragA*, *mchC_fragB* and *mchC_fragC*).

Table S1: Myxochromide biosynthetic gene clusters subjected to the gene design process in this study.

Producer strain	Strain abbrev.	Cluster	GenBank Accession*
Myxococcus xanthus DK1622	Mx1	A-type	KX622595
Myxococcus sp. 171	M1	B-type	KX622591
Myxococcus virescens ST200611	Mv1	C-type	KX622594
Stigmatella erecta Pde77	Se1	D-subtype 1	KX622602
Stigmatella aurantiaca DW4/3-1	Sa1	S-type	KX622599

*, annotated cluster files were additionally deposited in the MiBIG database.

Fig. S1 Design of splitter elements (SEs) for *mch* gene (cluster) assembly and engineering. SEs were inserted between PKS/NRPS domain encoding fragments (illustrated as grey boxes), except for the ER-CP linker region of *mchA*. They contain two recognition sites for a type IIS endonuclease (*Aar*I or *Bsa*I; highlighted in red) with variable R-sites representing the fusion sites for directed religation of the domain fragments after the "desplitting" process. Therefore, the 4 bp type IIS R-sites/fusion sites (highlighted in blue) are designed to be unique between different SEs and identical within each SE (see Table S3). Additionally, SEs habour a palindromic 6-8 bp R-site for a type II endocnuclease (shown in black) that is unique for SEs of a particular gene and enables engineering and assembly procedures via conventional restriction/ligation methods on "gene level". **A**: SE based on the type IIS restriction enzyme *Aar*I (32-34 bp in size). **B**: SE based on the type IIS restriction enzyme *Bsa*I (26-28 bp in size).

Table S2 Restriction enzyme sites used for pathway assembly and engineering.

Restriction enzyme	Recognition sequence	Function
*Aar*I	CACCTGC	Type IIS endonuclease R-site
*Bsa*I	GGTCTC	Type IIS endonuclease R-site
*Age*I	ACCGGT	R_{C14}
*Bsi*WI	CGTACG	R_{A1}
*Mlu*I	ACGCGT	R_{B1}, R_{C15}
*Mre*I	CGCCGGCG	R_{A6}, R_{C17}
*Not*I	GCGGCCGC	R_{B8}, R_{C16}
*Sph*I	GCATGC	R_{C1}
*Asi*SI *(Sfa*AI)	GCGATCGC	R_{A3}, R_{B3}, R_{C3}
*Afl*II *(Bsp*TI)	CTTAAG	R_{A5}, R_{B6}, R_{C7}
*Ase*I *(Vsp*I)	ATTAAT	R_{C9}
*Avr*II *(Xma*JI)	CCTAGG	R_{B7}, R_{C11}
*Bam*HI	GGATCC	R_{C10}
*Eco*RI	GAATTC	R_{C4}
*Hind*III	AAGCTT	R_{C12}
*Kpn*I	GGTACC	R_{L}
*Mfe*I *(Mun*I)	CAATTG	R_{C6}
*Nde*I	CATATG	R_{A4}, R_{B2}, R_{C5}
*Nhe*I	GCTAGC	R_{C13}
*Pvu*I	CGATCG	R_{R}
*Spe*I *(Bcu*I)	ACTAGT	R_{A2}, R_{B5}, R_{C2}
*Xba*I	TCTAGA	R_{A6}, R_{B4}, R_{C8}
*Pac*I	TTAATTAA	Vector backbone modification
*Pme*I *(Mss*I)	GTTTAAAC	Vector backbone modification
*Swa*I *(Smi*I)	ATTTAAAT	Vector backbone modification
*Dra*I	TTTAAA	Destruction of cloning vector backbone

*, to allow for the assembly and interchangeability of *mch* cluster parts, the recognition sequences of 6 type II restriction enzymes (highlighted in red) were introduced into the coding sequence of *mch* genes; the recognition sequences of other 19 restriction enzymes were eliminated from *mch* genes; according to the assembly strategy depicted in Fig. 2, the functions of the restriction enzymes are shown.

Table S3 Design of SEs between catalytic domain encoding regions and terminal regions of *mchA'/B'/C'* fragments.

Sequence of SEs and terminal regions	Restriction site and position [b]	Location in the gene (bp) [c]
***mchA* (A-type cluster)**		
5'-GGTCTCCGCAAGACGTACG**-KS**	*Bsi*WI (R_{A1})	191–194

KS-CACCTGAGACCACTAGTGGTCTCCCACC**-AT**	*Spe*I (R_{A2})	1498–1501
AT-GGCAGGAGACCGCGATCGCGGTCTCTGGCA**-DH**	*Asi*SI (R_{A3})	2645–2648
DH-ACGGAGAGACCCATATGGGTCTCGACGG**-ER**	*Nde*I (R_{A4})	4295–4298
ER-CGTTCGAGACCCTTAAGGGTCTCTCGTT**-KR/CP**	*Afl*II (R_{A5})	5186–5189
KR/CP-CGCCGGCGN_{27}ATCGCGAGACC**-3'**	*Mre*I (R_{A6})	6361–6364
***mchB* (A-, D- or S-type cluster)**		
5'-GGTCTCCTTCGN_{18}ACGCGT **-C_1**	*Mlu*I (R_{B1})	232–235
C_1-GCGCCGAGACCCATATGGGTCTCCGCGC**-A_1**	*Nde*I (R_{B2})	1304–1307
A_1-CGCGGGAGACCGCGATCGCGGTCTCTCGCG**-CP_1**	*Asi*SI (R_{B3})	4282–4285 (in A-type), 4312–4315 (in D / S-type)
CP_1-AGCGAGAGACCTCTAGAGGTCTCGAGCG**-C_2**	*Xba*I (R_{B4})	4604–4607 (in A-type), 4634–4637 (in D / S-type)
C_2-CAGCCGAGACCACTAGTGGTCTCGCAGC**-A_2**	*Spe*I (R_{B5})	5826–5829 (in A-type), 5856–5859 (in D / S-type)
A_2-GAAGTGAGACCCTTAAGGGTCTCCGAAG**-CP_2**	*Afl*II (R_{B6})	7437–7440 (in A-type), 7467–7470 (in D / S-type)
CP_2-GCAGGGAGACCCCTAGGGGTCTCTGCAG**-E_2**	*Avr*II (R_{B7})	7739–7742 (in A-type), 7769–7772 (in D / S-type)
E_2- GCGGCCGCN$_{20}$TCCCCGAGACC**-3'**	*Not*I (R_{B8})	9080–9083 (in A-type), 9107–9110 (in D / S-type)
***mchC* (A-, D- or S-type cluster)**		
5'-GGTCTCTAGCACGGCATGC**-C3**	*Sph*I (R_{C1})	50–53
C_3-GAGCCGAGACCACTAGTGGTCTCGGAGC**-A_3**	*Spe*I (R_{C2})	1240–1243
A_3-GGAGCGAGACCGCGATCGCGGTCTCGGGAG**-CP_3**	*Asi*SI (R_{C3})	2853–2856 (in A-type), 2880–2883 (in D-type), 2862–2865 (in S-type)
CP_3-GGACTGAGACCGAATTCGGTCTCCGGAC**-C_4**	*Eco*RI (R_{C4})	3147–3150 (in A-type), 3156–3159 (in D-type), 3156–3159 (in S-type)
C_4-ACACCGAGACCCATATGGGTCTCTACAC**-A_4**	*Nde*I (R_{C5})	4325–4328 (in A-type), 4334–4337 (in D-type), 4337–4340 (in S-type)
A_4-CCGCAGAGACCCAATTGGGTCTCTCCGC**-CP_4**	*Mfe*I (R_{C6})	5960–5963 (in A-type), 5969–5972 (in D-type), 5972–5975 (in S-type)
CP_4-CGAGCGAGACCCTTAAGGGTCTCTCGAG**-C_5**	*Afl*II (R_{C7})	6270–6273 (in A-type), 6276–6279 (in D-type), 6279–6282 (in S-type)
C_5-CGGACGAGACCTCTAGAGGTCTCTCGGA**-A_5**	*Xba*I (R_{C8})	7469–7472 (in A-type), 7475–7478 (in D-type), 7478–7481 (in S-type)
A_5-TGGAGGAGACCATTAATGGTCTCATGGA**-CP_5**	*Ase*I (R_{C9})	9083–9086 (in A-type), 9089–9092 (in D-type), 9092–9095 (in S-type)
CP_5-CGCCAGAGACCGGATCCGGTCTCACGCC**-C_6**	*Bam*HI (R_{C10})	9400–9403 (in A-type), 9406–9409 (in D-type), 9409–9412 (in S-type)
C_6-CGACCGAGACCCCTAGGGGTCTCACGAC**-A_6**	*Avr*II (R_{C11})	10605–10608 (in A-type), 10611–10614 (in D-type), 10614–10617 (in S-type)
A_6-GCGATGAGACCAAGCTTGGTCTCCGCGA**-CP_6**	*Hind*III (R_{C12})	12235–12238 (in A-type), 12241–12244 (in D-type), 12244–12247 (in S-type)
CP_6-CGCTGGAGACCGCTAGCGGTCTCTCGCT**-TE**	*Nhe*I (R_{C13})	12527–12530 (in A-type), 12533–12536 (in D-type), 12536–12539 (in S-type)
TE-ACCGGTN$_{19}$GCTCCGAGACC**-3'**	*Age*I (R_{C14})	13227–13230 (in A-type), 13239–13242 (in D-type), 13242–13245 (in S-type)
***mchC* (B-type cluster)**		

5'-GGTCTCTAGCACGGCATGC-**C_3**	*Sph*I (R_{C1})	50–53
C_3-GAGCCGAGACCACTAGTGGTCTCGGAGC-**A_3**	*Spe*I (R_{C2})	1240–1243
A_3-GGAGCGAGACCGCGATCGCGGTCTCGGGAG-**CP_3**	*Asi*SI (R_{C3})	2853–2856
CP_3-GGACTGAGACCGAATTCGGTCTCCGGAC-**C_4**	*Eco*RI (R_{C4})	3147–3150
C_4-ACCTCGAGACCACGCGTGGTCTCGACCT-**A_4**	*Mlu*I (R_{C15})	4414–4417
A_4-TCGCCGAGACCGCGGCCGCGGTCTCGTCGC-**CP_4**	*Not*I (R_{C16})	5971–5974
CP_4-TCTCCGAGACCCGCCGGCGGGTCTCGTCTC-**C_5**	*Mre*I (R_{C17})	6239–6242
C_5-ACACCGAGACCCATATGGGTCTCTACAC-**A_5**	*Nde*I (R_{C5})	7439–7442
A_5-CCGCAGAGACCCAATTGGGTCTCTCCGC-**CP_5**	*Mfe*I (R_{C6})	9074–9077
CP_5-CGAGCGAGACCCTTAAGGGTCTCTCGAG-**C_6**	*Afl*III (R_{C7})	9381–9384
C_6-CGGACGAGACCTCTAGAGGTCTCTCGGA-**A_6**	*Xba*I (R_{C8})	10580–10583
A_6-TGGAGGAGACCATTAATGGTCTCATGGA-**CP_6**	*Ase*I (R_{C9})	12194–12197
CP_6-CGCCAGAGACCGGATCCGGTCTCACGCC-**C_7**	*Bam*HI (R_{C10})	12511–12514
C_7-CGACCGAGACCCCTAGGGGTCTCACGAC-**A_7**	*Avr*II (R_{C11})	13716–13719
A_7-GCGATGAGACCAAGCTTGGTCTCCGCGA-**CP_7**	*Hind*III (R_{C12})	15346–15349
CP_7-CGCTGGAGACCGCTAGCGGTCTCTCGCT-**TE**	*Nhe*I (R_{C13})	15638–15641
TE- ACCGGTN$_{19}$GCTCCGAGACC-**3'**	*Age*I (R_{C14})	16335–16338
***mchC* (C-type cluster)**		
5'-GGTCTCTAGCACGGCATGC–**C_3**	*Sph*I (R_{C1})	50–53
C_3-GAGCCGAGACCACTAGTGGTCTCGGAGC-**A_3**	*Spe*I (R_{C2})	1240–1243
A_3-GGAGCGAGACCGCGATCGCGGTCTCGGGAG-**CP_3**	*Asi*SI (R_{C3})	2853–2856
CP_3-GGACTGAGACCGAATTCGGTCTCCGGA**C**-**C_4**	*Eco*RI (R_{C4})	3147–3150
C_4-ACACCGAGACCCATATGGGTCTCTACAC-**A_4**	*Nde*I (R_{C5})	4325–4328
A_4-CCGCAGAGACCCAATTGGGTCTCTCCGC-**T_4**	*Mfe*I (R_{C6})	5960–5963
CP_4-CGAGCGAGACCCTTAAGGGTCTCTCGAG-**C_5**	*Afl*III (R_{C7})	6270–6273
C_5-CGGACGAGACCTCTAGAGGTCTCTCGGA-**A_6**	*Xba*I (R_{C8})	7469–7472
A_6-GCGATGAGACCAAGCTTGGTCTCCGCGA-**CP_6**	*Hind*III (R_{C12})	9100–9103
CP_6-CGCTGGAGACCGCTAGCGGTCTCTCGCT-**C_6**	*Nhe*I (R_{C13})	9392–9395
TE- ACCGGTN$_{19}$GCTCCGAGACC-**3'**	*Age*I (R_{C14})	10098–10101

a, SEs were introduced between each domain fragment of the *mch* genes (except between the KR and CP domain of *mchA*). For the *mchA* gene, only the PKS coding sequence from the A-type producer (Mx1) was subjected to the sequence design. For the *mchB* gene, the NRPS sequences from the A-, D- and S-type producers (Mx1, Se1 and Sa1) were subjected to the sequence design. For the *mchC* gene, the NRPS sequences from the A-, B-, C-, D- and S-type producers (Mx1, M1, Mv1, Se1 and Sa1) were subjected to the designed. *Bsa*I recognition sequences are labeled in red, the corresponding restriction sites (= fusion sites) are labeled in blue, the spacer nucleotide which is skipped by the type IIS restriction enzyme is shown in grey; type II enzyme recognition sites are underlined;
b, positions of the type II endonuclease recognition sites (underlined) corresponding to Fig. 2 in the main text;
c, calculation of location of fusion sites is based on the *mch* clusters deposited in GeneBank (see Table S1).

Table S4 Modified nucleotides/amino acids in the SEs and the terminal regions listed in Table S3 during the constructional design.*

Position of modified sequences	Modified nucleotides **	Modified amino acids ***
A-type cluster		
SE between CP_3 and C_4 in *mchC* (3147–3150 bp), *Bsa*I fusion site	GGG GAC ACG (GGA GAC ACG)	G D T (G D T)
SE between CP_5 and C_6 in *mchC* (9400–9403 bp), *Bsa*I fusion site	GTC CGC CTG (GTC CGA CTG)	V R L (V R L)
3'-term in *mchC* (13202–13207 bp), *Age*I (R_{C14}) site	GAC CGG TGT (GAC CGC AGT)	D R C (D R S)
B-type cluster		
SE between CP_3 and C_4 in *mchC* (3147–3150 bp), *Bsa*I fusion site	GGG GAC ACG (GGA GAC ACG)	G D T (G D T)
SE between CP_5 and C_6 in *mchC* (9381–9384 bp), *Bsa*I fusion site	CCC GAG GGC (CCC GAA GGC)	P E G (P E G)
SE between CP_6 and C_7 in *mchC* (12511–12514 bp), *Bsa*I fusion site	GTC CGC CTG (GTC CGG TTG)	V R L (V R L)
3'-term in *mchC* (16310–16315 bp), *Age*I (R_{C14}) site	GAC CGG TGC (GAC CGT GGC)	D R C (D R G)
C-type cluster		

SE between CP_4 and C_5 in *mchC* (6270–6273 bp), *Bsa*I fusion site	CCC GAG GGC (CCG GAG GGC)	P E G (P E G)
SE between A_6 and CP_6 in *mchC* (9100–9103 bp), *Bsa*I fusion site	GGC GCG ATG (GGC GCG CTG)	G A M (G A L)
3'-term in mchC (10073–10078 bp), *Age*I (R_{C14}) site	GAC CGG TGC (GAC CGG AGC)	D R C (D R S)
D-type cluser		
5'-term in *mchB* (254–259 bp), *Mlu*I (R_{B1}) site	CAC GCG TGC (CAC CCG AGC)	H A C (H P S)
SE between A_1 and CP_1 in *mchB* (4312–4315 bp), *Bsa*I fusion site	CGG CGC GCC (CGG CGA GCC)	R R A (R R A)
SE between CP_2 and E_2 in *mchB* (7769–7772 bp), *Bsa*I fusion site	ACG GGC AGT (ACG GGG AGT)	T G S (T G S)
3'-term in *mchB* (9079–9086 bp), *Not*I (R_{B8}) site	GCG GCC GCG (GCC GCG ACG)	A A A (A A T)
SE between A_3 and CP_3 in *mchC* (2880–2883 bp), *Bsa*I fusion site	ACG GAG CAC (ACA GAG CAC)	T E H (T E H)
SE between CP_3 and C_4 in *mchC* (3156–3159 bp), *Bsa*I fusion site	GGG GAC GGG (GGT GAC GGG)	G D G (G D G)
SE between CP_4 and C_5 in *mchC* (6276–6279 bp), *Bsa*I fusion site	CCC GAG AGC (CCG GAG AGC)	P E S (P E S)
SE between CP_5 and C_6 in *mchC* (9406–9409 bp), *Bsa*I fusion site	GTC CGC CTG (GTC CGG CTG)	V R L (V R L)
SE between A_6 and CP_6 in *mchC* (12241–12244 bp), *Bsa*I fusion site	GGG GCG ATG (GGG ACG ATG)	G T M (G A M)
SE between CP_6 and TE in *mchC* (12533–12536 bp), *Bsa*I fusion site	CCG CTC ACG (CCT CTC ACG)	P L T (P L T)
3'-term in *mchC* (13214–13219 bp), *Age*I (R_{C14}) site	GAC CGG TAT (GAC AGG GAT)	D R Y (D R D)
3'-term in *mchC* (13239–13242 bp), *Bsa*I fusion site	CCT GAG CTC (CCT GAG CTT)	P E L (P E L)
S-type cluster		
5'-term in *mchB* (254–259 bp), *Mlu*I (R_{B1}) site	CAC GCG TGC (CAC CCG AGC)	H A C (H P S)
3'-term in *mchB* (9079–9086 bp), *Not*I (R_{B8}) site	GCG GCC GCA (GCA GCC GCA)	A A A (A A A)
SE between CP_4 and C_5 in *mchC* (6279–6282 bp), *Bsa*I fusion site	CCC GAG AGC (CCG GAG AGC)	P E S (P E S)
SE between CP_5 and C_6 in *mchC* (9409–9412 bp), *Bsa*I fusion site	GTC CGC CTG (GTC CGG CTG)	V R L (V R L)
3'-term in *mchC* (13217–13222 bp), *Age*I (R_{C14}) site	GAC CGG TAT (GAC AGG GAC)	D R Y (D R D)

*, comparing to the BGCs in the native producers, only the SEs and the terminal regions containing mutated recognition/fusion sites in Table S3 are listed, while the elements with unmodified sites are not shown.
** fusion sites after *Bsa*I digestion are in shown in blue, type II restriction sites introduced for conventional cloning are underlined. The respective nucleotide and amino acid sequences in the native BGCs are shown in brackets, mutated nucleotides and amino acids are highlighted in red.

2.2 Design of the cloning vector pSynbio1 and the expression vector pSynbio2

For the assembly of large biosynthesis gene fragments and for 'desplitting' processes, the cloning vector pSynbio1, derived from the pSV vector (standard vector of ATG:biosynthetics GmbH), was designed and manufactured by DNA synthesis. The high-copy vector backbone pSynbio1 is composed of a minimal set of genetic elements required for the amplification and selection in *E. coli*. These include the *oriV* origin of replication from the broad-range RK2 plasmid,[4] the *trfA* gene, whose gene product binds to and activates *oriV*,[5] and an ampicillin resistance gene (*ampR*). Recognition sequences for *Kpn*I and *Pme*I were introduced into the vector backbone to allow for subcloning of synthetic fragments, and unique R-sites *Pac*I, *Swa*I and *Pme*I were introduced into the pSynbio2 for modification of the vector backbone. To meet the constructional requirements, the recognition sequences of endonucleases required for cloning and engineering of the synthetic cluster fragments/gene constructs (Table S2) were calculated out of the vector sequence. To deliver and functionally

express the synthetic *mch* pathways in *M. xanthus* DK1622 *ΔmchA-tet*, the expression vector pSynbio2 was designed and manufactured by DNA synthesis (Fig. S2). The minimal pSynbio2 vector backbone includes a p15A low-copy origin of replication to ensure stability of the large *mch* cluster constructs during propagation in *E.coli*, an antibiotic resistance gene (kanamycin, *kanR*) suitable for selection of *M. xanthus* DK1622 *ΔmchA-tet* transformants, an origin of transfer (*oriT*) to allow for conjugation as an alternative strategy to transformation via electroporation, and a multiple cloning site (MCS) which is composed of all the R-sites needed for pathway assembly and engineering (Table S2). In addition, unique restriction sites (*Pac*I, *Pme*I, *Swa*I) were introduced between the genetic elements to allow for the exchange or addition of vector backbone elements by conventional cloning techniques, *e.g.* to investigate other chromosomal integration sites.

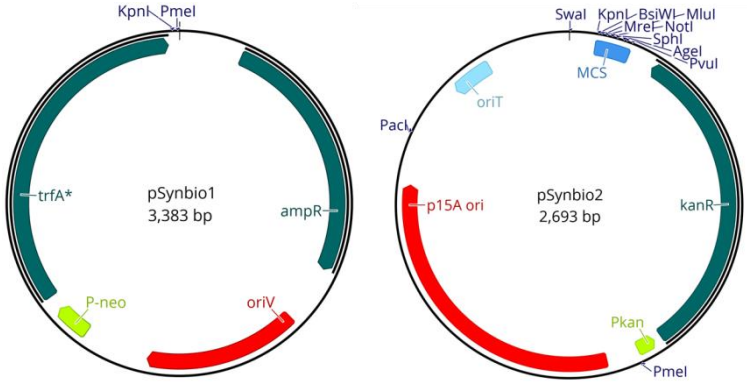

Fig. S2 Vector maps of pSynbio1 and pSynbio2.

2.3 Generation of *mch* cluster fragments via DNA synthesis

Artificial *mch* cluster fragments, which were designed and synthesized in this study, are shown in Table S5. Cluster fragments were delivered either in the pSV (standard vector of ATG:biosynthetics GmbH) vector or in the pUC57 vector backbone harboring an ampicillin resistance gene.

Table S5 Constructs generated via DNA synthesis.

Construct Name	Description	Size [bp]	Flanking restriction sites
A-type *mch* cluster fragments from *M. xanthus* DK1622[1)]			
pSV-P-5mchA_Ab	Promotor fragment (6607-7208 nt)	3539	*Kpn*I-*BsiW*I/*Pme*I
pSV-3mchA-5mchB_Ab	Linker region between *mchA* and *mchB* (13332-13720 nt)	3326	*Kpn*I/*Mre*I-*Mlu*I/*Pme*I
pSV-3mchB-5mchC_Ab	Linker region between *mchB* and *mchC* (22513-22701)	3126	*Kpn*I/*Not*I-*Sph*I/*Pme*I
pSV-T-3mchC_Ab	Terminator fragment (35867-38440 nt)	5547	*Kpn*I/*Age*I-*Pvu*I/*Pme*I
pSV-MchA_A_fragA	*mchA* gene fragment (7197-11354 nt)	7116	*Kpn*I/*BsiW*I-*Nde*I/*Pme*I
pSV-MchA_A_fragA_dcm	*mchA* gene fragment (7197-8507 nt)	4260	*Kpn*I/*BsiW*I-*Spe*I
pSV-MchA_A_fragB	*mchA* gene fragment (11301-13394 nt)	5063	*Kpn*I/*Nde*I-*Mre*I/*Pme*I
pSV-MchB_A_fragA	*mchB* gene fragment (13693-19364 nt)	8628	*Kpn*I/*Mlu*I-*Spe*I/*Pme*I
pSV-MchB_A_fragA_dcm	*mchB* gene fragment (13693-14768 nt)	4026	*Kpn*I/*Mlu*I-*Nde*I
pSV-MchB_A_fragB	*mchB* gene fragment (19287-22592 nt)	6275	*Kpn*I/*Spe*I-*Not*I/*Pme*I
pSV-MchC_A_fragA	*mchC* gene fragment (22690-27042 nt)	7295	*Kpn*I/*Sph*I-*Nde*I/*Pme*I
pSV-MchC_A_fragA_dcm	*mchC* gene fragment (22690-23883 nt)	4138	*Kpn*I/*Sph*I-*Spe*I
pSV-MchC_A_fragB	*mchC* gene fragment (26965-31798 nt)	7797	*Kpn*I/*Nde*I-*Ase*I/*Pme*I
pSV-MchC_A_fragC	*mchC* gene fragment (31723-35966 nt)	7207	*Kpn*I/*Ase*I-*Age*I/*Pme*I
pSV-MchC_A_fragC_dcm	*mchC* gene fragment (31723-32043 nt)	3264	*Ase*I-*Bam*HI
pUC57-CP1_A_inact1	Carrier protein fragment (17743-18068 nt)	3078	*Kpn*I/AsiSI-*Xba*I/*Pme*I
pUC57-CP2_A_inact1	Carrier protein fragment (20898-21203 nt)	3056	*Kpn*I/*Afl*II-*Avr*II/*Pme*I

pUC57-CP3_A_inact1	Carrier protein fragment (25494-25787 nt)	3050	*Kpn*I/*AsiS*I-*EcoR*I/*Pme*I
pSV-CP4_A_inact1	Carrier protein fragment (28601-28914 nt)	3079	*Kpn*I/*Mfe*I-*Afl*II/*Pme*I
pSV-CP4_A_inact2	Carrier protein fragment (28601-28914 nt)	3079	*Kpn*I/*Mfe*I-*Afl*II/*Pme*I
pUC57-CP5_A_inact1	Carrier protein fragment (31724-32042 nt)	3071	*Kpn*I/*Ase*I-*BamH*I/*Pme*I
pUC57-CP6_A_inact1	Carrier protein fragment (34876-35171 nt)	3046	*Kpn*I/*Hind*III-*Nhe*I/*Pme*I
pUC57-MchB_A_delM1	*mchB* gene fragment (14803-19299 nt)	5413	*Mlu*I-*Afl*II
pUC57-MchB_A_delM2	*mchB* gene fragment (19414-21210 nt)	5382	*Xba*I-*Not*I
pUC57-MchC_A_delM3	*mchC* gene fragment (23861-26974 nt)	5517	*Sph*I-*Mfe*I
pUC57-MchC_A_delM4	*mchC* gene fragment (27015-30155 nt)	5535	*EcoR*I-*Ase*I
pUC57-MchC_A_delM5	*mchC* gene fragment (30111-33245 nt)	5570	*Afl*II-*Hind*III
pUC57-MchC_A_delM6	*mchC* gene fragment (33372-35228 nt)	4674	*BamH*I-*Age*I
pUC57-MchB_A_duplM1	*mchB* gene fragment (15010-19509 nt)	8459	*Xba*I-*Spe*I
pUC57-MchB_A_duplM2	*mchB* gene fragment (18088-21213 nt)	6168	*Afl*II-*Avr*II
pUC57-MchC_A_duplM3	*mchC* gene fragment (24057-27186 nt)	7044	*EcoR*I-*Nde*I
pUC57-MchC_A_duplM4	*mchC* gene fragment (27183-30330 nt)	7086	*Afl*II-*Xba*I
pUC57-MchC_A_duplM5	*mchC* gene fragment (30324-33455 nt)	7071	*Bam*HI-*Avr*II
pUC57-MchC_A_duplM6	*mchC* gene fragment (32007-35138 nt)	6191	*Hind*III-*Nhe*I
pUC57-P-5mchA_opt_Ab	Promotor fragment (6607-7208 nt)	3332	*Kpn*I-*BsiW*I/*Pme*I
pUC57-3mchA-5mchB_opt_Ab	Linker region between *mchA* and *mchB* (13332-13720 nt)	3119	*Kpn*I/*Mre*I-*Mlu*I/*Pme*I
pUC57-3mchB-5mchC_opt_Ab	Linker region between *mchB* and *mchC* (22513-22701 nt)	2919	*Kpn*I/*Not*I-*Sph*I/*Pme*I
pUC57-T-3mchC_opt_Ab	Terminator fragment (35842-38439 nt)	5328	*Kpn*I/*Age*I-*Pvu*I/*Pme*I
pUC57-MchA_A_opt	*mchA* gene fragment (7197-13370 nt)	9169	*Kpn*I/*BsiW*I-*Mre*I/*Pme*I
pUC57-MchB_A_opt_fragA	*mchB* gene fragment (13693-19290 nt)	8335	*Kpn*I/*Mlu*I-*Spe*I/*Pme*I
pUC57-MchB_A_opt_fragB	*mchB* gene fragment (19287-22544 nt)	6003	*Kpn*I/*Spe*I-*Not*I/*Pme*I
pUC57-MchC_A_opt_fragA	*mchC* gene fragment (22690-28913 nt)	8961	*Kpn*I/*Sph*I-*Afl*II/*Pme*I
pUC57-MchC_A_opt_fragB	*mchC* gene fragment (28910-35870 nt)	9706	*Kpn*I/*Afl*II-*Age*I/*Pme*I
B-type *mch* cluster fragments from *Myxococcus* sp. 171[2)]			
pSV-3mchB-5mchC_Bb	Linker region between *mchB* and *mchC* (22379-22578 nt)	3126	*Kpn*I/*Not*I-*Sph*I/*Pme*I
pSV-T-3mchC_Bb	Terminator fragment (38817-41402 nt)	5547	*Kpn*I/*Age*I-*Pvu*I/*Pme*I
pSV-MchC_B_fragA_woSE	*mchC* gene fragment (22557-26925 nt)	7760	*Kpn*I/*Sph*I-*Mlu*I/*Pme*I
pSV-MchC_B_fragB_woSE	*mchC* gene fragment (26921-31584 nt)	8061	*Kpn*I/*Mlu*I-*Mfe*I/*Pme*I
pSV-MchC_B_fragC_woSE	*mchC* gene fragment (31581-34704 nt)	6521	*Kpn*I/*Mfe*I-*Ase*I/*Pme*I
pSV-MchC_B_fragC	*mchC* gene fragment (31581-34704 nt)	7807	*Kpn*I/*Mfe*I-*Ase*I/*Pme*I
pSV-MchC_B_fragD_woSE	*mchC* gene fragment (34701-38845 nt)	7542	*Kpn*I/*Ase*I-*Age*I/*Pme*I
C-type *mch* cluster fragments from *M. virescens* ST200611[3)]			
pSV-3mchB-5mchC_Cb	Linker region between *mchB* and *mchC* (23091-23279 nt)	3126	*Kpn*I/*Not*I-*Sph*I/*Pme*I
pSV-T-3mchC_Cb	Terminator fragment (33291-35906 nt)	5525	*Kpn*I/*Age*I-*Pvu*I/*Pme*I
pSV-MchC_C_fragA	*mchC* gene fragment (50-4328 nt)	7311	*Kpn*I/*Sph*I-*Nde*I/*Pme*I
pSV-MchC_C_fragA_dcm	*mchC* gene fragment (23268-24461 nt)	4142	*Kpn*I/*Sph*I-*Spe*I
pSV-MchC_C_fragB	*mchC* gene fragment (4325-10101 nt)	8860	*Kpn*I/*Nde*I-*Age*I/*Pme*I
D-type *mch* cluster fragments from *S. erecta* Pde77[4)]			
pSV-3mchA-5mchB_Db	Linker region between *mchA* and *mchB* (11825-12206 nt)	3760	*Kpn*I/*Mre*I-*Mlu*I/*Pme*I
pSV-3mchB-5mchC_Db	Linker region between *mchB* and *mchC* (21027-21217 nt)	3568	*Kpn*I/*Not*I-*Sph*I/*Pme*I
pSV-T-3mchC_Db	Terminator fragment (34376-35036 nt)	5550	*Kpn*I/*Age*I-*Pvu*I/*Pme*I
pSV-MchB_D_fragA	*mchB* gene fragment (12178-17812 nt)	8660	*Kpn*I/*Mlu*I-*Spe*I/*Pme*I
pSV-MchB_D_fragB	*mchB* gene fragment (17804-21058 nt)	6226	*Kpn*I/*Spe*I-*Not*I/*Pme*I
pSV-MchC_D_fragA	*mchC* gene fragment (21207-25568 nt)	7319	*Kpn*I/*Sph*I-*Nde*I/*Pme*I

pSV-MchC_D_fragB	*mchC* gene fragment (25492-30322 nt)	7793	*Kpn*I/*Nde*I-*Vsp*I/*Pme*I
pSV-MchC_D_fragC	*mchC* gene fragment (30245-34493 nt)	7213	*Kpn*I/*Vsp*I-*Age*I/*Pme*I
S-type *mch* cluster fragments from *S. aurantiaca* DW4/3-1[5)]			
pSV-3mchB-5mchC_Sb	Linker region between *mchB* and *mchC* (22680-22869 nt)	3127	*Kpn*I/*Not*I-*Sph*I/*Pme*I
pSV-T-3mchC_Sb	Terminator fragment (36025-36702 nt)	5544	*Kpn*I/*Age*I-*Pvu*I/*Pme*I
pSV-MchA_S_fragA	*mchA* gene fragment (7314-11450 nt)	7146	*Kpn*I/*BsiW*I-*Nde*I/*Pme*I
pSV-MchA_S_fragB	*mchA* gene fragment (11446-13510 nt)	5051	*Kpn*I/*Nde*I-*Mre*I/*Pme*I
pSV-MchB_S_fragA	*mchB* gene fragment (13833-19510 nt)	8650	*Kpn*I/*Mlu*I-*Spe*I/*Pme*I
pSV-MchB_S_fragA_dcm	*mchB* gene fragment (13833-14908 nt)	4020	*Kpn*I-*Nde*I
pSV-MchB_S_fragB	*mchB* gene fragment (19456-22711 nt)	6272	*Kpn*I/*Spe*I/*Not*I/*Pme*I
pSV-MchC_S_fragA	*mchC* gene fragment (22858-27148 nt)	7329	*Kpn*I/*Sph*I/*Nde*I/*Pme*I
pSV-MchC_S_fragA_dcm	*mchC* gene fragment (22858-24051 nt)	4138	*Kpn*I/*Spe*I
pSV-MchC_S_fragB	*mchC* gene fragment (27145-31903 nt)	7800	*Kpn*I/*Nde*I/*Vsp*I/*Pme*I
pSV-MchC_S_fragC	*mchC* gene fragment (31900-36101 nt)	7211	*Kpn*I/*Vsp*I/*Age*I/*Pme*I
pSV-MchC_S_fragC_dcm	*mchC* gene fragment (31900-32220 nt)	3264	*Ase*I/*Bam*HI
pSV-CP4_S_react	Carrier protein fragment (28780-29090 nt)	3076	*Kpn*I/*Mfe*I-*Afl*II/*Pme*I
A-type *mch* cluster fragments from *M. xanthus* DK1622[6)]			
pSV-P-5mchA_A_AarI	Promotor fragment (6603-7206 nt)	4003	*Kpn*I-*BsiW*I/*Pme*I
pSV-3mchA-5mchB_A_AarI	Linker region between *mchA* and *mchB* (13335-13718 nt)	3783	*Kpn*I/*Mre*I-*Mlu*I/*Pme*I
pSV-3mchA-5mchB_A_AarI	Linker region between *mchB* and *mchC* (22517-22699 nt)	3582	*Kpn*I/*Not*I-*Sph*I/*Pme*I
pSV-T-3mchC_A_AarI	Terminator fragment (35842-38443 nt)	6001	*Kpn*I/*Age*I-*Pvu*I/*Pme*I
pSV-MchA_A_AarI_SE	*mchA* gene fragment (7203-13468 nt)	9665	*Kpn*I/*BsiW*I-*Mre*I/*Pme*I
pSV-MchB_A_AarI_SE	*mchB* gene fragment (13715-22746 nt)	12431	*Kpn*I/*Mlu*I-*Not*I/*Pme*I
pSV-MchC_A_AarI_fragABCE	*mchC* gene fragment (22697-27083 nt)	9404	*Kpn*I/*Sph*I-*Bam*HI/*Mlu*I
pSV-MchC_A_AarI_fragD	*mchC* gene fragment (26971-30113 nt)	6186	*Nde*I-*Xba*I
pSV-MchC_A_AarI_fragF	*mchC* gene fragment (32059-35845 nt)	6863	*Bam*HI-*Mlu*I
Cloning and expression vectors			
pSynbio1_AarI	Cloning vector	3383	-
pSynbio2_AarI	Expression vector	2700	-
pSV-Amp_Synbio1mut	*ampR* gene fragment	3587	*Pst*I-*Msc*I
pSV-MCS_Synbio2	Multiple cloning site fragment	3415	*Swa*I-*Hind*III

1) *Bsa*I design based on *mch* cluster retrieved from GeneBank entry KX622595
2) *Bsa*I design based on *mch* cluster retrieved from GeneBank entry KX622591
3) *Bsa*I design based on *mch* cluster retrieved from GeneBank entry KX622593
4) *Bsa*I design based on *mch* cluster retrieved from GeneBank entry KX622602
5) *Bsa*I design based on *mch* cluster retrieved from GeneBank entry KX622599
6) *Aar*I design based on *mch* cluster retrieved from GeneBank entry KX622595

2.4 Assembly of artificial *mch* genes and gene clusters

The synthetic fragments of biosynthetic genes were stitched and subcloned to pSynbio1 vector. The resulting intermediate constructs, pSyn1-mchA_SE, pSyn1-mchB_SE and pSyn1-mchC_SE, were hydrolyzed by *Bsa*I to retrieve the splitter elements. After purification with QIAquick PCR Purification Kit (Qiagen), SEs were removed and the SE-free fragments were ligated by T4 DNA ligase. The reassembled biosynthetic genes as well as synthetic promoter, intergenic linkers and terminator were subcloned to pSynbio2, generating final *mch* expression vector. To generate CP-mutations, module duplications and module deletions, dedicated synthetic fragments were subcloned to pSyn1-mchB_SE or pSyn1-mchC_SE. After desplitting and reassembly, modified *mchB* or *mchC* replaced the corresponding gene on pSynMch13 by conventional cloning to yield modified *mch* expression vector. Detailed information for the construction of expression vectors is available in Table S6 and Table S7. The point mutations in final expression constructs were excluded by Illumina MiSeq sequencing.

Table S6 Constructs for *mch* gene library generated in this study.

Plasmid	Construction
A-type *mch* cluster fragments from *M. xanthus* DK1622	
pSyn1-MchA_A_SE	(1) 2122 bp *Nde*I/*Pme*I MchA_A_fragB fragment from pSV-MchA_A_fragB ligated into pSV-MchA_A_fragA hydrolyzed with *Nde*I/*Pme*I to generate pSV-MchA_A_fragAB (2) 6302 bp *Kpn*I/*Pme*I MchA_A_fragAB fragment from pSV-MchA_A_fragAB ligated into pSynbio1 hydrolyzed with *Kpn*I/*Pme*I to generate pSyn1-MchA_A_SE_pre (3) 1336 bp *Kpn*I/*Spe*I MchA_A_fragA_dcm fragment from pSV-MchA_A_fragA_dcm ligated into pSyn1-MchA_A_SE_pre to generate pSyn1-MchA_A_SE
pSyn1-MchA_A	Hydrolysis of pSyn1-MchA_A_SE by *Bsa*I followed by re-ligation to remove SE*
pSyn1-MchB_A_SE	(1) 3335 bp *Spe*I/*Pme*I MchB_A_fragB fragment from pSV-MchB_A_fragB ligated into pSV-MchB_A_fragA hydrolyzed with *Spe*I/*Pme*I to generate pSV-MchB_A_fragAB (2) 9028 bp *Kpn*I/*Pme*I MchB_A_fragAB fragment from pSV-MchB_A_fragAB ligated into pSynbio1 hydrolyzed with *Kpn*I/*Pme*I to generate pSyn1-MchB_A_SE_pre (3) 1100 bp *Kpn*I/*Nde*I MchB_A_fragA_dcm fragment from pSV-MchB_A_fragA_dcm ligated into pSyn1-MchB_A_SE_pre to generate pSyn1-MchB_A_SE
pSyn1-MchB_A	Hydrolysis of pSyn1-MchB_A_SE by *Bsa*I followed by re-ligation to remove SE
pSyn1-MchC_A_SE	(1) 4862 bp *Nde*I/*Pme*I MchC_A_fragB fragment from pSV-MchC_A_fragB ligated into pSV-MchC_A_fragA hydrolyzed with *Nde*I/*Pme*I to generate pSV-MchC_A_fragAB (2) 9237 bp *Kpn*I/*Pme*I MchC_A_fragAB fragment from pSV-MchC_A_fragAB ligated into pSynbio1 hydrolyzed with *Kpn*I/*Pme*I to generate pSyn1-MchC_A_fragAB (3) 4272 bp *Ase*I/*Pme*I MchC_A_fragC fragment from pSV-MchC_A_fragC ligated into pSyn1-MchC_A_fragAB digested with *Ase*I/*Pme*I to generate pSyn1-MchC_A_SE_pre (4) 1219 bp *Kpn*I/*Spe*I MchC_A_fragA_dcm fragment from pSV-MchC_A_fragA_dcm ligated into pSyn1-MchC_A_SE_pre to generate pSyn1-MchC_A_SE_pre2 (5) 344 bp *Ase*I/*Bam*HI MchC_A_fragC_dcm fragment from pSV-MchC_A_fragC_dcm ligated into pSyn1-MchC_A_SE_pre2 to generate pSyn1-MchC_A_SE
pSyn1-MchC_A	Hydrolysis of pSyn1-MchC_A_SE by *Bsa*I followed by re-ligation to remove SE
pSyn1-MchB_A_CP1inact1_SE	350 bp *Asi*SI/*Xba*I MchB_A_CP1inact1 fragment from pUC57-MchB_A_CP1inact1 ligated into pSyn1-MchB_A_SE to generate pSyn1-MchB_A_CP1inact1_SE
pSyn1-MchB_A_CP1inact1	Hydrolysis of pSyn1-MchB_A_CP1inact1_SE by *Bsa*I followed by re-ligation to remove SE
pSyn1-MchB_A_CP2inact1_SE	330 bp *Afl*II/*Avr*II MchB_A_CP2inact1 fragment from pUC57-MchB_A_CP2inact1 ligated into pSyn1-MchB_A_SE to generate pSyn1-MchB_A_CP2inact1_SE
pSyn1-MchB_A_CP2inact1	Hydrolysis of pSyn1-MchB_A_CP2inact1_SE by *Bsa*I followed by re-ligation to remove SE
pSyn1-MchC_A_CP3inact1_SE	322 bp *Asi*SI/*Eco*RI MchC_A_CP3inact1 fragment from pUC57-MchC_A_CP3inact1 ligated into pSyn1-MchC_A_SE to generate pSyn1-MchC_A_CP3inact1_SE
pSyn1-MchC_A_CP3inact1	Hydrolysis of pSyn1-MchC_A_CP3inact1_SE by *Bsa*I followed by re-ligation to remove SE
pSyn1-MchC_A_CP4inact1_SE	338 bp *Mfe*I/*Afl*II MchC_A_CP4inact1 fragment from pUC57-MchC_A_CP4inact1 ligated into pSyn1-MchC_A_SE to generate pSyn1-MchC_A_CP4inact1_SE
pSyn1-MchC_A_CP4inact1	Hydrolysis of pSyn1-MchC_A_CP4inact1_SE by *Bsa*I followed by re-ligation to remove SE
pSyn1-MchC_A_CP4inact2_SE	338 bp *Mfe*I/*Afl*II MchC_A_CP4inact2 fragment from pUC57-MchC_A_CP4inact2 ligated into pSyn1-MchC_A_SE to generate pSyn1-MchC_A_CP4inact2_SE
pSyn1-	Hydrolysis of pSyn1-MchC_A_CP4inact2_SE by *Bsa*I followed by re-ligation to

MchC_A_CP4inact2	remove SE
pSyn1-MchC_A_CP5inact1_SE	344 bp *Ase*I/*Bam*HI MchC_A_CP5inact1 fragment from pUC57-MchC_A_CP5inact1 ligated into pSyn1-MchC_A_SE to generate pSyn1-MchC_A_CP5inact1_SE
pSyn1-MchC_A_CP5inact1	Hydrolysis of pSyn1-MchC_A_CP5inact1_SE by *Bsa*I followed by re-ligation to remove SE
pSyn1-MchC_A_CP6inact1_SE	320 bp *Hind*III/*Nhe*I MchC_A_CP6inact1 fragment from pUC57-MchC_A_CP6inact1 ligated into pSyn1-MchC_A_SE to generate pSyn1-MchC_A_CP6inact1_SE
pSyn1-MchC_A_CP6inact1	Hydrolysis of pSyn1-MchC_A_CP6inact1_SE by *Bsa*I followed by re-ligation to remove SE
pSyn1-MchB_A_duplM1_SE	5743 bp *Xba*I/*Spe*I MchB_A_duplM1 fragment from pUC57-MchB_A_duplM1 ligated into pSyn1-MchB_A_SE to generate pSyn1-MchB_A_duplM1_SE
pSyn1-MchB_A_duplM1	Hydrolysis of pSyn1-MchB_A_duplM1_SE by *Bsa*I followed by re-ligation to remove SE
pSyn1-MchB_A_duplM2_SE	3452 bp *Afl*II/*Avr*II MchB_A_duplM2 fragment from pUC57-MchB_A_duplM2 ligated into pSyn1-MchB_A_SE to generate pSyn1-MchB_A_duplM2_SE
pSyn1-MchB_A_duplM2	Hydrolysis of pSyn1-MchB_A_duplM2_SE by *Bsa*I followed by re-ligation to remove SE
pSyn1-MchC_A_duplM3_SE	4329 bp *Eco*RI/*Nde*I MchC_A_duplM3 fragment from pUC57-MchC_A_duplM3 ligated into pSyn1-MchC_A_SE to generate pSyn1-MchC_A_duplM3_SE
pSyn1-MchC_A_duplM3	Hydrolysis of pSyn1-MchC_A_duplM3_SE by *Bsa*I followed by re-ligation to remove SE
pSyn1-MchC_A_duplM4_SE	4370 bp *Afl*II/*Xba*I MchC_A_duplM4 fragment from pUC57-MchC_A_duplM4 ligated into pSyn1-MchC_A_SE to generate pSyn1-MchC_A_duplM4_SE
pSyn1-MchC_A_duplM5_SE	4355 bp *BamH*I/*Avr*II MchC_A_duplM5 fragment from pUC57-MchC_A_duplM5 ligated into pSyn1-MchC_A_SE to generate pSyn1-MchC_A_duplM5_SE
pSyn1-MchC_A_duplM6_SE	3475 bp *Hind*III/*Nhe*I MchC_A_duplM6 fragment from pUC57-MchC_A_duplM6 ligated into pSyn1-MchC_A_SE to generate pSyn1-MchC_A_duplM6_SE
pSyn1-MchC_A_duplM6	Hydrolysis of pSyn1-MchC_A_duplM6_SE by *Bsa*I followed by re-ligation to remove SE
pSyn1-MchB_A_delM1_SE	2697 bp *Mlu*I/*Afl*II MchB_A_delM1 fragment from pUC57-MchB_A_delM1 ligated into pSyn1-MchB_A_SE to generate pSyn1-MchB_A_delM1_SE
pSyn1-MchB_A_delM1	Hydrolysis of pSyn1-MchB_A_delM1_SE by *Bsa*I followed by re-ligation to remove SE
pSyn1-MchB_A_delM2_SE	2665 bp *Xba*I/*Not*I MchB_A_delM2 fragment from pUC57-MchB_A_delM2 ligated into pSyn1-MchB_A_SE to generate pSyn1-MchB_A_delM2_SE
pSyn1-MchB_A_delM2	Hydrolysis of pSyn1-MchB_A_delM2_SE by *Bsa*I followed by re-ligation to remove SE
pSyn1-MchC_A_delM3_SE	2797 bp *Sph*I/*Mfe*I MchC_A_delM3 fragment from pUC57-MchC_A_delM3 ligated into pSyn1-MchC_A_SE to generate pSyn1-MchC_A_delM3_SE
pSyn1-MchC_A_delM3	Hydrolysis of pSyn1-MchC_A_delM3_SE by *Bsa*I followed by re-ligation to remove SE
pSyn1-MchC_A_delM4_SE	2820 bp *Eco*RI/*Ase*I MchC_A_delM4 fragment from pUC57-MchC_A_delM4 ligated into pSyn1-MchC_A_SE to generate pSyn1-MchC_A_delM4_SE
pSyn1-MchC_A_delM4	Hydrolysis of pSyn1-MchC_A_delM4_SE by *Bsa*I followed by re-ligation to remove SE
pSyn1-MchC_A_delM5_SE	2584 bp *Afl*II/*Hind*III MchC_A_delM5 fragment from pUC57-MchC_A_delM5 ligated into pSyn1-MchC_A_SE to generate pSyn1-MchC_A_delM5_SE
pSyn1-MchC_A_delM5	Hydrolysis of pSyn1-MchC_A_delM5_SE by *Bsa*I followed by re-ligation to remove SE
pSyn1-MchC_A_delM6_SE	1958 bp *BamH*I/*Age*I MchC_A_delM6 fragment from pUC57-MchC_A_delM6 ligated into pSyn1-MchC_A_SE to generate pSyn1-MchC_A_delM6_SE
B-type *mch* cluster fragments from *Myxococcus* sp. 171	
pSyn1-MchC_B_SE	(1) 2954 bp *Kpn*I/*Mlu*I MchC_B_fragA fragment from pSV-MchC_B_fragA_woSE and 2947 bp *Mlu*I/*Pme*I MchC_B_fragB fragment from pSV-MchC_B_fragB_woSE ligated into pSynbio1 hydrolyzed with *Kpn*I/*Pme*I to generate pSyn1-MchC_B_fragAB (2) 4854 bp *Kpn*I/*Ase*I MchC_B_fragC fragment from pSV-MchC_B_fragC_woSE and 4269 *Ase*I/*Pme*I MchC_B_fragD fragment from pSV-

	MchC_B_fragD_woSE ligated into pSynbio1 hydrolyzed with *Kpn*I/*Pme*I to generate pSyn1-MchC_B_fragCD (3) 7318 bp *Mun*I/*Pme*I MchC_B_fragA fragment from pSyn1-MchC_B_fragCD ligated into pSyn1-MchC_B_fragAB hydrolyzed with *Mun*I/*Pme*I to generate pSyn1-MchC_B_SE_pre (4) 3193 bp *Mun*I/*Ase*I MchC_B_fragC fragment from pSV-MchC_B_fragC ligated into pSyn1-MchC_B_SE_pre to generate pSyn1-MchC_B_SE
pSyn1-MchC_B	Hydrolysis of pSyn1-MchC_B_SE by *Bsa*I followed by re-ligation to remove SE
C-type *mch* cluster fragments from *M. virescens* ST200611	
pSyn1-MchC_C_SE	(1) 5923 bp *Nde*I/*Pme*I MchC_C_fragB fragment from pSV-MchC_C_fragB ligated into pSV-MchC_C_fragA hydrolyzed with *Nde*I/*Pme*I to generate pSV-MchC_C_SE (2) 10296 bp *Kpn*I/*Pme*I MchC_C_SE fragment from pSV-MchC_C_SE ligated into pSynbio1 hydrolyzed with *Kpn*I/*Pme*I to generate pSyn1-MchC_C_SE_pre (3) 1211 bp *Kpn*I/*Spe*I MchC_C_fragA_dcm fragment from pSV-MchC_C_fragA_dcm ligated into pSyn1-MchC_C_SE_pre hydrolyzed with *Kpn*I/*Pme*I to generate pSyn1-MchC_C_SE
pSyn1-MchC_C	Hydrolysis of pSyn1-MchC_C_SE by *Bsa*I followed by re-ligation to remove SE
D-type *mch* cluster fragments from *S. erecta* Pde77	
pSyn1-MchB_D_SE	5719 bp *Kpn*I/*Spe*I MchB_D_fragA fragment from pSV-pMchB_D_fragA and 3332 bp *Spe*I/*Pme*I MchB_D_fragB fragment from pSV-pMchB_D_fragB ligated into pSynbio1 hydrolyzed with *Kpn*I/*Pme*I to generate pSyn1-MchB_D_SE
pSyn1-MchB_D	Hydrolysis of pSyn1-MchB_D_SE by *Bsa*I followed by re-ligation to remove SE
pSyn1-MchC_D_SE	(1) 4386 bp *Kpn*I/*Nde*I MchC_D_fragA fragment from pSV-MchC_D_fragA and 4859 bp *Nde*I/*Pme*I MchC_D_fragB fragment from pSV-MchC_D_fragB ligated into pSynbio1 hydrolyzed with *Kpn*I/*Pme*I to generate pSyn1-MchC_D_fragAB (2) 4278 bp *Ase*I/*Pme*I MchC_D_fragC fragment from pSV-pMchC_D_fragC ligated into pSyn1-MchB_D_fragAB hydrolyzed with *Ase*I/*Pme*I to generate pSyn1-MchC_D_SE
pSyn1-MchC_D	Hydrolysis of pSyn1-MchC_D_SE by *Bsa*I followed by re-ligation to remove SE
S-type *mch* cluster fragments from *S. aurantiaca* DW4/3-1	
pSyn1-MchB_S_SE	(1) 3328 bp *Spe*I/*Pme*I MchB_S_fragB fragment from pSV-MchB_S_fragB ligated into pSV-pMchB_S_fragA hydrolyzed with *Spe*I/*Pme*I to generate pSV-MchB_S_fragAB (2) 9051 bp *Kpn*I/*Pme*I MchB_S_fragAB fragment from pSV-MchB_S_fragAB ligated into pSynbio1 hydrolyzed with *Kpn*I/*Pme*I to generate pSyn1-MchB_S_SE_pre (3) 1100 bp *Kpn*I/*Nde*I MchB_S_fragA_dcm fragment from pSV-MchB_S_fragA_dcm ligated into pSyn1-MchB_S_SE_pre to generate pSyn1-MchB_S_SE
pSyn1-MchB_S	Hydrolysis of pSyn1-MchB_S_SE by *Bsa*I followed by re-ligation to remove SE
pSyn1-MchC_S_SE	(1) 4857 bp *Nde*I/*Pme*I MchC_S_fragB fragment from pSV-MchC_S_fragB ligated into pSV-MchC_S_fragA hydrolyzed with *Nde*I/*Pme*I to generate pSV-MchC_S_fragAB (2) 9234 bp *Kpn*I/*Pme*I MchC_S_fragAB fragment from pSV-MchC_S_fragAB ligated into pSynbio1 hydrolyzed with *Kpn*I/*Pme*I to generate pSyn1-MchC_S_fragAB (3) 4276 bp *Ase*I/*Pme*I MchC_S_fragC fragment from pSV-MchC_S_fragC ligated into pSyn1-MchC_S_fragAB hydrolyzed with *Ase*I/*Pme*I to generate pSyn1-MchC_S_SE_pre (4) 1219 bp *Kpn*I/*Spe*I MchC_S_fragA_dcm fragment from pSV-MchC_S_fragA_dcm ligated into pSyn1-MchC_S_SE_pre to generate pSyn1-MchC_S_SE_pre2 (5) 344 bp *Ase*I/*Bam*HI MchC_S_fragC_dcm fragment from pSV-MchC_S_fragC_dcm ligated into pSyn1-MchC_S_SE_pre2 to generate pSyn1-MchC_S_SE
pSyn1-MchC_S	Hydrolysis of pSyn1-MchC_S_SE by *Bsa*I followed by re-ligation to remove SE
pSyn1-	335 bp *Mfe*I/*Afl*II MchC_S_CP4react fragment from pUC57-MchC_S_CP4act

MchC_S_CP4react_SE	ligated into pSyn1-MchC_S_SE to generate pSyn1-MchC_S_CP4react_SE
pSyn1-MchC_S_CP4react	Hydrolysis of pSyn1-MchC_S_CP4react_SE by *Bsa*I followed by re-ligation to remove SE
A-type *mch* cluster fragments from *M. xanthus* DK1622**	
pSyn1-MchA_A_AarI_SE	6303 bp *Kpn*I/*Pme*I MchA_A_AarI_SE fragment from pSV-MchA_A_AarI_SE ligated into pSynbio1 hydrolyzed with *Kpn*I/*Pme*I to generate pSyn1-MchA_A_AarI_SE
pSyn1-MchA_A_AarI	Hydrolysis of pSyn1-MchA_A_AarI_SE by *Aar*I followed by re-ligation to remove SE
pSyn1-MchB_A_AarI_SE	9069 bp *Kpn*I/*Pme*I MchB_A_AarI_SE fragment from pSV-MchB_A_AarI_SE ligated into pSynbio1 hydrolyzed with *Kpn*I/*Pme*I to generate pSyn1-MchB_A_AarI_SE
pSyn1-MchB_A_AarI	Hydrolysis of pSyn1-MchB_A_AarI_SE by *Aar*I followed by re-ligation to remove SE
pSyn1-MchC_A_AarI_SE	(1) 3944 bp *Bam*HI/*Mlu*I MchC_A_AarI_fragF fragment from pSV-MchC_A_AarI_fragF ligated into pSV-MchC_A_AarI_fragABCE hydrolyzed with *Bam*HI/*Mlu*I to generate pSV-MchC_A_AarI_fragABCEF (2) 3256 bp *Nde*I/*Xba*I MchC_A_AarI_fragD fragment from pSV-MchC_A_AarI_fragD ligated into pSV-MchC_A_AarI_fragABCEF hydrolyzed with *Nde*I/*Xba*I to generate pSV-MchC_A_AarI_SE (3) 13637 bp *Kpn*I/*Pme*I MchC_A_AarI_SE fragment from pSV-MchC_A_AarI_SE ligated into pSynbio1 hydrolyzed with *Kpn*I/*Pme*I to generate pSyn1-MchC_A_AarI_SE
pSyn1-MchC_A_AarI	Hydrolysis of pSyn1-MchC_A_AarI_SE by *Aar*I followed by re-ligation to remove SE
pSyn1-P-5mchA_A_AarI	641 bp *Kpn*I/*Pme*I P-5mchA_A_AarI fragment from pSV- P-5mchA_A_AarI ligated into pSynbio1 hydrolyzed with *Kpn*I/*Pme*I to generate pSyn1-P-5mchA_A_AarI
pSyn1-3mchA-5mchB_A_AarI	421 bp *Kpn*I/*Pme*I 3mchA-5mchB_A_AarI fragment from pSV-3mchA-5mchB_A_AarI ligated into pSynbio1 hydrolyzed with *Kpn*I/*Pme*I to generate pSyn1-3mchA-5mchB_A_AarI
pSyn1-3mchB-5mchC_A_AarI	220 bp *Kpn*I/*Pme*I 3mchB-5mchC_A_AarI fragment from pSV-3mchB-5mchC_A_AarI ligated into pSynbio1 hydrolyzed with *Kpn*I/*Pme*I to generate pSyn1-3mchB-5mchC_A_AarI
pSyn1-T-3mchC_A_AarI	2639 bp *Kpn*I/*Pme*I T-3mchC_A_AarI fragment from pSV-T-3mchC_A_AarI ligated into pSynbio1 hydrolyzed with *Kpn*I/*Pme*I to generate pSyn1-T-3mchC_A_AarI

* SE = splitter element
** Based on *Aar*I design

Table S7 Constructs for *mch* cluster assemblies generated in this study.

Plasmid	Construction
pSynMch1	(1) 621 bp *Kpn*I/*Bsi*WI P5mchA$_A$ fragment from pSyn1-P-5mchA_A_AarI ligated into pSynbio2 hydrolyzed with *Kpn*I/*Bsi*WI to generate pSyn2-ca1 (2) 6134 bp *Bsi*WI/*Mre*I *mch*A$_A$ fragment from pSyn1-MchA_A_AarI ligated into pSyn2-ca1 hydrolyzed with *Bsi*WI/*Mre*I to generate pSyn2-ca2 (3) 386 bp *Mre*I/*Mlu*I 3A$_A$5B$_A$ fragment from pSyn1-3mchA-5mchB_A_AarI ligated into pSyn2-ca2 hydrolyzed with *Mre*I/*Mlu*I to generate pSyn2-ca3 (4) 8803 bp *Mlu*I/*Not*I *mch*B$_A$ fragment from pSyn1-MchB_A_AarI ligated into pSyn2-ca3 hydrolyzed with *Mlu*I/*Not*I to generate pSyn2-ca4 (5) 186 bp *Not*I/*Sph*I 3B$_A$5C$_A$ fragment from pSyn1-3mchB-5mchC_A_AarI ligated into pSyn2-ca4 hydrolyzed with *Not*I/*Sph*I to generate pSyn2-ca5 (6) 13150 bp *Sph*I/*Age*I mchC$_A$ fragment from pSyn1-MchC_A_AarI ligated into pSyn2-ca5 hydrolyzed with *Sph*I/*Age*I to generate pSyn2-ca6 (7) 2616 bp *Age*I/*Pvu*I T3mchC$_A$ fragment from pSyn1-T-3mchC_A_AarI ligated into pSyn2-ca6 hydrolyzed with *Age*I/*Pvu*I to generate pSynMch1
pSynMch2	(1) 606 bp *Kpn*I/*Bsi*WI P5mchA$_A$ fragment from pSV-P-5mchA_Ab ligated into pSynbio2

	hydrolyzed with *Kpn*I/*Bsi*WI to generate pSyn2-ca7
	(2) 6134 bp *Bsi*WI/*Mre*I *mch*A_A fragment from pSyn1-MchA_A ligated into pSyn2-ca7 hydrolyzed with *Bsi*WI/*Mre*I to generate pSyn2-ca8
	(3) 386 bp *Mre*I/*Mlu*I $3A_A5B_A$ fragment from pSV-3mchA-5mchB_Ab ligated into pSyn2-ca8 hydrolyzed with *Mre*I/*Mlu*I to generate pSyn2-ca9
	(4) 8803 bp *Mlu*I/*Not*I *mch*B_A fragment from pSyn1-MchB_A ligated into pSyn2-ca9 hydrolyzed with *Mlu*I/*Not*I to generate pSyn2-ca10
	(5) 186 bp *Not*I/*Sph*I $3B_A5C_A$ fragment from pSV-3mchB-5mchC_Ab ligated into pSyn2-ca10 hydrolyzed with *Not*I/*Sph*I to generate pSyn2-ca11
	(6) 13150 bp *Sph*I/*Age*I mchC_A fragment from pSyn1-MchC_A ligated into pSyn2-ca11 hydrolyzed with *Sph*I/*Age*I to generate pSyn2-ca12
	(7) 2601 bp *Age*I/*Pvu*I T3mchC_A fragment from pSV-T-3mchC_Ab ligated into pSyn2-ca12 hydrolyzed with *Age*I/*Pvu*I to generate pSynMch2_pre
	(8) 15917 bp *Kpn*I/*Not*I P5*mchA*$_A$-*mchA*$_A$-*3A*$_A$*5B*$_A$-*mchB*$_A$ fragment from pSyn2-ca10 ligated into pSynMch2_pre hydrolyzed with *Kpn*I/*Not*I to generate pSynMch2
pSynMch3	(1) 186 bp *Not*I/*Sph*I $3B_B5C_B$ fragment from pSV-3mchB-5mchC_Bb ligated into pSynbio2 hydrolyzed with *Not*I/*Sph*I to generate pSyn2-ca13
	(2) 2601 bp *Age*I/*Pvu*I T3*mchC*$_B$ fragment from pSV-T-3mchC_Bb ligated into pSyn2-ca13 hydrolyzed with *Age*I/*Pvu*I to generate pSyn2-ca14
	(3) 16250 bp *Sph*I/*Age*I *mchC*$_B$ fragment from pSyn1-MchC_B ligated into pSyn2-ca14 hydrolyzed with *Sph*I/*Age*I to generate pSyn2-ca15
	(4) 15909 bp *Kpn*I/*Not*I P5*mchA*$_A$-*mchA*$_A$-$3A_A5B_A$-*mchB*$_A$fragment from pSynMch2 ligated into pSyn2-ca15 hydrolyzed with *Kpn*I/*Not*I to generate pSynMch3
pSynMch4	(1) 186 bp *Not*I/*Sph*I $3B_C5C_C$ fragment from pSV-3mchB-5mchC_Cb ligated into pSyn2-ca10 hydrolyzed with *Not*I/*Sph*I to generate pSyn2-ca16
	(2) 10013 bp *Sph*I/*Age*I *mchC*$_C$ fragment from pSyn1-MchC_C ligated into pSyn2-ca16 hydrolyzed with *Sph*I/*Age*I to generate pSyn2-ca17
	(3) 2601 bp *Age*I/*Pvu*I T3*mchC*$_C$ fragment from pSV-T-3mchC_Cb ligated into pSyn2-ca17 hydrolyzed with *Age*I/*Pvu*I to generate pSynMch4
pSynMch5	(1) 205 bp *Not*I/*Sph*I $3B_D5C_D$ fragment from pSV-3mchB-5mchC_Db ligated into pSynbio2 hydrolyzed with *Not*I/*Sph*I to generate pSyn2-ca18
	(2) 2610 bp *Age*I/*Pvu*I T3*mchC*$_D$ fragment from pSV-T-3mchC_Db ligated into pSyn2-ca18 hydrolyzed with *Age*I/*Pvu*I to generate pSyn2-ca19
	(3) 13154 bp *Sph*I/*Age*I *mchC*$_D$ fragment from pSyn1-MchC_D ligated into pSyn2-ca19 hydrolyzed with *Sph*I/*Age*I to generate pSyn2-ca20
	(4) 8826 bp *Mlu*I/*Not*I *mchB*$_D$ fragment from pSyn1-MchB_D ligated into pSyn2-ca20 hydrolyzed with *Mlu*I/*Not*I to generate pSyn2-ca21
	(5) 7110 bp *Kpn*I/*Mlu*I P5*mchA*$_A$-*mchA*$_A$-$3A_A5B_A$ from pSynMch2 ligated into pSyn2-ca21 hydrolyzed with *Kpn*I/*Mlu*I to generate pSynMch5
pSynMch6	(1) 8830 bp *Mlu*I/*Not*I *mchB*$_S$ fragment from pSyn1-MchB_S ligated into pSyn2-ca9 hydrolyzed with *Mlu*I/*Not*I to generate pSyn2-ca22
	(2) 187 bp *Not*I/*Sph*I $3B_S5C_S$ fragment from pSV-3mchB-5mchC_Sb ligated into pSyn2-ca22 hydrolyzed with *Not*I/*Sph*I to generate pSyn2-ca23
	(3) 13157 bp *Sph*I/*Age*I *mchC*$_S$ fragment from pSyn1-MchC_S ligated into pSyn2-ca23 hydrolyzed with *Sph*I/*Age*I to generate pSyn2-ca24
	(4) 2620 bp *Age*I/*Pvu*I T3*mchC*$_S$ fragment from pSV-T-3mchC_Sb ligated into pSyn2-ca24 hydrolyzed with *Age*I/*Pvu*I T3*mchC*$_S$ to generate pSynMch6
pSynMch8	(1) 13165 bp *Sph*I/*Age*I *mchC*$_S$ fragment from pSyn1-MchC_S ligated into pSyn2-ca11 hydrolyzed with *Sph*I/*Age*I to generate pSyn2-ca31
	(2) 2620 bp *Age*I/*Pvu*I T3mchC_S fragment from pSV-T-3mchC_Sb ligated into pSyn2-ca31 hydrolyzed with *Age*I/*Pvu*I to generate pSynMch8_pre
	(3) 15917 bp *Kpn*I/*Not*I P5*mchA*$_A$-*mchA*$_A$-$3A_A5B_A$-*mch*B_A fragment from pSyn2-ca10 ligated into

	pSynMch8_pre hydrolyzed with *Kpn*I/*Not*I to generate pSynMch8
pSynMch9	(1) 186 bp *Not*I/*Sph*I $3B_A5C_A$ fragment from pSV-3mchB-5mchC_Ab into pSyn2-ca22 hydrolyzed with *Not*I/*Sph*I to generate pSyn2-ca32 (2) 13150 bp *Sph*I/*Age*I $mchC_A$ fragment from pSyn1-MchC_A ligated into pSyn2-ca32 hydrolyzed with *Sph*I/*Age*I to generate pSyn2-ca33 (3) 2608 bp *Age*I/*Pvu*I $T3mchC_A$ fragment from pSV-T-3mchC_Ab ligated into pSyn2-ca33 hydrolyzed with *Age*I/*Pvu*I to generate pSynMch9_pre (4) 15944 bp *Kpn*I/*Not*I $P5mchA_A$-$mchA_A$-$3A_A5B_A$-$mchB_S$ fragment from pSyn2-ca22 ligated into pSynMch9_pre hydrolyzed with *Kpn*I/*Not*I to generate pSynMch9
pSynMch10	(1) 186 bp *Not*I/*Sph*I $3B_C5C_C$ fragment from pSV-3mchB-5mchC_Cb into pSyn2-ca22 hydrolyzed with *Not*I/*Sph*I to generate pSyn2-ca34 (2) 10021 bp *Sph*I/*Age*I $mchC_C$ fragment from pSyn1-MchC_C ligated into pSyn2-ca34 hydrolyzed with *Sph*I/*Age*I to generate pSyn2-ca35 (3) 2601 bp *Age*I/*Pvu*I $T3mchC_C$ fragment from pSV-T-3mchC_Cb ligated into pSyn2-ca35 hydrolyzed with *Age*I/*Pvu*I to generate pSynMch10_pre (4) 15944 bp *Kpn*I/*Not*I $P5mchA_A$-$mchA_A$-$3A_A5B_A$-$mchB_S$ fragment from pSyn2-ca22 ligated into pSynMch10_pre hydrolyzed with *Kpn*I/*Not*I to generate pSynMch10
pSynMch11	19037 bp *Not*I/*Pvu*I $3B_B5C_B$-$mchC_B$-$T3mchC_B$ fragment from pSyn2-ca15 ligated into pSynMch10 hydrolyzed with *Not*I/*Pvu*I to generate pSynMch11
pSynMch12	15952 bp *Not*I/*Pvu*I $3B_D5C_D$-$mchC_D$-$T3mchC_D$ fragment from pSyn2-ca20 ligated into pSynMch10 hydrolyzed with *Not*I/*Pvu*I to generate pSynMch12
pSynMch13	(1) The native promoter of *mchA* gene cluster on pSynMch2 was replaced with *cmR-ccdB* cassette by Red/ET recombination to generate pSynMch2-cmccdB (2) The *cmR-ccdB* cassette on pSynMch2-cmccdB was substituted with overexpression promoter *Ptn5* by Red/ET recombination
pSynMch14	8830 bp *Mlu*I/*Not*I $mchB_S$ fragment from pSyn1-MchB_S ligated into pSynMch13 hydrolyzed with *Mlu*I/*Not*I to generate pSynMch14
pSynMch15	21643 bp *Kpn*I/*Not*I $3B_B5C_B$-$mchC_B$-$T3mchC_B$ fragment from pSyn2-ca15 ligated into pSynMch14 hydrolyzed with *Kpn*I/*Not*I to generate pSynMch15
pSynMch16	18558 bp *Kpn*I/*Not*I $3B_D5C_D$-$mchC_D$-$T3mchC_D$ fragment from pSyn2-ca20 ligated into pSynMch14 hydrolyzed with *Kpn*I/*Not*I to generate pSynMch16
pSynMch17	8803 bp *Mlu*I/*Not*I $mchB_A$ fragment from pSyn1-MchB_A_CP1inact1 ligated into pSynMch13 hydrolyzed with *Mlu*I/*Not*I to generate pSynMch17
pSynMch18	8803 bp *Mlu*I/*Not*I $mchB_A$ fragment from pSyn1-MchB_A_CP2inact1 ligated into pSynMch13 hydrolyzed with *Mlu*I/*Not*I to generate pSynMch18
pSynMch19	13150 bp *Sph*I/*Age*I $mchC_A$ fragment from pSyn1-MchC_A_CP3inact1 ligated into pSynMch13 hydrolyzed with *Sph*I/*Age*I to generate pSynMch19
pSynMch20	13150 bp *Sph*I/*Age*I $mchC_A$ fragment from pSyn1-MchC_A_CP4inact1 ligated into pSynMch13 hydrolyzed with *Sph*I/*Age*I to generate pSynMch20
pSynMch21	13150 bp *Sph*I/*Age*I $mchC_A$ fragment from pSyn1-MchC_A_CP4inact2 ligated into pSynMch13 hydrolyzed with *Sph*I/*Age*I to generate pSynMch21
pSynMch22	13150 bp *Sph*I/*Age*I $mchC_A$ fragment from pSyn1-MchC_A_CP5inact1 ligated into pSynMch13 hydrolyzed with *Sph*I/*Age*I to generate pSynMch22
pSynMch23	13150 bp *Sph*I/*Age*I $mchC_A$ fragment from pSyn1-MchC_A_CP6inact1 ligated into pSynMch13 hydrolyzed with *Sph*I/*Age*I to generate pSynMch23
pSynMch24	13165 bp *Sph*I/*Age*I $mchC_S$ fragment from pSyn1-MchC_S_CP4react ligated into pSynMch6 hydrolyzed with *Sph*I/*Age*I to generate pSynMch24
pSynMch25	13296 bp *Mlu*I/*Not*I $mchB_A$ fragment from pSyn1-MchB_A_duplM1 ligated into pSynMch13 hydrolyzed with *Mlu*I/*Not*I to generate pSynMch24
pSynMch26	11925 bp *Mlu*I/*Not*I $mchB_A$ fragment from pSyn1-MchB_A_duplM2 ligated into pSynMch13 hydrolyzed with *Mlu*I/*Not*I to generate pSynMch25
pSynMch27	16268 bp *Sph*I/*Age*I $mchC_A$ fragment from pSyn1-MchC_A_duplM3 ligated into pSynMch13 hydrolyzed with *Sph*I/*Age*I to generate pSynMch27

pSynMch28	16301 bp *Sph*I/*Age*I $mchC_A$ fragment from pSyn1-MchC_A_duplM6 ligated into pSynMch13 hydrolyzed with *Sph*I/*Age*I to generate pSynMch28
pSynMch29	4302 bp *Mlu*I/*Not*I $mchB_A$ fragment from pSyn1-MchB_A_delM1 ligated into pSynMch13 hydrolyzed with *Mlu*I/*Not*I to generate pSynMch29
pSynMch30	7002 bp *Mlu*I/*Not*I $mchB_A$ fragment from pSyn1-MchB_A_delM2 ligated into pSynMch13 hydrolyzed with *Mlu*I/*Not*I to generate pSynMch30
pSynMch31	10028 bp *Sph*I/*Age*I $mchC_A$ fragment from pSyn1-MchC_A_delM3 ligated into pSynMch13 hydrolyzed with *Sph*I/*Age*I to generate pSynMch31
pSynMch32	10001 bp *Sph*I/*Age*I $mchC_A$ fragment from pSyn1-MchC_A_delM4 ligated into pSynMch13 hydrolyzed with *Sph*I/*Age*I to generate pSynMch32
pSynMch33	10007 bp *Sph*I/*Age*I $mchC_A$ fragment from pSyn1-MchC_A_delM5 ligated into pSynMch13 hydrolyzed with *Sph*I/*Age*I to generate pSynMch33

3. Transformation of *M. xanthus* and verification by colony PCR

The *mch* expression constructs harboring synthetic *mch* cluster were transferred into *M. xanthus* DK1622 *ΔmchA-tet* via electroporation using established standard protocols.[6] The *mch* gene clusters were integrated to the chromosome of *M. xanthus* DK1622 *ΔmchA-tet* by homologous recombination (Fig. S3). The *rhlE* gene served as homologous sequence. The integration of the respective *mch* clusters in *M. xanthus* mutants were verified by colony PCR. Briefly, cells from a CTT agar plate were re-suspended in 100 µL water and heated at 100 °C for 10 min, 1 µL of the supernatant was used as template for PCR. Oligonucleotide sequences are given in the Table S8. As shown in Fig. S4, all *mch* clusters were integrated to the genome.

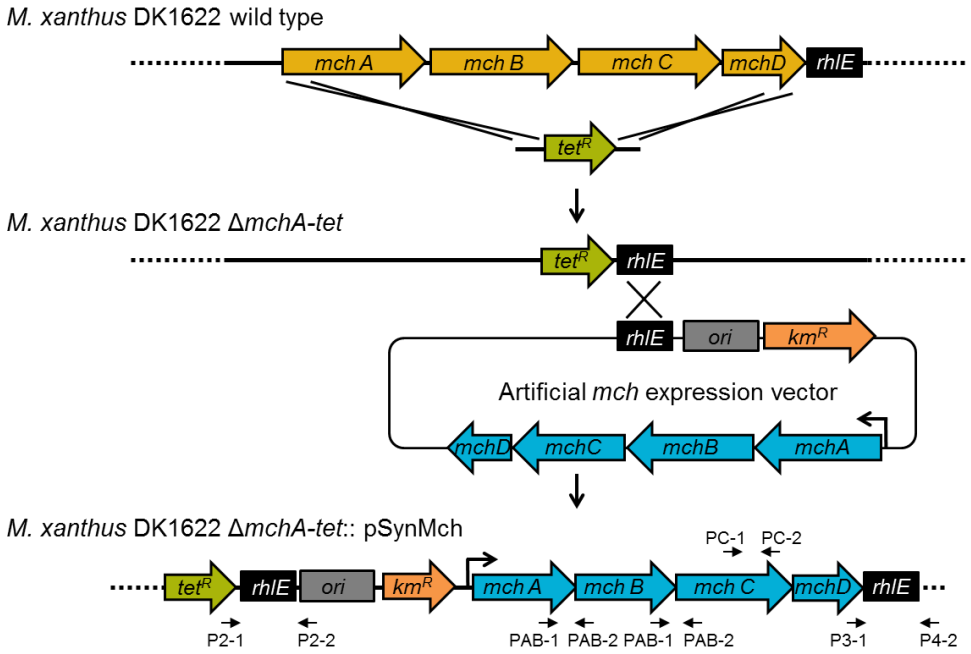

Fig. S3 Integration of artificial *mch* gene cluster into the chromosome of *M. xanthus* DK1622 *ΔmchA-tet*. The host *M. xanthus* DK1622 *ΔmchA-tet* was generated by deletion of the native A-type *mch* cluster with a tetracycline resistance gene (tet^R). The synthetic *mch* gene cluster on pSynbio2 vector was integrated downstream of the tet^R site by homologous recombination. The chromosomal integration of artificial *mch* clusters was verified by colony PCR. The positions of the primers (see Table S8) for colony PCR are illustrated.

Table S8 Oligonucleotides used in colony PCR.

Oligonucleotide	Sequence	Expected size (bp)
P2-1	CGGAGAACTGTGAATGCGC	1572
P2-2	GTTTCATTTGATGCTCGATG	

P3-1	CGCCGGACGCATGACTCAC	1563
P4-2	AGAGGCACTCCAGGCCTCTTA	
PAB-1	CGGCAGCCAGAGCTGGAGAA	880
PAB-2	TGGTGGACGGTCATCAGGAGG	
PBC-1	GGAGACGATTGAACGGCTGAACG	836
PBC-2	AAGGGCAGTGGCGTGGGTTG	
PC-1	GTGGAACCTCTACGGACCGACAG	857
PC-2	ACAGGGACACCAGCGGAAGC	

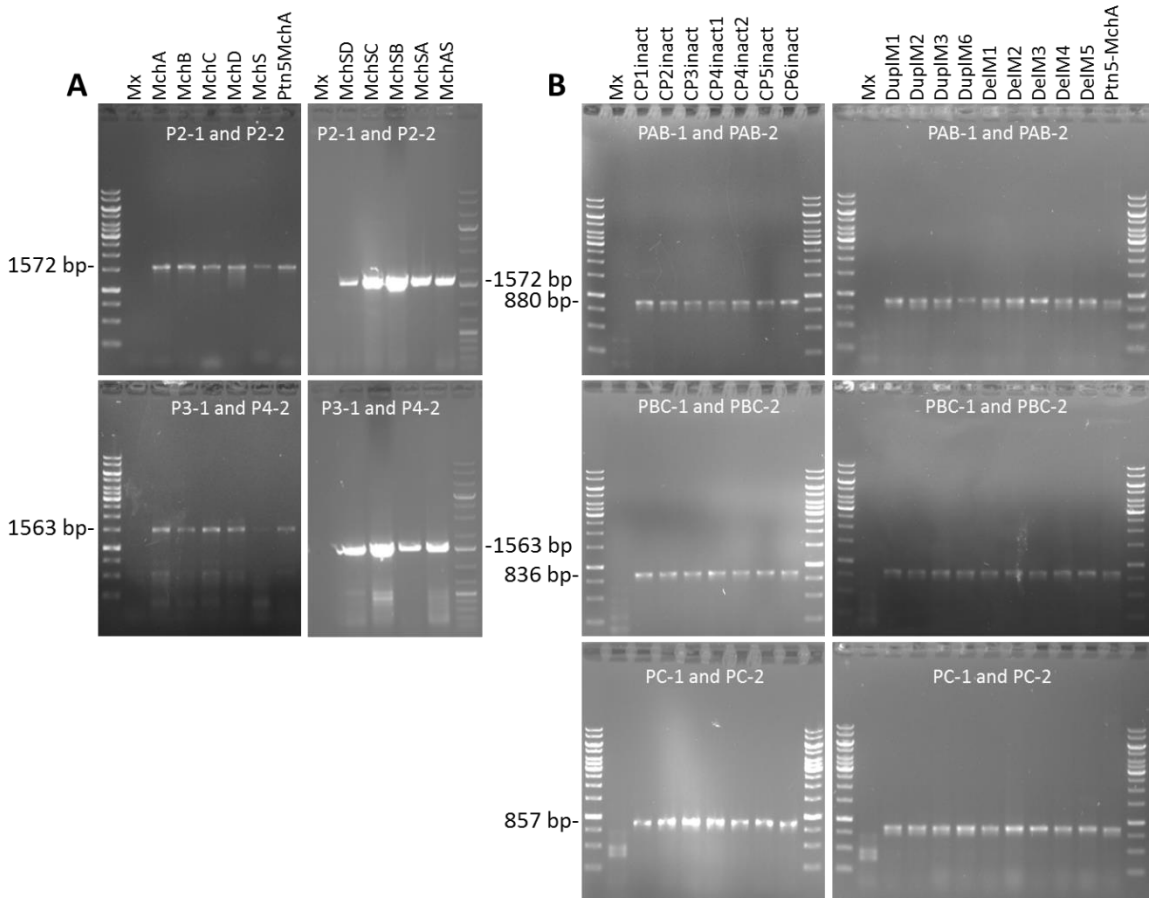

Fig. S4 Colony PCR analysis of *mch* cluster integration in *M. xanthus* mutants. (A) analysis of the integration of the native and hybrid *mch* clusters; (B) anlysis of the integration of the *mch* clusters with module engineering. The integrated *mch* gene clusters are shown on the top of figures; primer pairs used in the colony PCR are indicated in figures; the sizes of amplified fragments are illustrated. *M. xanthus* DK1622 *ΔmchA-tet* (Mx) served as negative control. MchA, *M. xanthus* DK1622 *ΔmchA-tet*::pSynMch2; Ptn5MchA, *M. xanthus* DK1622 *ΔmchA-tet*::pSynMch13; MchB, *M. xanthus* DK1622 *ΔmchA-tet*::pSynMch3; MchC, *M. xanthus* DK1622 *ΔmchA-tet*::pSynMch4; MchD, *M. xanthus* DK1622 *ΔmchA-tet*::pSynMch5; MchS, *M. xanthus* DK1622 *ΔmchA-tet*::pSynMch6; MchSD, *M. xanthus* DK1622 *ΔmchA-tet*::pSynMch12; MchSC, *M. xanthus* DK1622 *ΔmchA-tet*::pSynMch10; MchSB, *M. xanthus* DK1622 *ΔmchA-tet*::pSynMch11; MchSA, *M. xanthus* DK1622 *ΔmchA-tet*::pSynMch9; MchAS, *M. xanthus* DK1622 *ΔmchA-tet*::pSynMch8; CP1inact, *M. xanthus* DK1622 *ΔmchA-tet*::pSynMch17; CP2inact, *M. xanthus* DK1622 *ΔmchA-tet*::pSynMch18; CP3inact, *M. xanthus* DK1622 *ΔmchA-tet*::pSynMch19; CP4inact1, *M. xanthus* DK1622 *ΔmchA-tet*::pSynMch20; CP4inact2, *M. xanthus* DK1622 *ΔmchA-tet*::pSynMch21; CP5inact, *M. xanthus* DK1622 *ΔmchA-tet*::pSynMch22; CP6inact, *M. xanthus* DK1622 *ΔmchA-tet*::pSynMch23; DuplM1, *M. xanthus* DK1622 *ΔmchA-tet*::pSynMch25; DuplM2, *M. xanthus* DK1622 *ΔmchA-tet*::pSynMch26; DuplM3, *M. xanthus* DK1622 *ΔmchA-tet*::pSynMch27; DuplM6, *M. xanthus* DK1622 *ΔmchA-tet*::pSynMch28; DelM1, *M. xanthus* DK1622 *ΔmchA-tet*::pSynMch29; DelM2, *M. xanthus* DK1622 *ΔmchA-tet*::pSynMch30; DelM3, *M. xanthus* DK1622 *ΔmchA-tet*::pSynMch31; DelM4, *M. xanthus* DK1622 *ΔmchA-tet*::pSynMch32; DelM5, *M. xanthus* DK1622 *ΔmchA-tet*::pSynMch33.

4. Expression of artificial *mch* clusters in *M. xanthus* and production analysis

Myxochromide production analysis in the heterologous host was carried out on a 50 mL scale under routine cultivation conditions. Cells and Amberlite XAD-16 adsorber resin were harvested by centrifugation at 8,000 rpm for 10 min and subsequently extracted twice with 50 mL methanol and acetone (1:1). The extracts were evaporated to dryness, dissolved in methanol and subjected to UPLC-MS analysis using a Dionex Ultimate 3000 RSLC system coupled to a Bruker maXis 4G TOF mass spectrometer. Separation was performed using a Waters BEH C18, 100 × 2.1 mm, 1.7 µm d_p column. At a flow rate of 0.6 mL/min, the following gradient was applied (A: deionized water + 0.1% formic acid, B: acetonitrile + 0.1% formic acid): 0-0.5 min 5% B, 0.5-18.5 min 5-95% B, 18.5-20.5 min 95% B. Full scan mass spectra were acquired in positive ESI mode in a range from 150-2500 *m/z*.

4.1 Production of native myxochromides in *M. xanthus*

The constructs harboring synthetic *mch* clusters, pSynMch2 (A-tpye cluster), pSynMch3 (B-tpye cluster), pSynMch4 (C-tpye cluster), pSynMch5 (D-tpye cluster), pSynMch6 (S-tpye cluster) and pSynMch13 (A-tpye cluster controlled by *PTn5* promoter), were transferred into *M. xanthus* DK1622 *ΔmchA-tet*. Mutant strains were grown under routine conditions and the production of myxochromides was analyzed by UPLC-MS (Fig. S5).

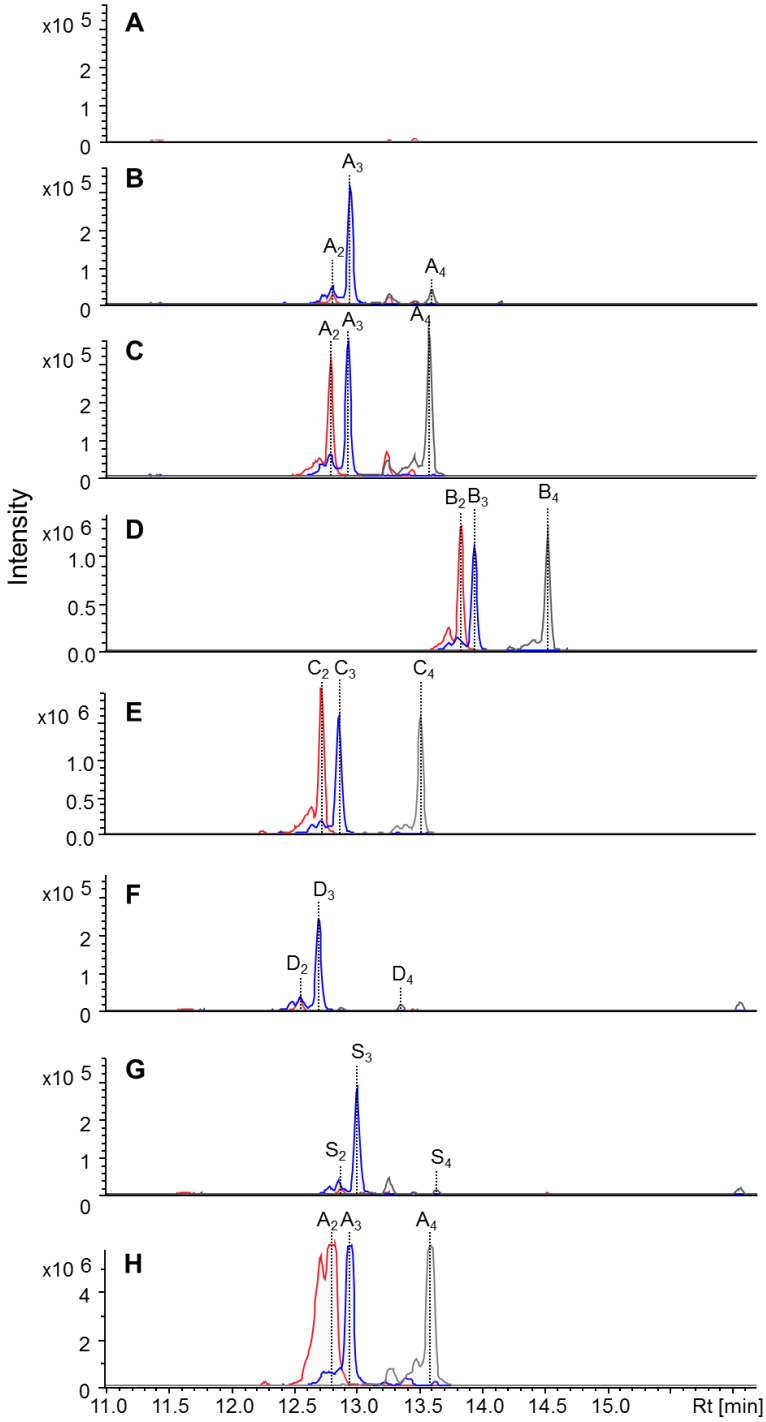

Fig. S5 UPLC-MS analysis of native myxochromide production in *M. xanthus*. Extracted ion chromatograms (EICs) for ±0.02 *m/z* corresponding to the $[M+H]^+$ ions of myxochromides are shown. **A**: No myxochromide production in *M. xanthus* DK1622 *ΔmchA-tet*. **B**: Detection of myxochromides A in *M. xanthus* DK1622 wild type; A_2 ($[M+H]^+$ = 834.47542), A_3 ($[M+H]^+$ = 846.47600) and A_4 ($[M+H]^+$ = 860.49223). **C**: Detection of myxochromides A in *M. xanthus* DK1622 *ΔmchA-tet::*pSynMch2; A_2 ($[M+H]^+$ = 834.47526), A_3 ($[M+H]^+$ = 847.47583), A_4 ($[M+H]^+$ = 860.49201). **D**: Detection of myxochromides B in *M. xanthus* DK1622 *ΔmchA-tet::*pSynMch3; B_2 ($[M+H]^+$ =947.56010), B_3 ($[M+H]^+$ = 959.56212), B_4 ($[M+H]^+$ = 973.57804). **E**: Detection of myxochromides C in *M. xanthus* DK1622 *ΔmchA-tet::*pSynMch4; C_2 ($[M+H]^+$ = 763.44022), C_3 ($[M+H]^+$ = 775.43935), C_4 ($[M+H]^+$ = 789.45619). **F**: Detection of myxochromides D in *M. xanthus* DK1622 *ΔmchA-tet::*pSynMch5; D_2 ($[M+H]^+$ = 737.42169), D_3 ($[M+H]^+$ = 749.42156), D_4 ($[M+H]^+$ = 763.43939). **G**: Detection of myxochromides S in *M. xanthus* DK1622 *ΔmchA-tet::*pSynMch6; S_2 ($[M+H]^+$ = 737.42423), S_3 ($[M+H]^+$ = 749.42284), S_4 ($[M+H]^+$ = 763.43604). **H**: Detection of myxochromides A in *M. xanthus* DK1622 *ΔmchA-tet::*pSynMch13; A_2 ($[M+H]^+$ = 834.47842), A_3 ($[M+H]^+$ = 846.47917) and A_4 ($[M+H]^+$ = 860.49366).

4.1.1 Estimation of myxochromide production yield

M. xanthus DK1622 wilde type and *M. xanthus* DK1622 Δ*mchA-tet* mutants harboring synthetic *mch* clusters were cultivated in 50 mL CTT medium for 3.5 and 4.5 days with adsorber resin Amberlite XAD-16. The cells and XAD-16 were collected by centrifugation and were extracted with 50 mL acetone and methonal (1:1). The dried extracts were dissolved in 500 µL MeOH. 1 and 2 µL of dilutions between 1:10 and 1:500 were injected on LC-UV/MS Thermo Scientific UltiMate 3000 coupled with Bruker amazon. Following HPLC conditions: Waters BEH C18 column (130 Å, 1.7 µm, 100 × 2.1 mm); eluent A: H_2O + 0.1% formic acid, eluent B: acetonitrile + 0.1% formic acid; flow rate: 0.6 mL/min; column temperature 45 °C; gradient: 0-0.5 min 5% B, 0.5-3.5 min 5-50% B, 3.5-18 min 50-60% B, 18-18.5 min 60-95%B, 18.5-20.5 min 95% B, 20.5-20.8 min 95-5% B and 20.8-22.5 min 5% B.

In order to estimate the production, the UV Peak at 420 nm was integrated using Data Analysis 4.2. The MS trace or MS/MS fragments were used to identify the corresponding UV peak before integration. Based on the UV peak areas of myxochromide standards, the concentrations of the myxochromides were calculated using OriginPro 2017 and Microsoft Excel 2010. The estimated yields of myxochromide representatives (myxochromide A_3, myxochromide B_2, myxochromide C_2, myxochromide D_3, myxochromide S_3, see Fig. S5) are shown in Fig. S6.

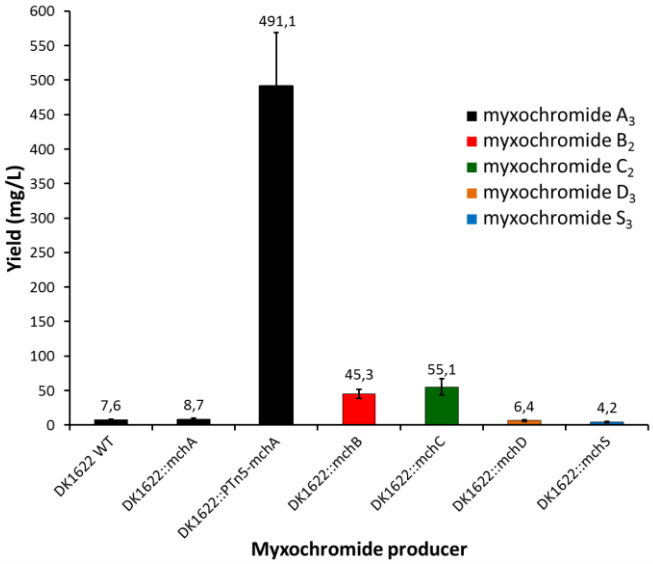

Fig. S6 Production yield of representative myxochromides in *M. xanthus* mutants. DK1622 WT, *M. xanthus* DK1622 wilde type; DK1622::mchA, *M. xanthus* DK1622 *ΔmchA-tet*::pSynMch2; DK1622::PTn5-mchA, *M. xanthus* DK1622 *ΔmchA-tet*::pSynMch13; DK1622::mchB, *M. xanthus* DK1622 *ΔmchA-tet*::pSynMch3; DK1622::mchC, *M. xanthus* DK1622 *ΔmchA-tet*::pSynMch4; DK1622::mchD, *M. xanthus* DK1622 *ΔmchA-tet*::pSynMch5; DK1622::mchS, *M. xanthus* DK1622 *ΔmchA-tet*::pSynMch6.

4.2 Heterologous expression of artificial hybrid *mch* clusters in *M. xanthus*

To heterologously produce novel hybrid myxochromides in *M. xanthus* DK1622, the expression constructs pSynMch8 (AS-type), pSynMch9 (SA-type), pSynMch10 (SC-type), pSynMch11 (SB-type) and pSynMch12 (SD-type) harboring the artificial hybrid *mch* clusters were subsequently transformed into the heterologous host *M. xanthus* DK1622 *ΔmchA-tet*. The production of hybrid myxochromides was checked by UPLC-MS (Fig. S7). Although the hybrid *mch* clusters were controlled by *PTn5* promoter, the production levels were comparable to the yield achieved by the artitifical *mchA* cluster controlled by the native promoter.

Myxochromides AS – novel engineered lipopentapeptides

Myxochromide derivatives with $[M+H]^+$ masses corresponding to the expected hybrid myxochromides AS_2, AS_3 and AS_4 (Fig. S7) were detected in the extracts of *M. xanthus* DK1622 *ΔmchA-tet::*pSynMch8. The most prominent derivative was AS_2 under the applied cultivation conditions, whereas derivatives AS_3 and AS_4 were produced in lower yields but at similar levels compared to each other (Fig. S7).

Myxochromides SA – novel engineered lipohexapeptides

Myxochromide derivatives with $[M+H]^+$ masses corresponding to the expected novel hybrid lipohexapeptides myxochromides SA_2, SA_3 and SA_4 (Fig. S7) were detected in the extracts of *M. xanthus* DK1622 *ΔmchA-tet::*pSynMch9. Compound SA_3 was found to be the major derivative under the applied cultivation conditions, whereas derivatives SA_2 and SA_4 were produced in significantly lower amounts (Fig. S7).

Myxochromides SB – novel engineered lipoheptapeptides

Myxochromide derivatives with $[M+H]^+$ masses corresponding to the assumed hybrid lipoheptapeptides myxochromides SB_2, SB_3 and SB_4 (Fig. S7) were detected in the extracts of *M. xanthus* DK1622 *ΔmchA-tet::*pSynMch11. The major derivative was SB_4 under the applied cultivation conditions followed by SB_3 and SB_2, which were produced in significantly lower amounts (Fig. S7).

Myxochromides SC – novel engineered lipopentapeptides

Myxochromide derivatives with $[M+H]^+$ masses corresponding to the expected novel lipopentapeptides myxochromides SC_2, SC_3 and SC_4 (Fig. S7) were detected in the extracts of *M. xanthus* DK1622 *ΔmchA-tet::*pSynMch10. The production profile was found to be highly similar to that of the myxochromide SB producing mutant strain (Fig. S7). Compound SC_4 was identified as most prominent derivative under the applied cultivation conditions, whereas derivatives SC_2 and SC_3 were produced as minor products.

Myxochromides SD – novel engineered lipopentapeptides

Myxochromide derivatives with $[M+H]^+$ masses corresponding to the expected hybrid myxochromides SD_2, SD_3 and SD_4 (Fig. S7) were detected in the extracts of *M. xanthus* DK1622 *ΔmchA-tet::*pSynMch12. In comparison to the other hybrid myxochromides, production of myxochromides SD was found to be significantly lower, and was also observed for several independent clones. The major derivative was SD_3 under the applied cultivation conditions and was roughly produced at similar levels as some minor compounds in the other extracts. Derivatives SD_2 and SD_4 were produced in even lower yields (Fig. S7).

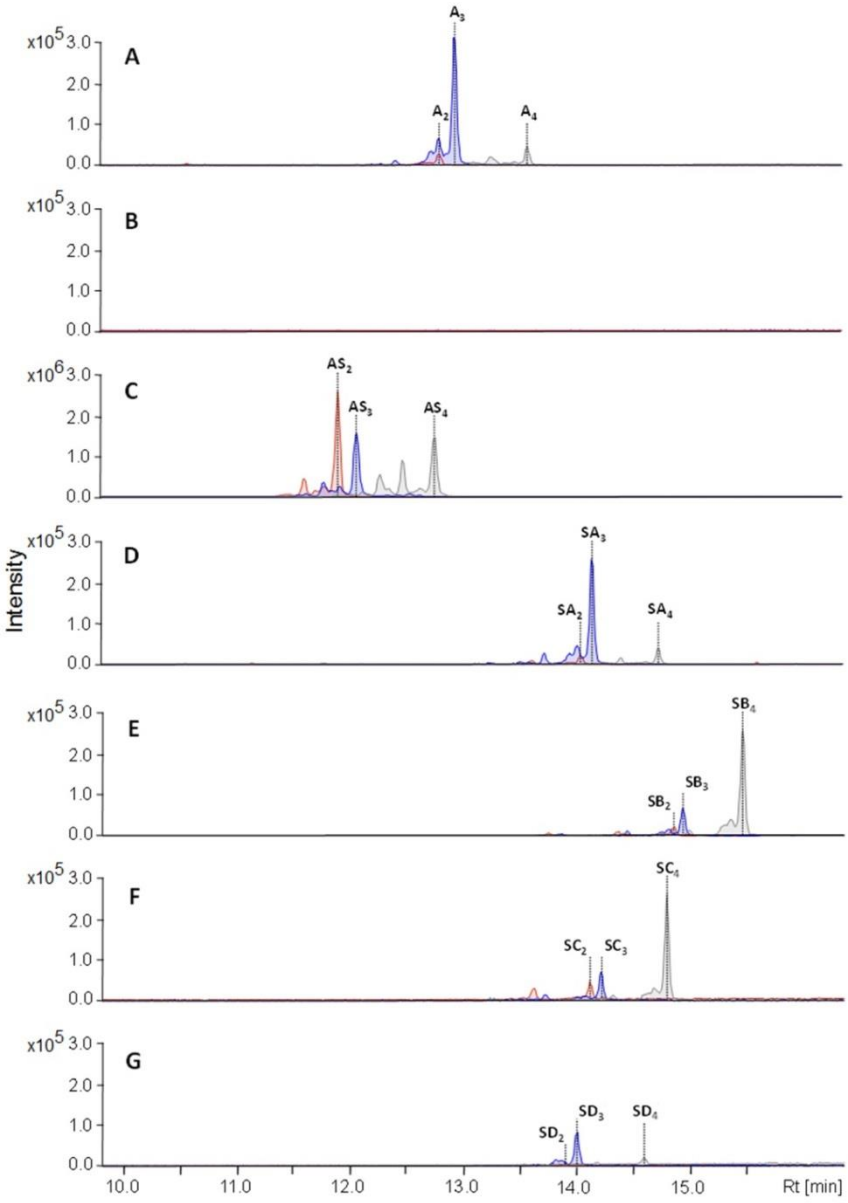

Fig. S7 UPLC-MS analysis of hybrid myxochromide production in myxobacterial mutant strains. Extracted ion chromatograms (EICs) for ±0.02 *m/z* corresponding to the $[M+H]^+$ ions of myxochromides are shown. **A**: Detection of myxochromides A in *M. xanthus* DK1622 wild type; A_2 ($[M+H]^+$ = 834.47655), A_3 ($[M+H]^+$ = 846.47655) and A_4 ($[M+H]^+$ = 860.49220). **B**: No myxochromide production in *M. xanthus* DK1622 *ΔmchA-tet*. **C**: Detection of myxochromides AS in *M. xanthus* DK1622 *ΔmchA-tet*::pSynMch8; AS_2 ($[M+H]^+$ = 695.37684), AS_3 ($[M+H]^+$ = 707.37684), AS_4 ($[M+H]^+$ = 721.39249). **D**: Detection of myxochromides SA in *M. xanthus* DK1622 *ΔmchA-tet*::pSynMch9; SA_2 ($[M+H]^+$ =876.52350), SA_3 ($[M+H]^+$ = 888.52350), SA_4 ($[M+H]^+$ = 902.53915). **E**: Detection of myxochromides SB in *M. xanthus* DK1622 *ΔmchA-tet*::pSynMch11; SB_2 ($[M+H]^+$ = 989.60757), SB_3 ($[M+H]^+$ = 1001.60757), SB_4 ($[M+H]^+$ = 1015.62322). **F**: Detection of myxochromides SC in *M. xanthus* DK1622 *ΔmchA-tet*::pSynMch10; SC_2 ($[M+H]^+$ = 805.48639), SC_3 ($[M+H]^+$ = 817.48639), SC_4 ($[M+H]^+$ = 831.50204). **G**: Detection of myxochromides SD in *M. xanthus* DK1622 *ΔmchA-tet*::pSynMch12; SD_2 ($[M+H]^+$ = 779.47074), SD_3 ($[M+H]^+$ = 791.47074), SD_4 ($[M+H]^+$ = 805.48639).

4.3 Heterologous expression of CP-mutated *mch* clusters in *M. xanthus*

In order to imitate the 'module-skipping' process observed in MchD and MchS pathways, we replaced the CP domains in the artificial A-type myxochromide pathway with CP-inactivated synthetic fragments. The expression constructs pSynMch17 (CP1 inactivated), pSynMch18 (CP2 inactivated), pSynMch19 (CP3 inactivated), pSynMch20 (CP4 inactivated, version 1), pSynMch21 (CP4 inactivated, version 2), pSynMch22

(CP5 inactivated), pSynMch23 (CP6 inactivated) and pSynMch24 (CP4 reactivated in S-type *mch* cluster) were transformed into *M. xanthus* DK1622 *ΔmchA-tet*. The production of myxochromides was detected by UPLC-MS. Myxochromides D were produced in *M. xanthus* DK1622 *ΔmchA-tet*::pSynMch20 and *M. xanthus* DK1622 *ΔmchA-tet*::pSynMch21, while the production of myxochromides was abolished in other mutants (Fig. S8).

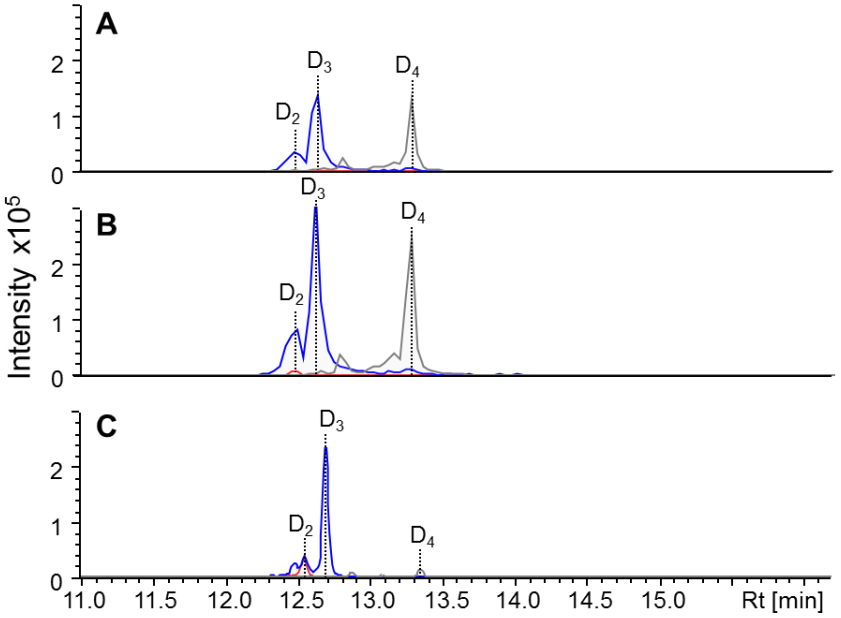

Fig. S8 HPLC-MS analysis of myxochromide production in CP4-mutants. Extracted ion chromatograms (EICs) for ±0.02 *m/z* corresponding to the $[M+H]^+$ ions of myxochromides D are shown. **A**, Detection of myxochromides D in *M. xanthus* DK1622 *ΔmchA-tet*::pSynMch20; D_2 ($[M+H]^+$ = 737.42474), D_3 ($[M+H]^+$ = 749.42289), D_4 ($[M+H]^+$ = 763.43882). **B**, Detection of myxochromides D in *M. xanthus* DK1622 *ΔmchA-tet*::pSynMch21; D_2 ($[M+H]^+$ = 737.42269), D_3 ($[M+H]^+$ = 749.42317), D_4 ($[M+H]^+$ = 763.43833). **C**, *M. xanthus* DK1622 *ΔmchA-tet*::pSynMch5 was set as reference; D_2 ($[M+H]^+$ = 737.42169), D_3 ($[M+H]^+$ = 749.42156), D_4 ($[M+H]^+$ = 763.43939).

4.4 Heterologous expression of *mch* clusters with duplication or deletion of biosynthetic domains

The duplicated A_n-CP_n-C_{n+1} encoding fragments of the A-type BGC were inserted to the previously identified fusion site (F-site) in A domains (Fig. S9).[3] In the cases of DuplM2 and DuplM6, A_2-CP_2-C_2 and A_6-CP_6-C_6 encoding fragments were inserted to the F-site in A_2 domain and A_6 domain, respectively. For the deletions of biosynthetic domains, the unit A_n-CP_n-C_{n+1} encoding fragments of A-type BGCs were deleted between two F-sites locate at the C-terminus of C_n and C_{n+1} domains (Fig. S10). In the case of DelM2, A_2-CP_2 encoding fragment was deleted between C_2 and E_2 encoding fragments.

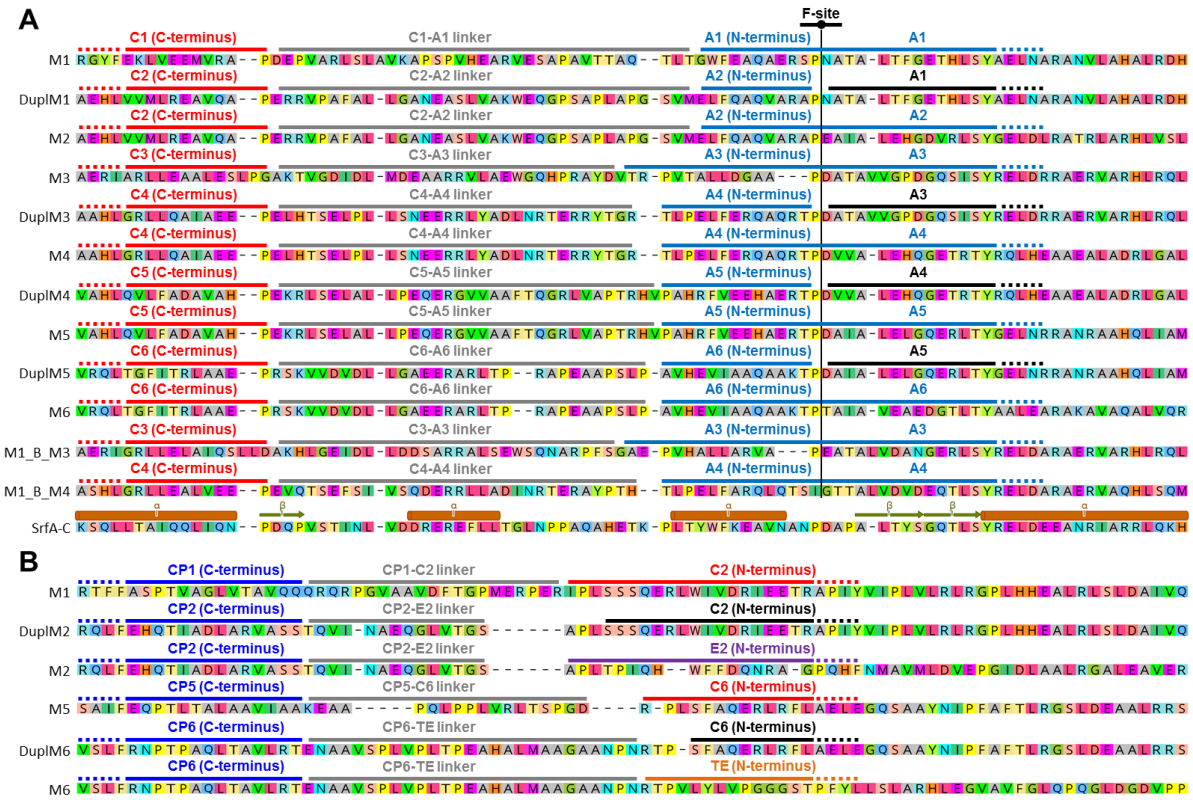

Fig. S9 Protein alignment of the fusion regions for the duplication of biosynthetic domains in the A-type pathway. The 'fusion site' (F-site) for the construction of DuplM1, DuplM3, DuplM4 and DuplM5 locates at the N-terminus of A domain. (A) alignment of the fusion regions in DuplM1, DuplM3, DuplM4 and DuplM5, in which domain set was duplicated in A_n-CP_n-C_{n+1} unit. (B) alignment of the fusion regions in DuplM2 and DuplM6, in which domain set was duplicated in C_n-A_n-CP_n unit. In DuplM2 and DuplM6 the fusion sites locate at the N-termimus of the E2 domain and the TE domain, respectively. The respective regions in the native modules (M1-M6) and the previously identified F-site in B-type pathway (M1_B_M4) after a proposed module duplication event serve as references.[3] The respective regions were aligned with the surfactin synthetase subunit SrfA-C (PDB:2VSQ).

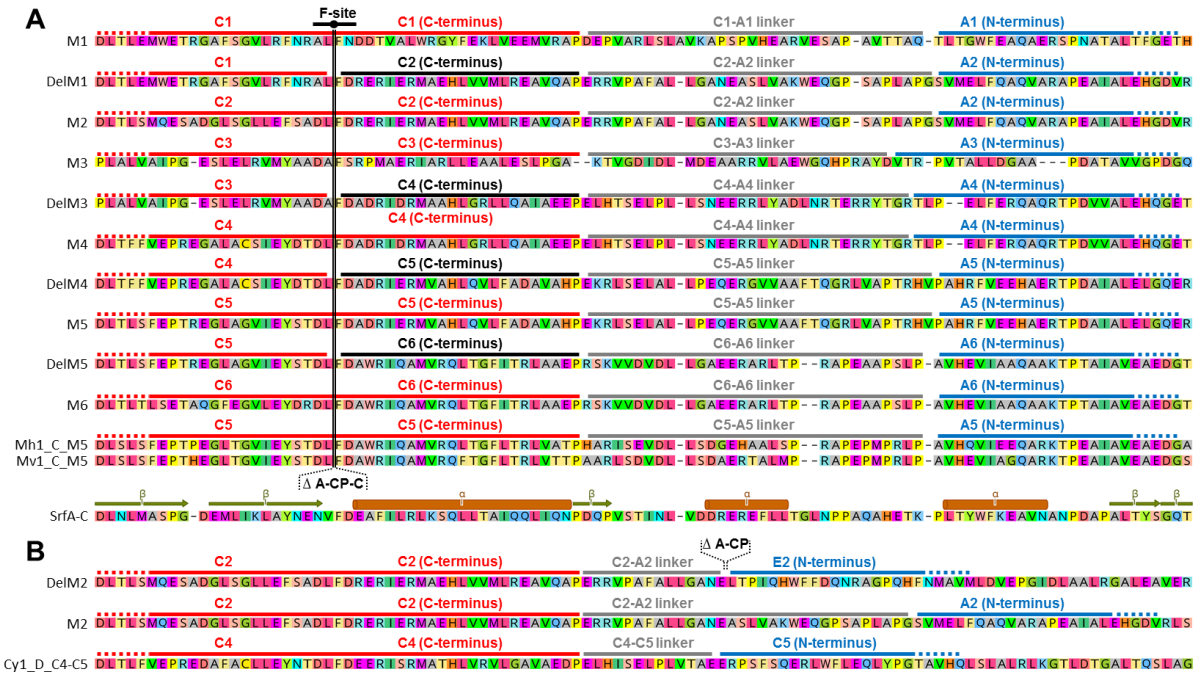

Fig. S10 Protein alignment of the fusion regions for the deletions of biosynthetic domains in the A-type pathway. (A) alignment of the fusion regions in DelM1, DelM3, DelM4 and DelM5, in which domain set was deleted in A_n-CP_n-C_{n+1} unit. The 'fusion site' (F-site) for the construction of the deletions locates at the C-terminus of C domain. (B) alignment of the fusion region in DelM2. Due to the E domain downstream of the CP_2 domain, the A_2-CP_2 unit was deleted in the case of DelM2 deletion, which is in analogy to the naturally occurred A_4-CP_4 deletion in D-type pathway (Cy1_D_C4-C5). The respective regions in the native modules (M1-M6) and the previously identified F-site in C-type pathways (Mh1_C_M5 and Mv1_C_M5) after a proposed module deletion event serve as references.[3] The respective regions were aligned with the surfactin synthetase subunit SrfA-C (PDB:2VSQ).

The constructs with DuplM1 (pSynMch25), DuplM2 (pSynMch26), DuplM3 (pSynMch27) and DuplM6 (pSynMch28), as well as constructs with DelM1 (pSynMch29), DelM2 (pSynMch30), DelM3 (pSynMch31), DelM4 (pSynMch32) and DelM5 (pSynMch33), were transferred into *M. xanthus* DK1622 Δ*mchA-tet*. The production of myxochromides was analyzed by UPLC-MS. *M. xanthus* DK1622 *ΔmchA-tet*::pSynMch25, *M. xanthus* DK1622 *ΔmchA-tet*::pSynMch26 and *M. xanthus* DK1622 *ΔmchA-tet*::pSynMch28 produced only myxochromide A. Six mutants of *M. xanthus* DK1622 *ΔmchA-tet*::pSynMch27 were checked, five of them produced myxochromide B as major products and myxochromide A as minor products, while one mutant (*M. xanthus* DK1622 *ΔmchA-tet*::pSynMch27-2#) produced only myxochromide A (Fig. S11). Production of myxochromide D was detected in *M. xanthus* DK1622 *ΔmchA-tet*::pSynMch32, and myxochromide C was detected in *M. xanthus* DK1622 *ΔmchA-tet*::pSynMch33 (Fig. S12).

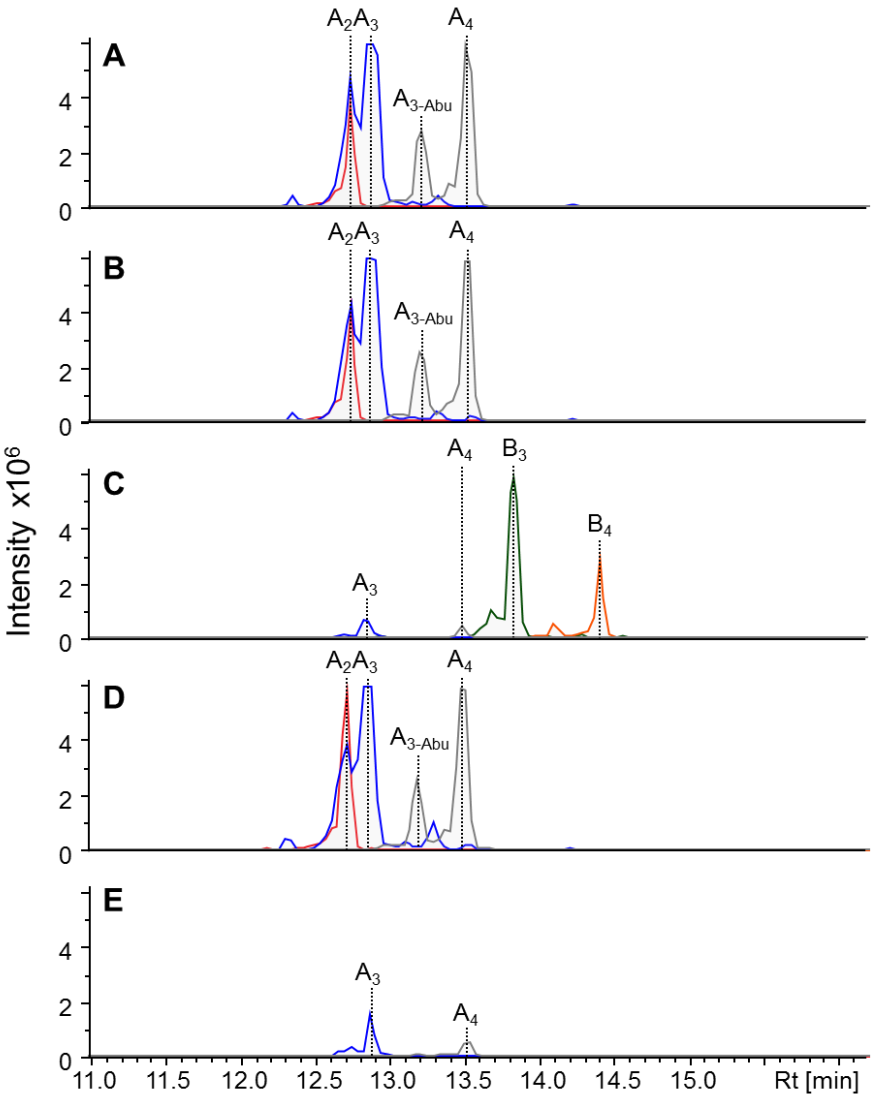

Fig. S11 HPLC-MS analysis of myxochromide production in *M. xanthus* mutants with module duplication. Extracted ion chromatograms (EICs) for ±0.02 *m/z* corresponding to the $[M+H]^+$ ions of myxochromides are shown. Myxochromides A were detected in *M. xanthus* DK1622 *ΔmchA-tet*::pSynMch25 (**A**), *M. xanthus* DK1622 *ΔmchA-tet*::pSynMch26 (**B**), *M. xanthus* DK1622 *ΔmchA-tet*::pSynMch27 (**C**), *M. xanthus* DK1622 *ΔmchA-tet*::pSynMch27-2# (**D**), *M. xanthus* DK1622 *ΔmchA-tet*::pSynMch28 (**E**). The MS/MS analysis of the peaks with *m/z* ($[M+H]^+$) of 860.49376 in **A**, **B** and **D** suggested them as A_3-Abu in which the Ala of myxochromide A is supposed to be replace by aminobutyric acid (Abu), similar with the case observed in previously reported myxochromide S-Abu.[3] Myxochromide B was detected in **C**; B_3 ($[M+H]^+$ = 959.56398) and B_4 ($[M+H]^+$ = 973.57673).

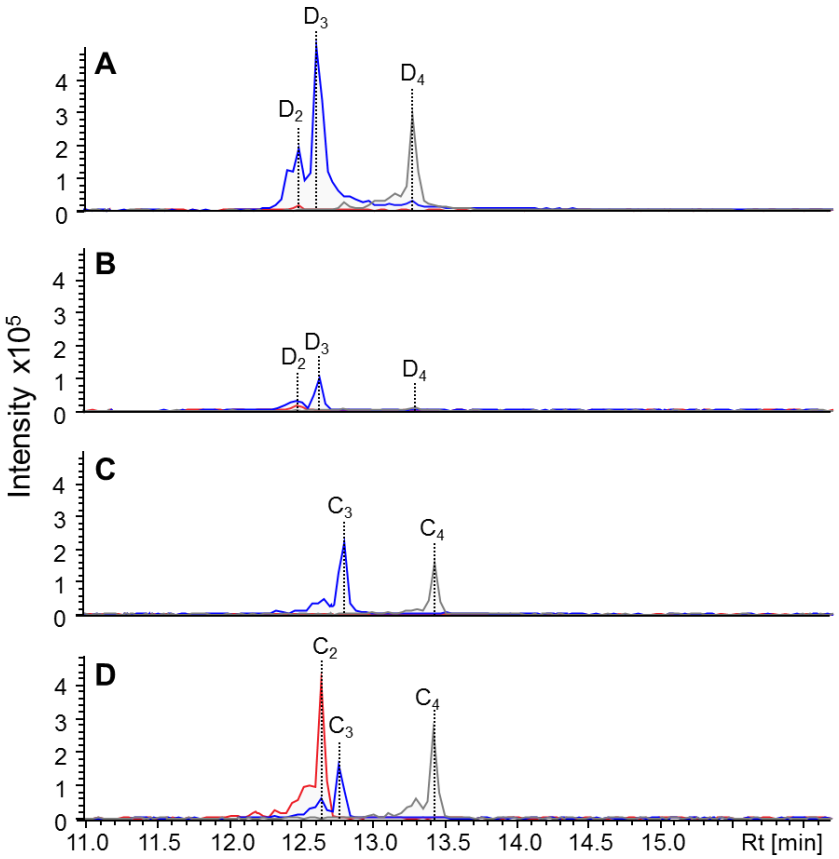

Fig. S12 HPLC-MS analysis of myxochromide production in *M. xanthus* mutants with module deletion. Extracted ion chromatograms (EICs) for ±0.02 *m/z* corresponding to the $[M+H]^+$ ions of myxochromides are shown. **A,** *M. xanthus* DK1622 *ΔmchA-tet*::pSynMch32; D_2 ($[M+H]^+$ = 737.42423), D_3 ($[M+H]^+$ = 749.42404), D_4 ($[M+H]^+$ = 763.43837). **B**, *M. xanthus* DK1622 *ΔmchA-tet*::pSynMch5 was set as reference; **C**, *M. xanthus* DK1622 *ΔmchA-tet*::pSynMch33; C_3 ($[M+H]^+$ = 775.43860), C_4 ($[M+H]^+$ = 789.45437). **D**, *M. xanthus* DK1622 *ΔmchA-tet*::pSynMch4 was set as reference.

4.5 Verification of *M. xanthus* mutants by Southern blot

The chromosomal integration of expression constructs harboring the duplicated encoding sequences of modules 1, 2, 3 and 6 (DuplM1, DuplM2, DuplM3 and DuplM6) in *M. xanthus* mutants was analyzed by Southern blot. *M. xanthus* DK1622 *ΔmchA-tet* served as negative control, *M. xanthus* DK1622 *ΔmchA-tet*::pSynMch2 (with one copy of A-type *mch* cluster) was set as reference, and pSynMch25~pSynMch28 served as positive control. Genomic DNA of *M. xanthus* DK1622 *ΔmchA-tet*, *M. xanthus* DK1622 *ΔmchA-tet*::pSynMch2, *M. xanthus* DK1622 *ΔmchA-tet*::pSynMch25 (DuplM1), *M. xanthus* DK1622 *ΔmchA-tet*::pSynMch26 (DuplM2), *M. xanthus* DK1622 *ΔmchA-tet*::pSynMch27 (DuplM3) and *M. xanthus* DK1622 *ΔmchA-tet*::pSynMch28 (DuplM6) were extracted by phenol/chloroform/isoamyl alcohol. Genomic DNA was digested with *Nco*I (DuplM1, DuplM3 and references) or *Eco47*III (DuplM2, DuplM6 and references) and was separated by 1% TAE agarose gel at 25 V for 20 hours. 1.5 ng DIG labeled DNA Molecular Weight Marker VII (Roch) was loaded in parallel. The gels were incubated twice in denaturation solution (0.5 M NaOH and 1.5 M NaCl) with 15 min for each time, and were then washed twice (15 min for each) in neutralizing solution (1 M Tris/HCl and 1.5 M NaCl, pH 7.5) after short wash in MilliQ water. After 30 min equilibration in 20× SSC buffer (3 M NaCl and 300 mM trisodium citrate, pH 7.0), DNA was transferred to a positively charged nylon membrane (Roche Applied Science) by capillary blotting for overnight. Afterwards, membranes were briefly soaked in 2× SSC buffer and baked at 80 °C for 2 hours. For hybridization, the membranes were prehybridized in hybridization buffer (DIG Easy hybrid granules, Roche) in roller bottle, gently shaking at 42 °C for 2 hours. DIG labelled nucleotide probes, generated by PCR DIG Labeling Mix (Roche) and targeting on each duplicated module, were then added to hybridization buffer to the final concentration 12 ng/mL and the hybridization was performed at 42 °C overnight. After two washes (5 min for each) in 2× SSC including 0.1% SDS and two washes (15 min for

each) in 0.5× SSC including 0.1% SDS at 68 °C, membranes were equilibrated in maleic acid buffer (150 mM NaCl, 100 mM maleic acid, pH 7.5) and then incubated in blocking solution (1% Blocking Reagent (Roche Applied Science) in maleic acid buffer) for 1 hour at room temperature with gentle shaking. Anti-digoxigenin-AP Fab fragments (Roche Applied Science) was then added to the blocking solution and gently shook at room temperature for 30 min. Membranes were subsequently washed twice in maleic acid buffer and detection buffer (100 mM NaCl, 100 mM Tris-HCl pH 9.5). Several drops of CDP-Star chemiluminescent substrate (Roche Applied Science) were added to the surface of the membranes and chemiluminescence was detected by documentation device.

As shown in Fig. S13, two copies of module 1, 2, 3 and 6 encoding fragments were detected in *M. xanthus* DK1622 *ΔmchA-tet*::pSynMch25 (DuplM1), *M. xanthus* DK1622 *ΔmchA-tet*::pSynMch26 (DuplM2), *M. xanthus* DK1622 *ΔmchA-tet*::pSynMch27 1# (DuplM3) and *M. xanthus* DK1622 *ΔmchA-tet*::pSynMch28 (DuplM6), respectively. In *M. xanthus* DK1622 *ΔmchA-tet*::pSynMch27 2# (DuplM3) producing only myxochromide A, only one copy of module 3 encoding fragment was detected.

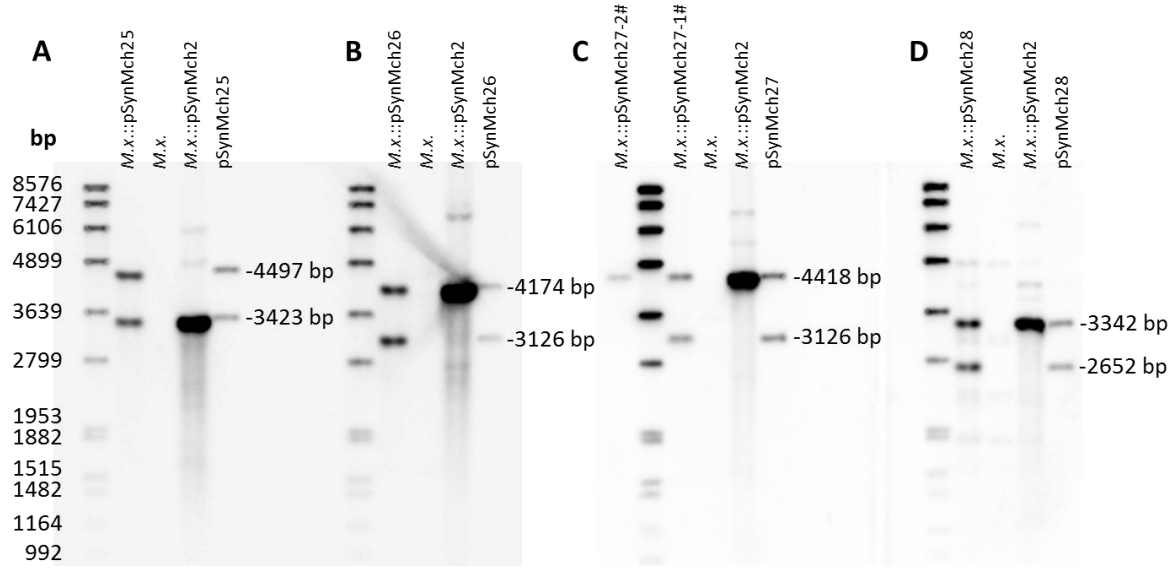

Fig. S13 Southern blot analysis of chromosomal integration of duplicated domain set-encoding fragments in *M. xanthus* mutants. Blotting results for the DuplM1 in *M. xanthus* DK1622 *ΔmchA-tet*::pSynMch25 (A), DuplM2 in *M. xanthus* DK1622 *ΔmchA-tet*::pSynMch26 (B), DuplM3 in *M. xanthus* DK1622 *ΔmchA-tet*::pSynMch27 (C) and DuplM6 in *M. xanthus* DK1622 *ΔmchA-tet*::pSynMch28 (D) are shown. The sizes of expected fragments are illustrated. *M.x.*, *M. xanthus* DK1622 *ΔmchA-tet* was set as negative control; *M.x.*::pSynMch2, reference with one copy of A-type *mch* cluster; pSynMch25~pSynMch28, plasmids were set as positive control.

5. Structure elucidation of novel hybrid myxochromides

5.1 Cultivation of heterologous production strains and isolation of myxochromides

The heterologous producers *M. xanthus* DK1622 *ΔmchA-tet*::pSynMch8 (Myxochromides AS) and DK1622 *ΔmchA-tet*::pSynMch11 (Myxochromides SC) were cultivated in 18 L (18× 1 L) and the producers *M. xanthus* DK1622 *ΔmchA-tet*::pSynMch14 (Myxochromides SA), *M. xanthus* DK1622 *ΔmchA-tet*::pSynMch15 (Myxochromides SB) and *M. xanthus* DK1622 *ΔmchA-tet*::pSynMch16 (Myxochromides SD) were cultivated in 9L (10× 1 L) CTT medium including 2% XAD-16 resin for 5-6 days at 30 °C and 180 rpm.
For the isolation of myxochromides AS, SA and SC, cells and XAD-16 Amberlite adsorber resin were harvested by centrifugation at 10,500 rpm and 4 °C for 15 min and were extracted five times with 1 L methanol and acetone (1:1). The organic solvents were removed under reduced pressure and the residues were extracted five times with 200 mL of ethyl acetate. After removal of the solvent, the crude extracts were dissolved in up to 10 mL methanol for subsequent separation via reverse phase HPLC. A Dionex UltiMate 3000 system equipped with a Luna 5 µm C18(2) 100Å column (250 × 10 mm, Phenomenex) was used. At constant flow rate (5.0 mL/min), the following multi-step gradient was applied for isolation of myxochromides AS_4 and SC_4 (A: deionized water, B: acetonitrile): 0-5 min 10-45% B, 5-30 min 45-65% B, 30-40 min 65-80% B, 40-41 min 80-10% B, 41-47 min 10% B. Myxochromide SC_4 was further purified by applying the following modified gradient (A: deionized water, B: acetonitrile): 0-5 min 10% B, 5-50 min 10-95% B, 50-55 min 95% B, 55-56 min 95-10% B, 56-60 min 10% B. For separation of myxochromide SA, the following modified gradient was applied (A: deionized water, B: acetonitrile): 0-4 min 5% B, 4-8 min 5-65%, 8-41 min 65-95% B, 41-43 min 95% B, 43-45 min 95-5% B, 45-51 min 5% B).
For the isolation of myxochromides SB and SD, cells and XAD adsorber resin were placed in a glass column over glass wool and a sand layer. Myxochromides were extracted by pouring 600 mL *n*-hexane, 900 mL dichloromethane, 600 mL ethyl acetate, 600 mL acetone and 600 mL methanol through the packed column. The fractions were concentrated and analyzed for target myxochromides via HPLC-MS. Separation was performed on a Dionex UltiMate 3000 system using a Waters BEH C18 (100 × 2.1 mm, 1.7 µm) column. At a flow rate of 0.6 mL/min, the following gradient was applied (A: deionized water + 0.1% formic acid, B: acetonitrile + 0.1% formic acid): 0-0.5 min 5% B, 0.5-18.5 min 5-95% B, 18.5-20.5 min 95% B. Full scan mass spectra were acquired in positive ESI mode in a range from 200-2000 *m/z*. After removal of the solvent, myxochromides were dissolved in 3 mL of methanol for further separation via reverse phase HPLC. Myxochromides SB were purified on a Dionex Ultimate 3000 system equipped with an Eclipse C8 column (250 × 10 mm, 4 µm) at constant flowrate (5 mL/min) by applying the following gradient (A: deionized water, B: acetonitrile): 0-2 min 5% B, 2-10 min 5-65% B, 10-30 min 65-70% B, 30-31 min 70-95% B, 31-34 min 95 %B, 34-35 min 95-5% B, 35-38 min 5% B. Myxochromides SD were purified on a Dionex UltiMate 3000 system equipped with a Jupiter column (250 × 10 mm, 4 µm) at constant flow rate (5 mL/min) by applying the following modified gradient (A: deionized water, B: acetonitrile): 0-2 min 5% B, 2-10 min 5-66% B, 10-30 min 66-68% B, 30-31 min 68-95% B, 31-34 min 95% B, 34-35 min 95-5% B, 35-38 min 5% B.
UV traces were recorded by a diode array detector (DAD) with specified wave lengths (210, 300 and 410 nm) with myxochromides showing good UV absorption at 410 nm. Retention times (R_t) and yields of the isolated compounds are shown in Table S9.

Table S9 Retention times and total amounts of hybrid myxochromides isolated in this study.

Mutant strain	Isolated compound	R_t [min]	Yield [mg]
DK1622 *ΔmchA-tet*::pSynMch8	Myxochromide AS_4	27.6	4.5
DK1622 *ΔmchA-tet*::pSynMch14	Myxochromide SA_3	18.9	7.2
DK1622 *ΔmchA-tet*::pSynMch15	Myxochromide SB_4	23.0	7.5
DK1622 *ΔmchA-tet*::pSynMch10	Myxochromide SC_4	39.2	0.5
DK1622 *ΔmchA-tet*::pSynMch16	Myxochromide SD_3	19.6	0.7

5.2 Structure elucidation of hybrid myxochromides

Structure elucidation of myxochromide AS_4, myxochromide SA_3, myxochromide SB_4, myxochromide SC_4 and myxochromide SD_3 was achieved using 1D and 2D NMR spectroscopy as well as HR-MS data. NMR spectra were acquired in CD_3OD at a Bruker Ascend 700 or 500 MHz spectrometer equipped with a 5 mm TXI cryoprobe. 1D ^1H and 2D ^1H–^1H COSY, HSQC, HMBC (and if necessary) ROESY spectra were recorded using standard pulse programs. Carbon chemical shifts were extracted from 2D NMR data. NMR spectroscopic data are listed in the Tables S11, S13, S15, S17 and S19. HR-ESI-MS data were obtained on a Bruker Maxis 4G mass spectrometer. Full scan mass spectra were acquired in a range from 150-2500 *m/z* in a positive mode. HR-ESI-MS data of hybrid myxochromides are shown in Table S10.

Table S10 HR-ESI-MS data of isolated hybrid myxochromides.

Compound	Formula	$[M+H]^+$ calc.	$[M+H]^+$ exp.	Δ*m/z* [ppm]
Myxochromide AS_4	$C_{38}H_{52}N_6O_8$	721.39194	721.39373	2.48
Myxochromide SA_3	$C_{48}H_{69}N_7O_9$	888.52295	888.52409	1.28
Myxochromide SB_4	$C_{54}H_{80}N_8O_{10}$	1015.62267	1015.62390	1.21
Myxochromide SC_4	$C_{46}H_{66}N_6O_8$	831.50149	831.50222	0.88
Myxochromide SD_3	$C_{44}H_{64}N_6O_8$	791.47019	791.47051	0.40

For the assignment of the absolute configuration, Marfey's method based on amino acid derivatization was applied.[7] 0.1-0.3 mg of pure compound was hydrolyzed with 37% HCl (0.2 mL) in a 1.5 mL glass vial for 3 days at 110 °C. The hydrolysate was evaporated to dryness and dissolved in H_2O (100 µL). A 50 µL aliquot was supplemented with 1N $NaHCO_3$ (20 µL) and 1% 1-fluoro-2,4-dinitrophenyl-5-*L*/*D*-leucinamide (*L*-FDLA or *D*-FDLA) solution in acetone (20 µL), and the mixtures were heated to 40 °C for 8 h at 700 rpm. After cooling down to room temperature, the solutions were neutralized with 2N HCl (20 µL), evaporated to dryness and the derivatized amino acids were dissolved in 300 µL acetonitrile. An amino acid standard mix (Sigma Aldrich) as well as *N*-Me-*L*-Threonine (Sigma Aldrich) were derivatized via the same procedure and all samples were analyzed on a Dionex Ultimate 3000 RSLC system coupled to a Bruker Maxis 4G mass spectrometer. Separation was performed using a Waters BEH C18, 100 × 2.1 mm, 1.7 µm d_p column. At a flow rate of 0.6 mL/min, the following gradient was applied (A: deionized water + 0.1% formic acid, B: acetonitrile + 0.1% formic acid): 0 min 5% B, 0-1 min 5-10% B, 1-15 min 10-35% B, 15-22 min 35-55% B, 22-25 min 55-80% B, 25-26 min 80% B, 26-26.5 min 80-5% B, 26.5-31 min 5% B. Full scan mass spectra were acquired in a range from 100-1000 *m/z*.

5.2.1 Structure of myxochromide AS_4

Structure elucidation of myxochromide AS_4 was achieved using 1D ^1H and 2D ^1H-^1H COSY, HSQC and HMBC spectra (Fig. S15). Carbon chemical shifts were extracted from 2D NMR data. NMR spectroscopic data are listed in Table S11. The ^1H NMR spectrum exhibited signals corresponding to five α-CH protons (δ_H 3.8-5.6), four CH_3 groups (δ_H 1.3-1.7) and two CH_2 groups (δ_H 2.0-2.3) together with a *N*-Me group (δ_H 3.29, 3H, s). Moreover, a number of downfield signals belonging to the unsaturated polyketide side chain (δ_H 5.8-7.3) and a CH_3 signal (δ_H 1.04, 3H, t) were observed. 2D NMR data revealed the presence *N*-Me-threonine, glutamine, alanine and a polyene side chain. Amino acid sequence was established by means of key HMBC correlations and final structure was elucidated as shown in Fig. S14. For the assignment of the absolute configuration of myxochromide AS_4, hydrolysis and Marfey analysis of the obtained amino acids,[7] was applied as described above. The chromatograms obtained from HPLC-MS analysis are illustrated in Fig. S16 and stereochemical assignments are illustrated in Table S12. Comparison of the retention times and masses of derivatized standard amino acids and the hydrolyzed lipopeptide revealed that all amino acids of the myxochromide AS_4 peptide core show *L*-configuration, while glutamine was converted to glutamic acid during hydrolysis. This correlates with the assumption that in the underlying hybrid pathway, the condensation domain of module 3 specifically

processes the *L*-configured aminoacyl donor ($^{L}C_{L}$ domain), although the presence of an epimerization domain in module 2 of the assembly line points to the incorporation of *D*-Ala into this position of the peptide core.

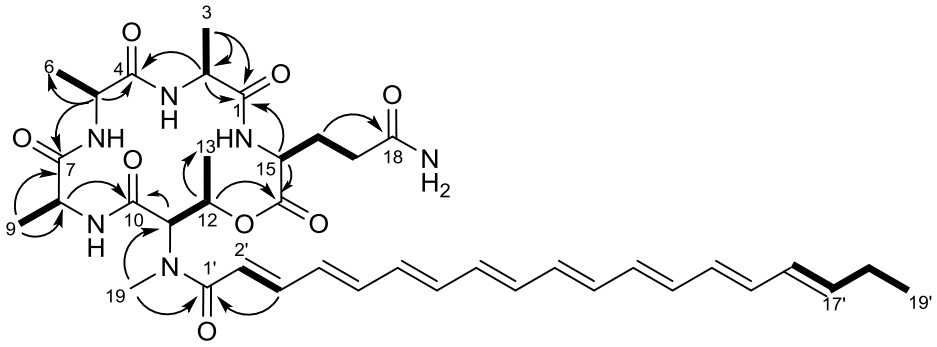

Fig. S14 Structure of myxochromide AS_4 showing selected COSY (bold line) and key HMBC (arrow) correlations.

Table S11 NMR spectroscopic data of myxochromide AS_4.

Moiety			**Position**	**δ_C[a]**	**δ_H[b] (*J* in Hz)**	**HMBC[c]**
L-Ala (1)			1	173.2		
			2	53.0	3.77, *q* (7.3)	1, 3, 4
			3	15.3	1.65, *d* (7.3)	1, 2
L-Ala (2)			4	173.7		
			5	51.6	3.82, *q* (7.0)	4, 6,7
			6	14.9	1.39, *d* (7.0)	4, 5
L-Ala (3)			7	176.6		
			8	51.1	4.03, *q* (7.3)	7, 9,10
			9	16.1	1.32, *m*	7, 8
N-Me-*L*-Thr	10	171.1				
	11	59.5	5.55, *d* (4.2)	1',10, 12, 19		
	12	74.0	5.46, *m*	13, 14		
	13	16.5	1.26, *d* (6.5)	11, 12		
	19	35.0	3.27, *s*	1', 11		
L-Gln	14	170.9				
	15	51.9	4.67, *dd* (3.2, 9.6)	1, 14, 16, 17		
	16a	27.8	1.93, *m*	15, 17, 18		
	16b		2.04, *m*			
	17a	31.9	2.26, *m*	14, 16		
	17b		2.32, *m*			
	18	178.2				
Side chain	1'	170.6				
	2'	119.7	6.57, *d* (14.6)	1'		
	3'	145.2	7.29, *dd* (11.4, 14.6)	1', 2', 5'		
	4'	138.4	6.52, *m*			
	5'	141.8	6.69, *m*			
	6'-14'	*d*	*d*			

15'	135.1	6.24, *m*	
16'	130.9	6.12, *m*	15', 18'
17'	138.1	5.79, *m*	15', 18', 19'
18'	26.7	2.14, *m*	16', 17', 19'
19'	13.7	1.02, *t* (7.2)	18'

[a] acquired at 125 MHz and assigned from 2D NMR spectra, referenced to solvent signal CD_3OD at δ 49.15 ppm.
[b] acquired at 500 MHz, referenced to solvent signal CD_3OD at δ 3.31 ppm.
[c] proton showing HMBC correlations to indicated carbons.
[d] overlapped signals.

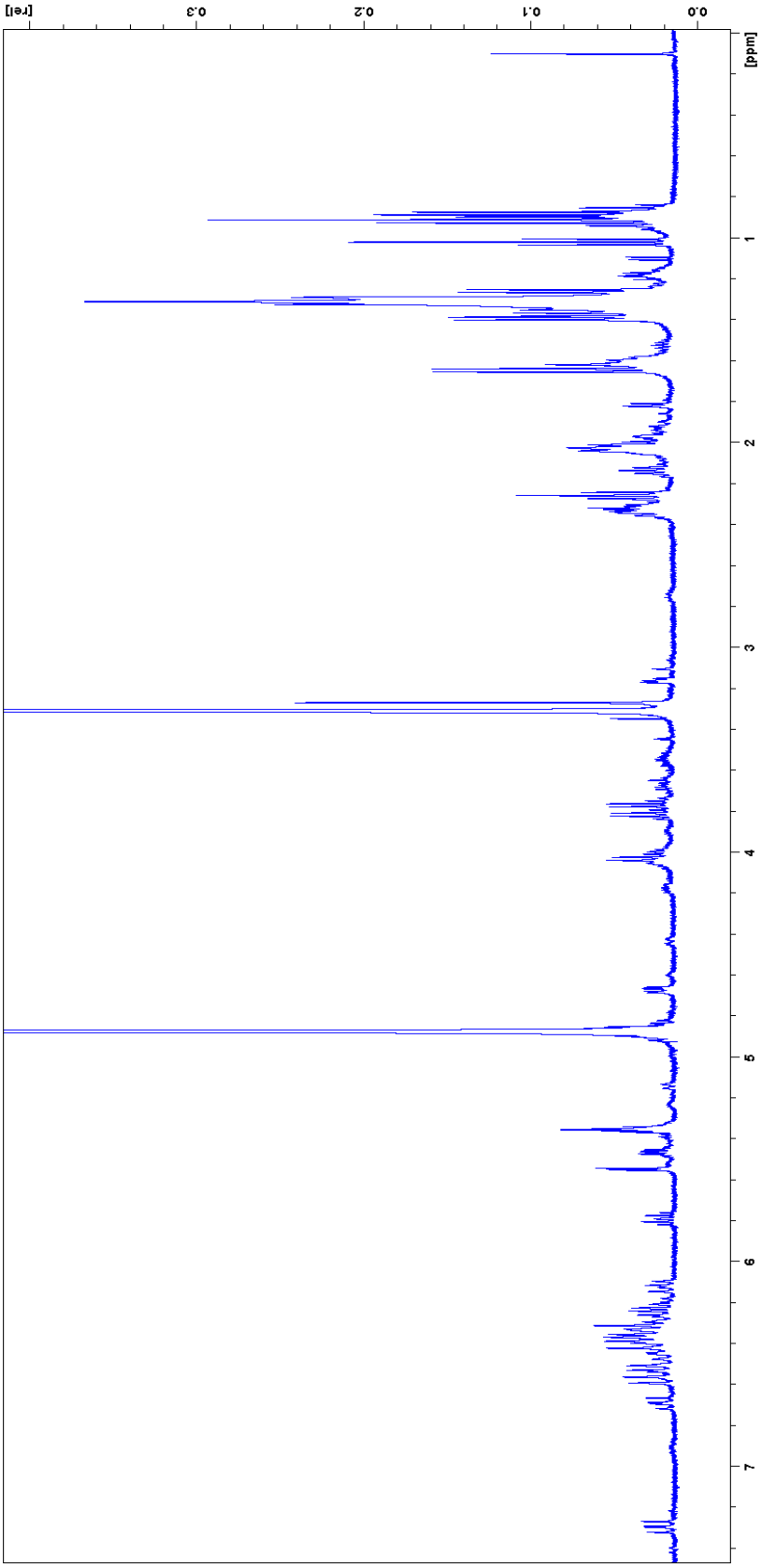

^{1}H-NMR spectrum of myxochromide AS_4 in CD_3OD (500 MHz)

Fig. S15 ***(continued on next page)***

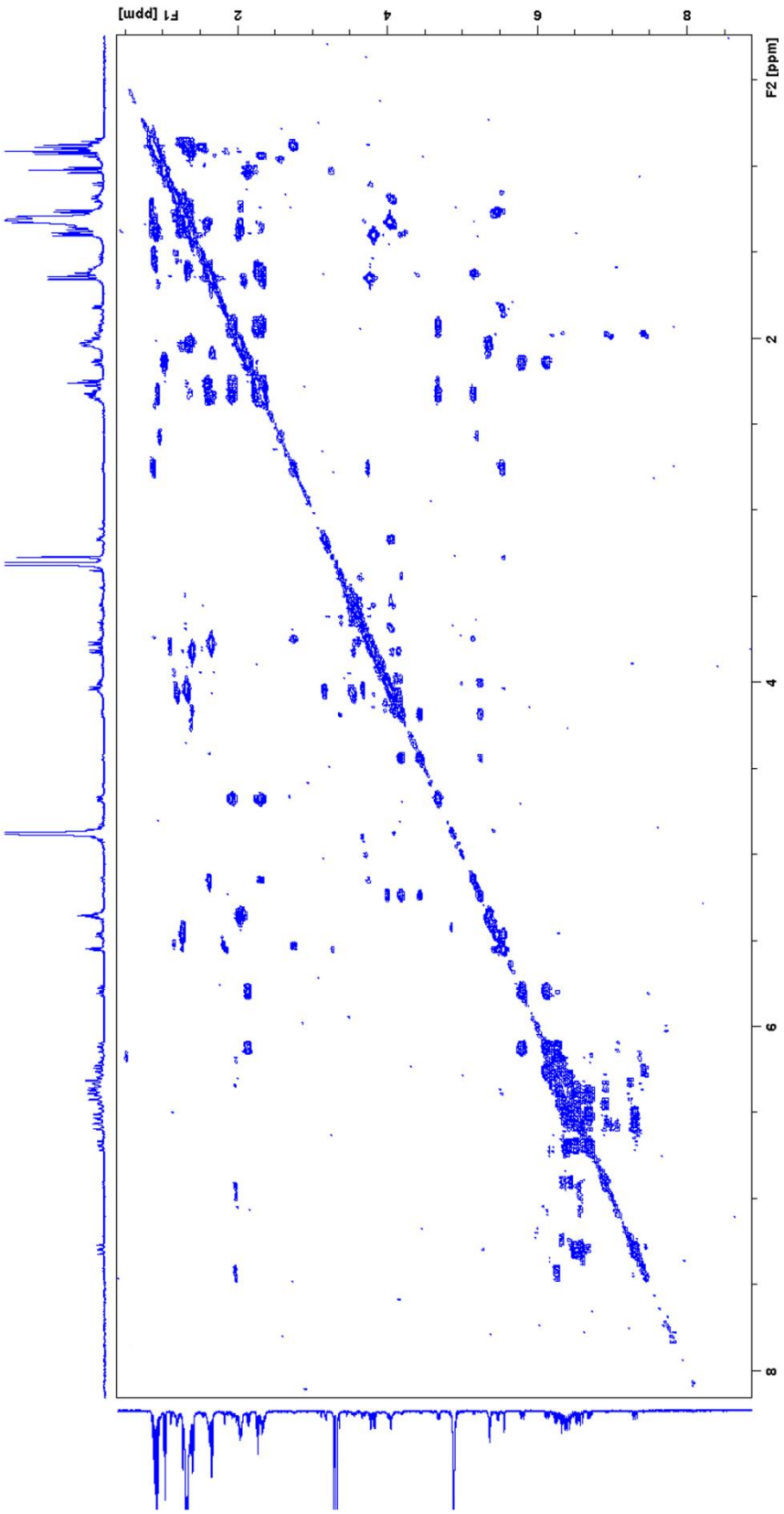

^{1}H-^{1}H COSY spectrum of myxochromide AS_4 in CD_3OD (500 MHz)

Fig. S15 ***(continued on next page)***

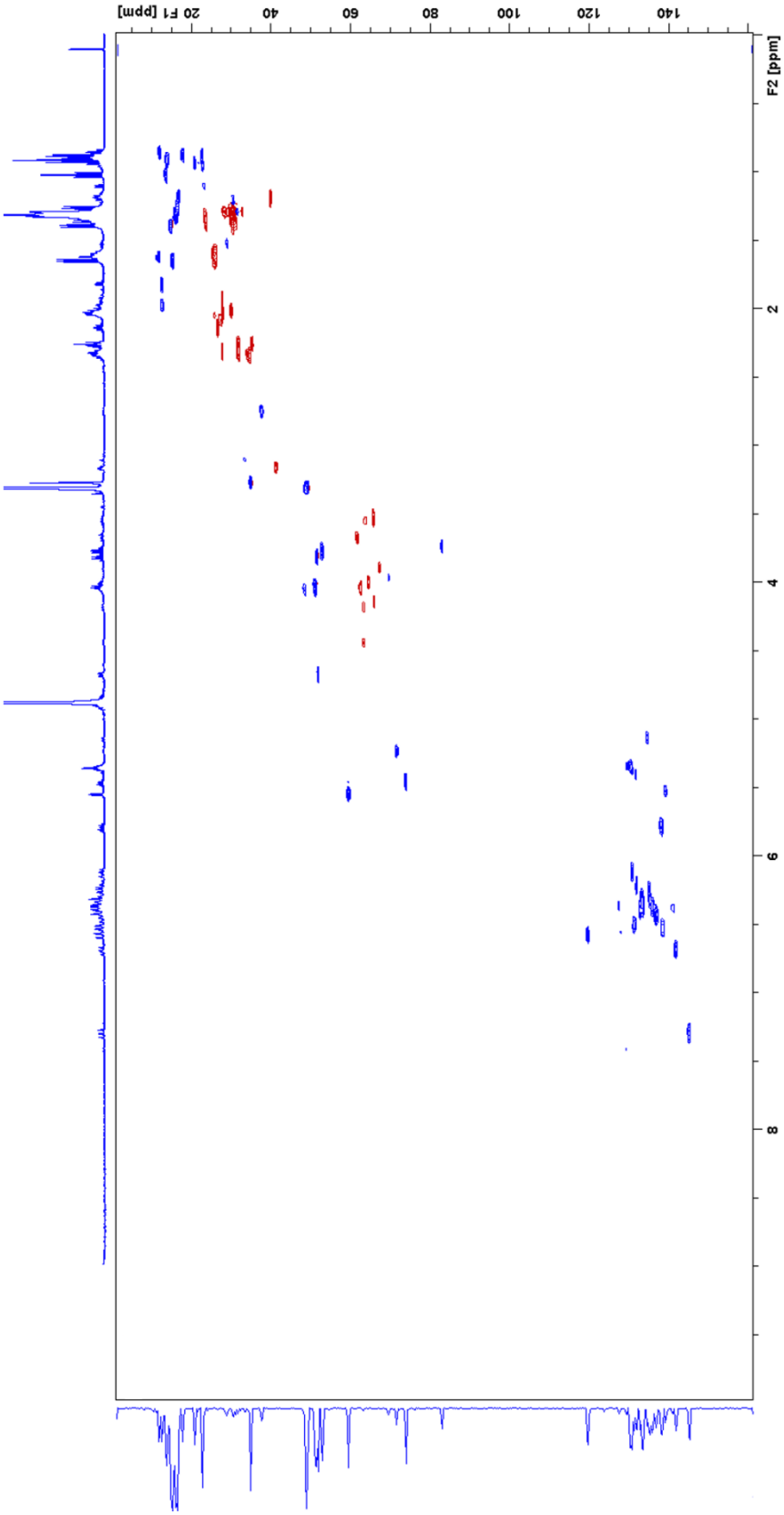

HSQC spectrum of myxochromide AS_4 in CD_3OD (500 MHz)

Fig. S15 ***(continued on next page)***

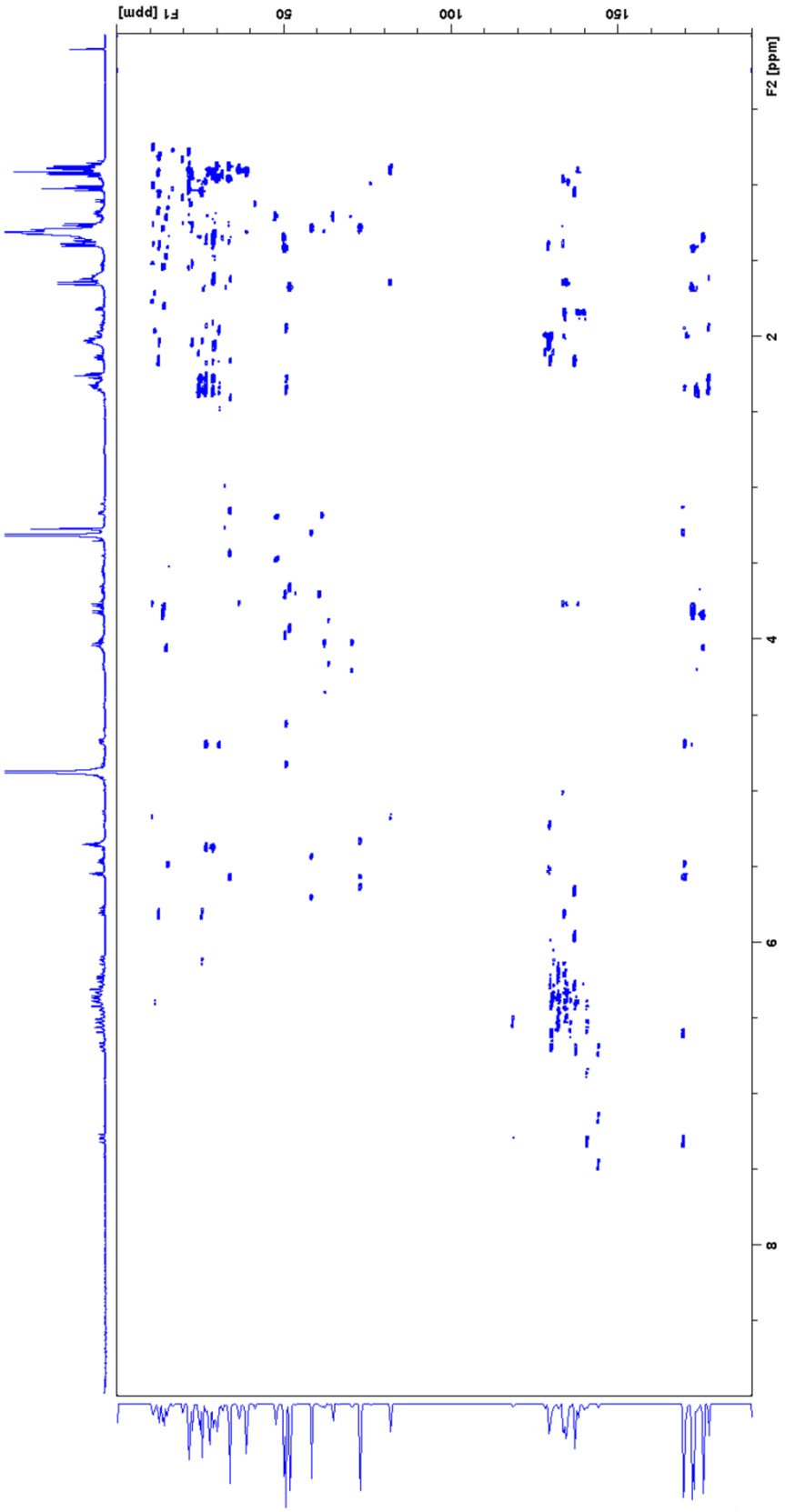

HMBC spectrum of myxochromide AS_4 in CD_3OD (500 MHz)

Fig. S15 NMR spectra of myxochromide AS_4.

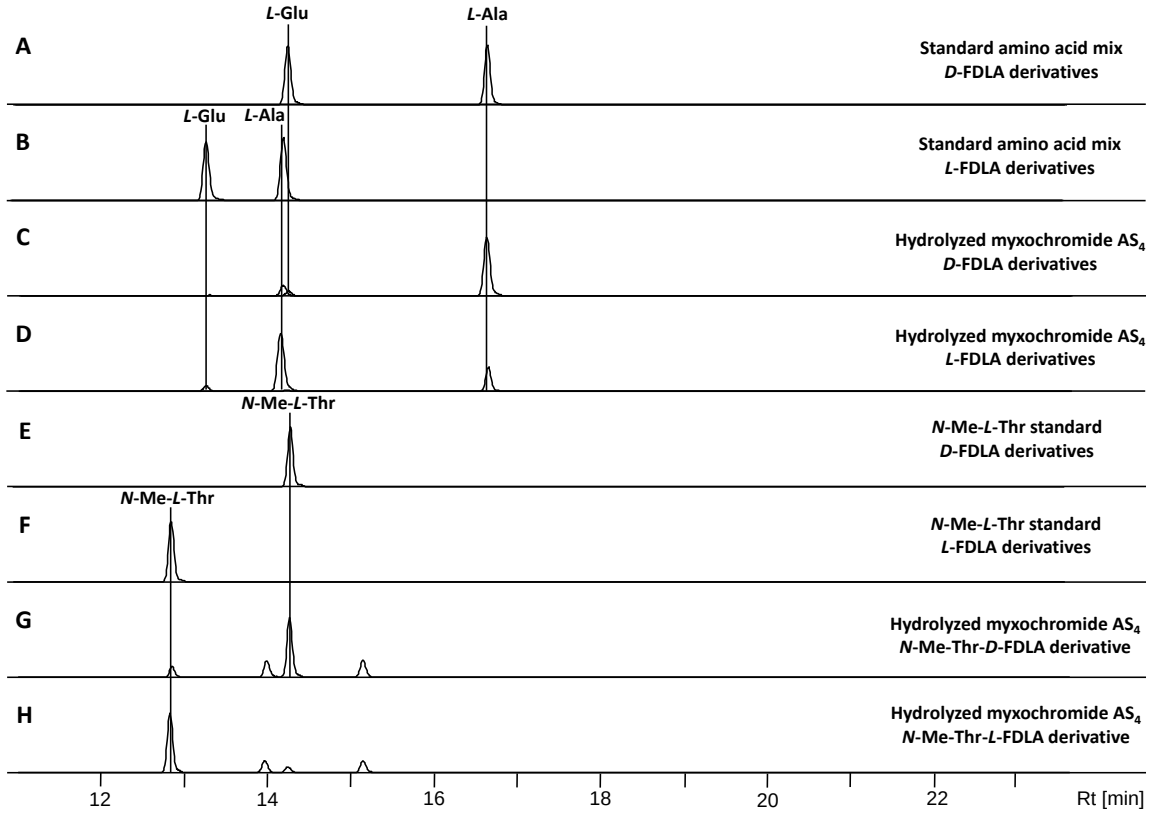

Fig. S16 Analysis of the absolute configuration of myxochromide AS_4. Extracted ion chromatograms (EIC) for ±0.05 *m/z* corresponding to the $[M+H]^+$ ions of derivatized amino acids, which are present in the peptide scaffold, are shown. **A**: Standard amino acid mix derivatized with *D*-FDLA reagent. **B**: Standard amino acid mix derivatized with *L*-FDLA reagent. **C**: Hydrolyzed myxochromide AS_4 derivatized with *D*-FDLA reagent. **D**: Hydrolyzed myxochromide AS_4 derivatized with *L*-FDLA reagent. **E**: Standard solution of *N*-Me-*L*-threonine derivatized with *D*-FDLA. **F**: Standard solution of *N*-Me-*L*-threonine derivatized with *L*-FDLA. **G**: Same sample as in **C** analyzed for the *N*-Me-*L*-threonine *D*-FDLA derivative. **H**: Same sample as in **D** analyzed for the *N*-Me-*L*-threonine *L*-FDLA derivative.

Table S12 Analytical data of detected amino acid derivatives and assignment of the absolute configuration of the amino acids in myxochromide AS_4.

aa-FDLA derivative	*L*-aa standards		Peptide hydrolysate		Assigned configuration
	R_t [min]	*m/z* $[M+H]^+$	R_t [min]	*m/z* $[M+H]^+$	
Glu-*D*-FDLA	14.3	442.1578	14.3	442.1563	**L**
Glu-*L*-FDLA	13.3	442.1579	13.3	442.1574	
Ala-*D*-FDLA	16.7	384.1520	16.7	384.1517	**L**
Ala-*L*-FDLA	14.3	384.1524	14.3	384.1518	
Ala-*D*-FDLA	16.7	384.1520	16.7	384.1517	**L**
Ala-*L*-FDLA	14.3	384.1524	14.3	384.1518	
Ala-*D*-FDLA	16.7	384.1520	16.7	384.1517	**L**
Ala-*L*-FDLA	14.3	384.1524	14.3	384.1518	
N-Me-Thr-*D*-FDLA	14.4	428.1782	14.3	428.1774	**L**
N-Me-Thr-*L*-FDLA	12.9	428.1786	12.8	428.1776	

5.2.2 Structure of myxochromide SA_3

Structure elucidation of myxochromide SA_3 was achieved using 1D ^1H and 2D ^1H-^1H COSY, HSQC and HMBC spectra (Fig. S18). Carbon chemical shifts were extracted from 2D NMR data. NMR spectroscopic data are listed in Table S13. The COSY spectrum supported by HSQC and HMBC data showed presence of spin systems corresponding to *N*-Me-threonine, glutamine, alanine, proline and leucine residues as well as a polyene side chain. Amino acid sequence was established by means of key HMBC correlations and final structure was elucidated as shown in Fig. S17. For the assignment of the absolute configuration of myxochromide SA_3, Marfey analysis of the obtained amino acids[7] was applied as described above. The chromatograms obtained from HPLC-MS analysis are illustrated in Fig. S19 and stereochemical assignments are illustrated in Table S14. Comparison of the retention times and *m/z* values of derivatized standard amino acids and the hydrolyzed lipopeptide revealed the presence of a *D*-configured leucine residue (C16) in myxochromide SA_3. The amino acids alanine (C2), proline (C5), another leucine (C10), *N*-Me-threonine (C22) and glutamine (C26), which was converted to glutamic acid during hydrolysis, were found to be *L*-configured. These findings demonstrate that the epimerization domain of module 2 in the underlying hybrid assembly line is not specific for alanine, but also accepts the more bulky leucine residue. The downstream condensation domain from module 3 originating from the A-type *mch* pathway is obviously a ^DC_L-type domain, thereby processing the *D*-configured dipeptide intermediate.

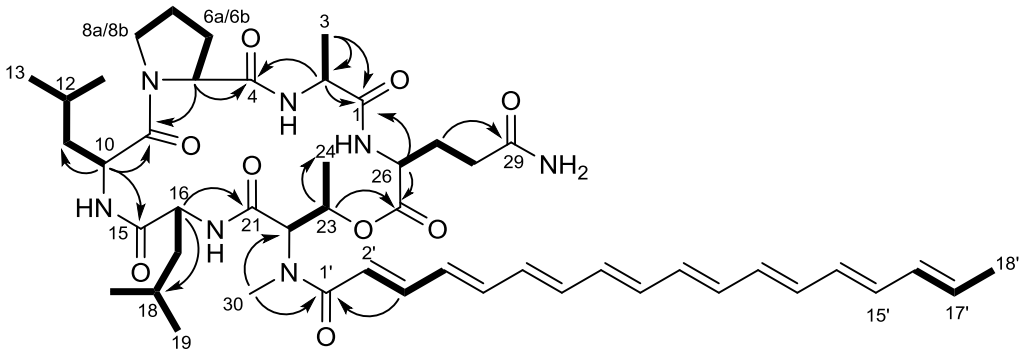

Fig. S17 Structure of myxochromide SA_3 showing selected COSY (bold line) and key HMBC (arrow) correlations.

Table S13 NMR spectroscopic data of myxochromide SA_3.

Moiety	Position	$\delta_C{}^a$	$\delta_H{}^b$ (*J* in Hz)	HMBC[c]
L-Ala	1	172.9		
	2	52.1	3.84, *q* (7.3)	1, 3, 4
	3	15.8	1.56, *d* (7.3)	1, 2
L-Pro	4	174.3		
	5	63.5	4.00, *dd* (9.6, 6.9)	4, 6, 9
	6a	29.8	1.89, *m*	5, 7
	6b		2.24, *m*	5, 7
	7a	26.4	2.02, *m*	6, 8
	7b		2.16, *m*	6, 8
	8a	47.8	3.55, *m*	7
	8b		3.74, *m*	7
L-Leu	9	172.0		
	10	52.1	4.40, *m*	9, 11, 12, 15
	11a	38.0	1.51, *m*	10

	11b		1.56, *m*	10
	12	25.8	1.53, *m*	10, 11, 13, 14
	13	23.4	0.98, *d* (6.9)	11, 12, 14
	14	23.4	0.98, *d* (6.9)	13
D-Leu	15	174.8		
	16	51.7	4.78, *t* (7.5)	15, 18, 21
	17a	40.4	1.49, *m*	18, 19, 20
	17b		1.57, *m*	18, 19, 20
	18	25.9	1.52, *m*	
	19	22.6	0.94, *m*	20
	20	22.6	0.94, *m*	19
N-Me-*L*-Thr	21	169.0		
	22	60.7	5.57, *d* (3.3)	1', 21, 23
	23	72.2	5.73, *m*	24, 25
	24	16.3	1.09, *d* (6.6)	21, 22
	30	35.2	3.21, *s*	1', 22
L-Gln	25	171.5		
	26	54.0	4.51, *dd* (8.4, 8.1)	1, 25, 27, 28
	27a	28.8	1.80, *m*	29
	27b		2.34, *m*	29
	28a	32.1	2.23, *m*	29
	28b		2.32, *m*	29
	29	177.2		
Side chain	1'	170.9		
	2'	120.0	6.60, *d* (14.7)	1'
	3'	144.8	7.35, *dd* (14.7, 11.5)	1'
	4'	131.3	6.49, *m*	
	5'-15'	[d]	[d]	[d]
	16'	133.1	6.14, *m*	
	17'	131.1	5.75, *m*	18'
	18'	18.2	1.78, *d* (6.6)	17'

[a] acquired at 125 MHz and assigned from 2D NMR spectra, referenced to solvent signal CD_3OD at δ 49.15 ppm.
[b] acquired at 500 MHz, referenced to solvent signal CD_3OD at δ 3.31 ppm.
[c] proton showing HMBC correlations to indicated carbons.
[d] overlapped signals.

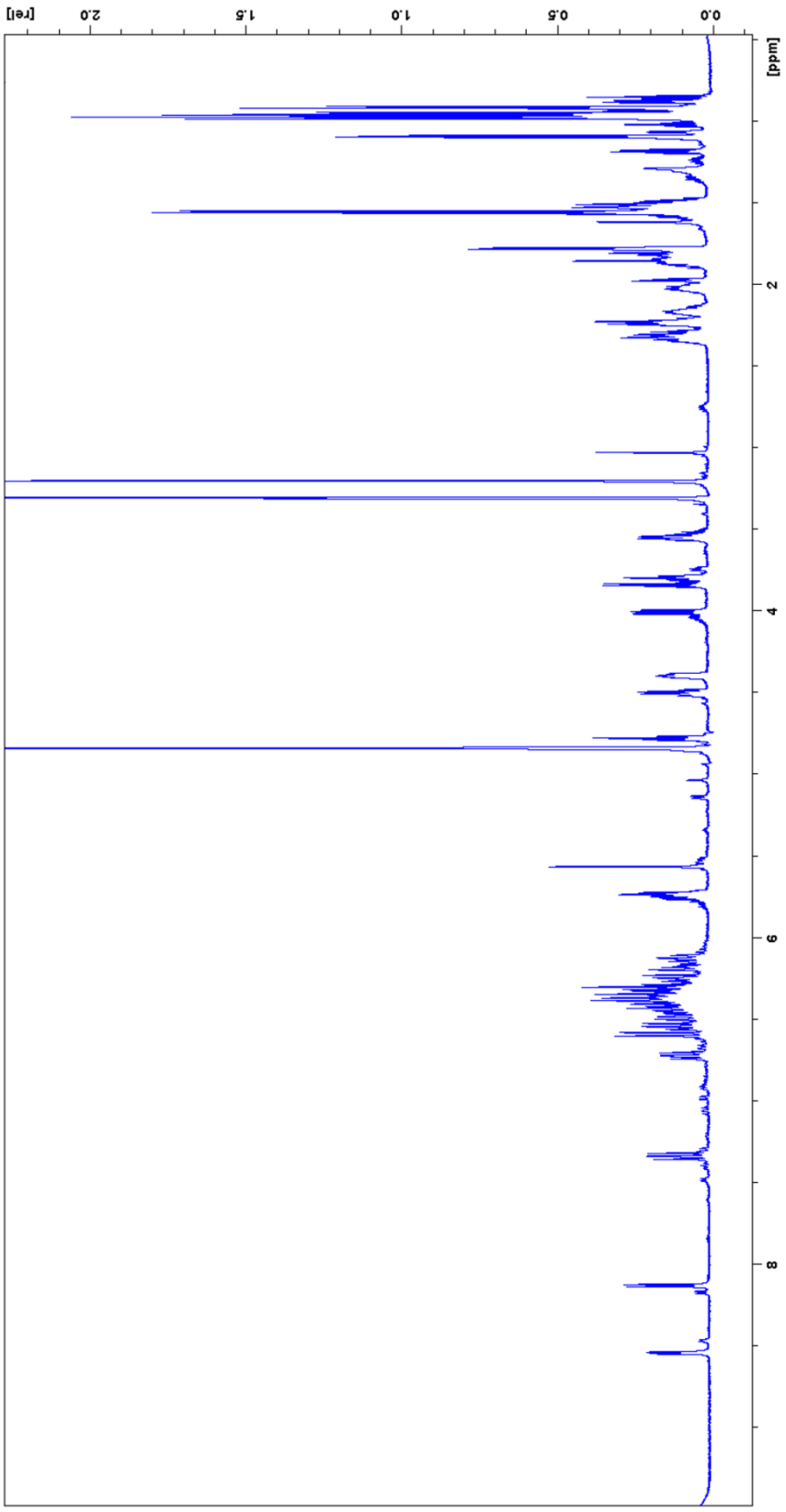

^{1}H-NMR spectrum of myxochromide SA_3 in CD_3OD (500 MHz)

Fig. S18 ***(continued on next page)***

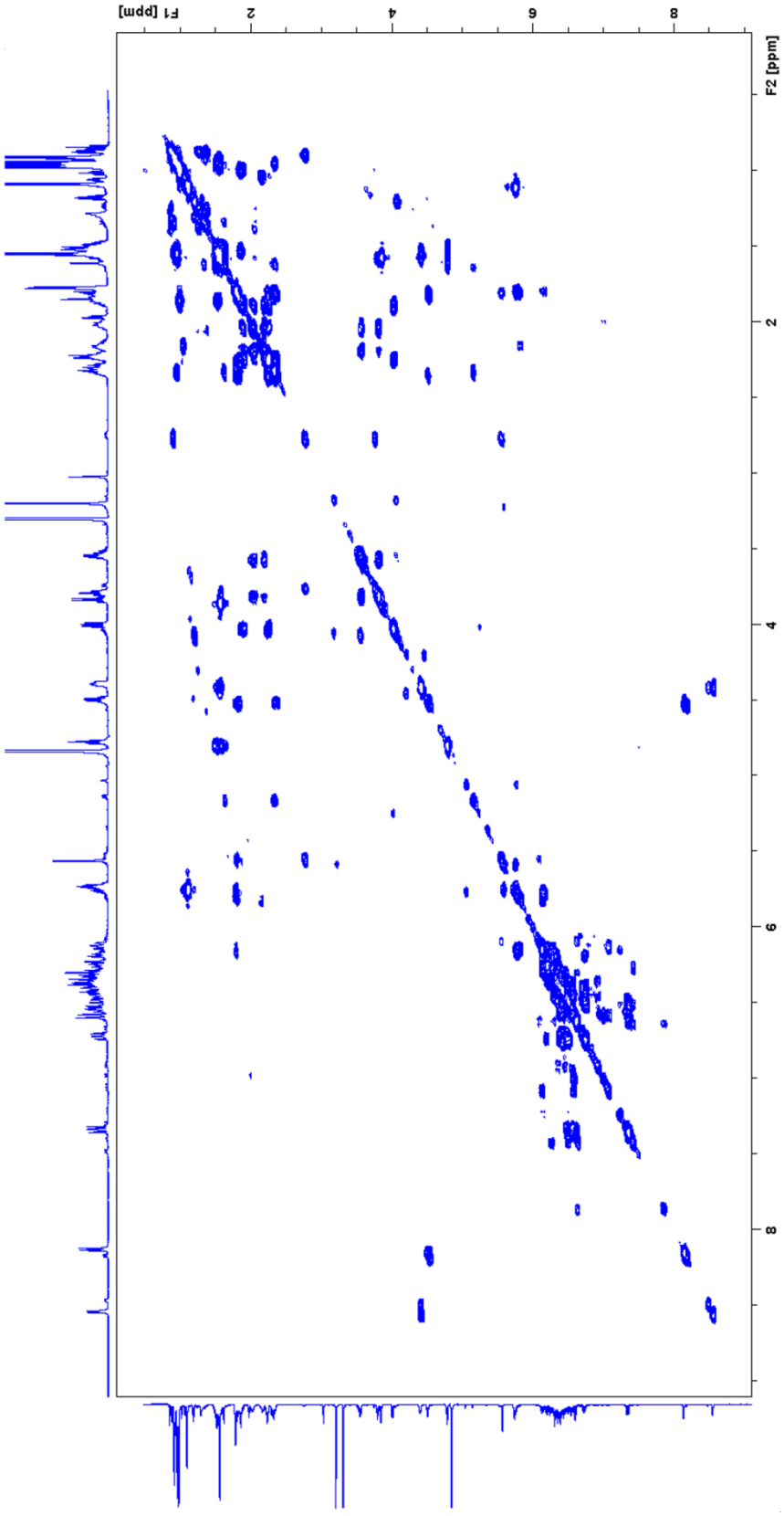

^{1}H-^{1}H COSY spectrum of myxochromide SA$_3$ in CD_3OD (500 MHz)

Fig. S18 ***(continued on next page)***

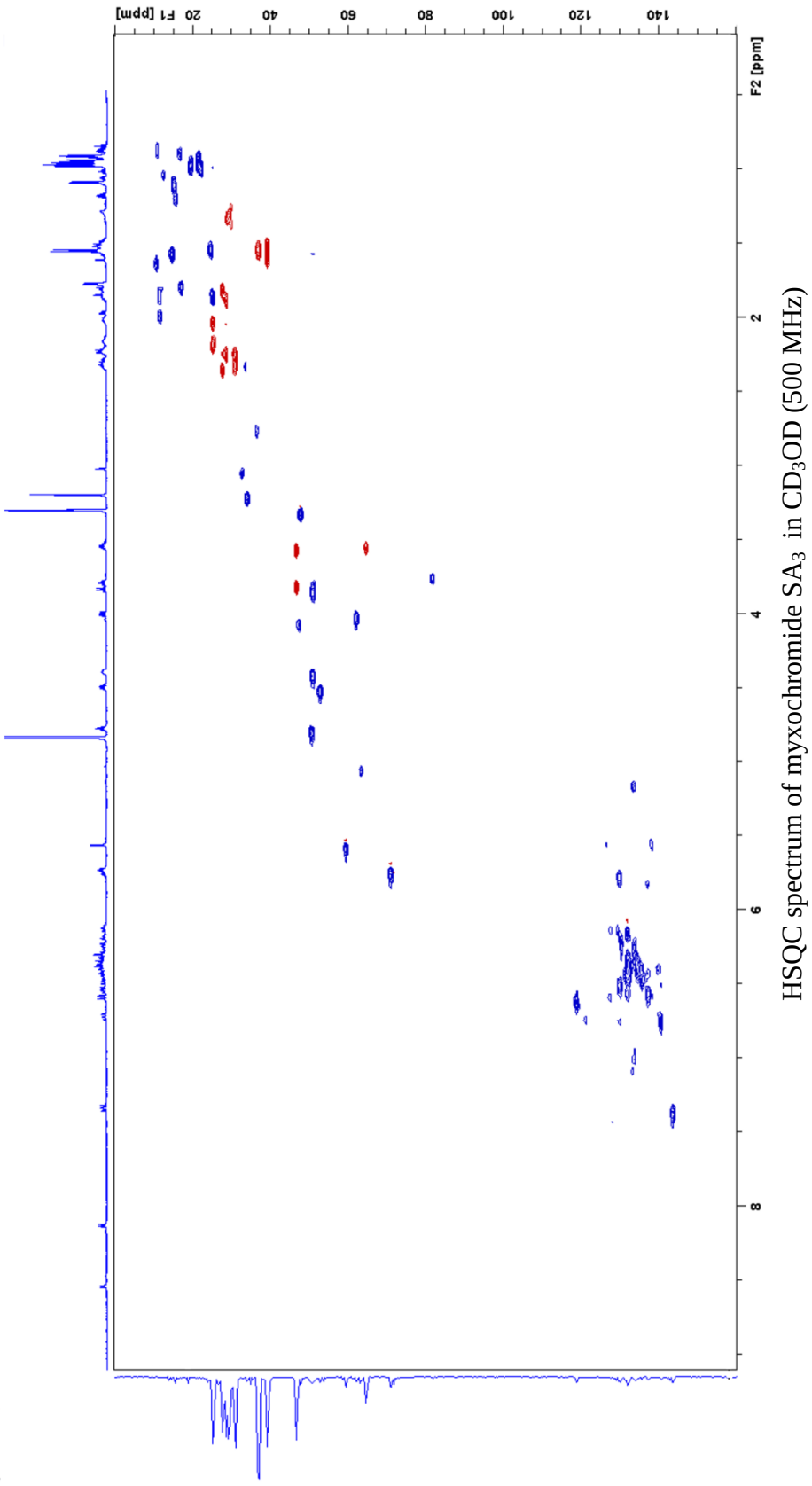

HSQC spectrum of myxochromide SA_3 in CD_3OD (500 MHz)

Fig. S18 ***(continued on next page)***

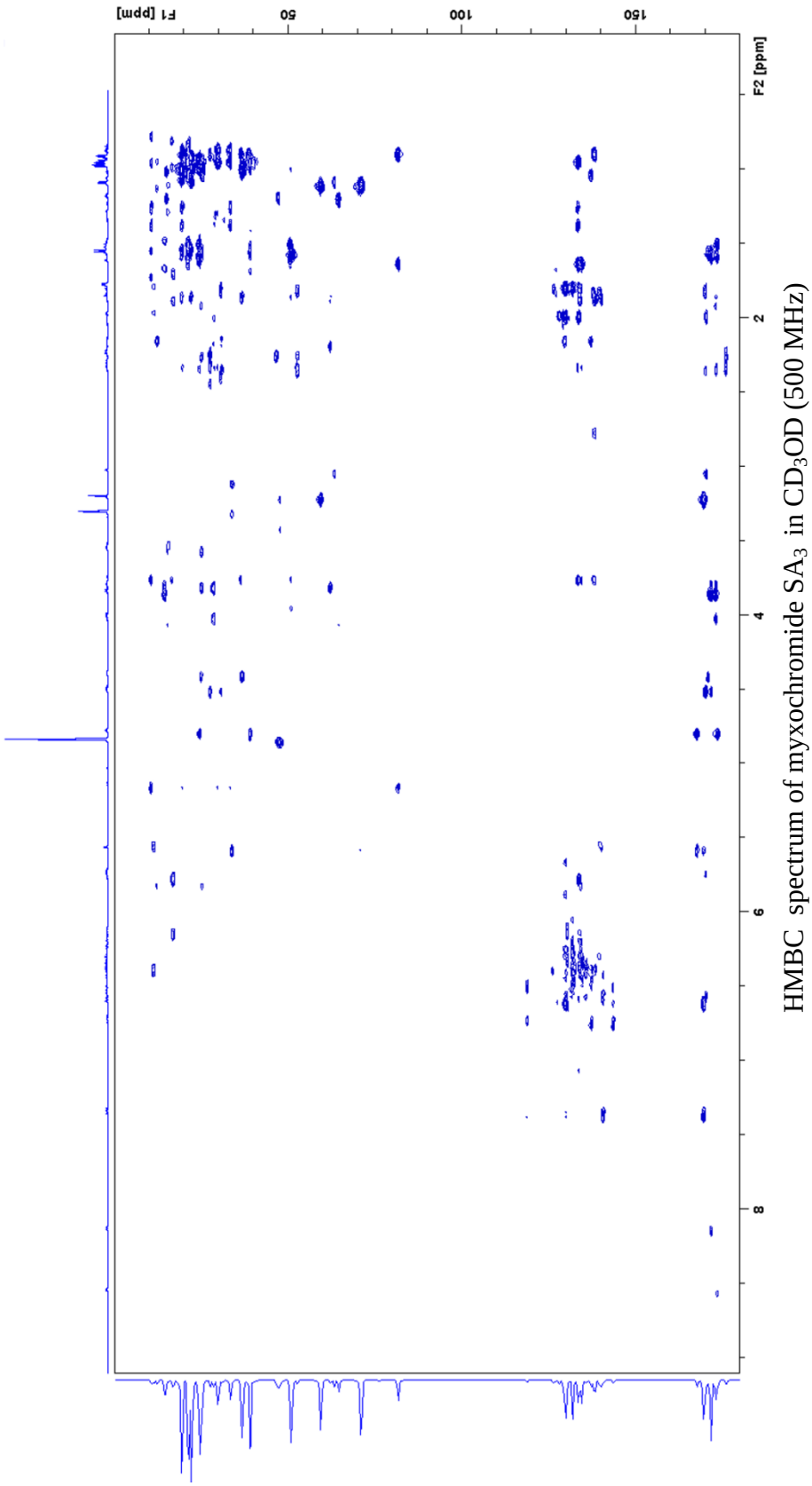

Fig. S18 NMR spectra of myxochromide SA_3.

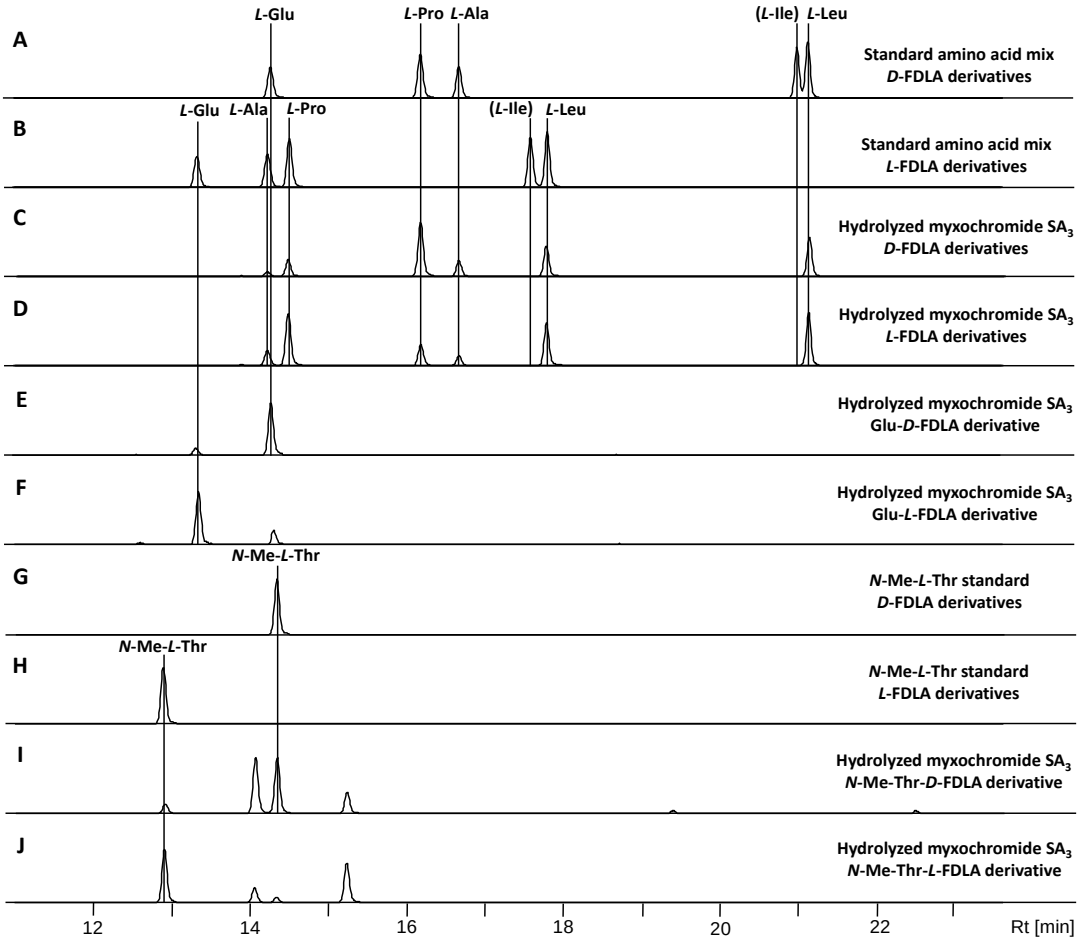

Fig. S19 Analysis of the absolute configuration of myxochromide SA_3. Extracted ion chromatograms (EIC) for ±0.05 *m/z* corresponding to the $[M+H]^+$ ions of derivatized amino acids, which are present in the peptide scaffold, are shown. **A**: Standard amino acid mix derivatized with *D*-FDLA reagent. **B**: Standard amino acid mix derivatized with *L*-FDLA reagent. **C**: Hydrolyzed myxochromide SA_3 derivatized with *D*-FDLA reagent. **D**: Hydrolyzed myxochromide SA_3 derivatized with *L*-FDLA reagent. **E**: Same sample as in **C** analyzed for the *L*-glutamic acid *D*-FDLA derivative. **F**: Same sample as in **D** analyzed for the *L*-glutamic acid *L*-FDLA derivative. **G**: Standard solution of *N*-Me-*L*-threonine derivatized with *D*-FDLA. **H**: Standard solution of *N*-Me-*L*-threonine derivatized with *L*-FDLA. **I**: Same sample as in **C** analyzed for the *N*-Me-*L*-threonine *D*-FDLA derivative. **J**: Same sample as in **D** analyzed for the *N*-Me-*L*-threonine *L*-FDLA.

Table S14 Analytical data of detected amino acid derivatives and assignment of the absolute configuration of the amino acids in myxochromide SA_3.

aa-FDLA derivative	*L*-aa standards		Peptide hydrolysate		Assigned configuration
	t_R [min]	*m/z* $[M+H]^+$	t_R [min]	*m/z* $[M+H]^+$	
Glu-*D*-FDLA	14.3	442.1578	14.3	442.1576	**L**
Glu-*L*-FDLA	13.3	442.1579	13.3	442.1570	
Ala-*D*-FDLA	16.7	384.1520	16.7	384.1515	**L**
Ala-*L*-FDLA	14.3	384.1524	14.3	384.1511	
Pro-*D*-FDLA	16.2	410.1675	16.2	410.1676	**L**
Pro-*L*-FDLA	14.5	410.1675	14.5	410.1673	
Leu-*D*-FDLA	21.1	426.1989	21.1	426.1993	**L**
Leu-*L*-FDLA	17.8	426.1988	17.8	426.1986	
Leu-*D*-FDLA	**21.1**	426.1989	**17.8**	426.1993	**D**
Leu-*L*-FDLA	**17.8**	426.1988	**21.1**	426.1982	
N-Me-Thr-*D*-FDLA	14.4	428.1782	14.4	428.1786	**L**
N-Me-Thr-*L*-FDLA	12.9	428.1786	12.9	428.1785	

5.2.3 Structure of myxochromide SB_4

Structure elucidation of myxochromide SB_4 was achieved using ^1H and 2D ^1H-^1H COSY, HSQC, HMBC and ROESY spectra (Fig. S21). Carbon chemical shifts were extracted from 2D NMR data. NMR spectroscopic data are listed in the Table S15. The ^1H NMR spectrum closely resembled to that of myxochromide SA_3. In addition to the common structural parts, analysis of 2D NMR spectra corroborated the presence of an additional leucine residue compared to myxochromide SA_3. Key HMBC and ROESY correlations established the amino acid sequence and finalized its planar structure as depicted in Fig. S20. Length of the polyene side chain was deduced based on the HR-MS data and molecular formula. For the assignment of the absolute configuration of myxochromide SB_4, hydrolysis and Marfey analysis of the obtained amino acids,[7] was applied as described above. The chromatograms obtained from HPLC-MS analysis are illustrated in Fig. S22 and stereochemical assignments are illustrated in Table S16. Comparison of the retention times and masses of derivatized standard amino acids and the hydrolyzed lipopeptide revealed that one of the three leucine residues (C10, C16 and C22) from myxochromide SA_3 has *D* configuration. The remaining leucine residues as well as the amino acids alanine (C2), proline (C5), *N*-Me-threonine (C28) and glutamine (C32), which was converted to glutamic acid during hydrolysis, were found to be *L*-configured. According to the domain organization of the underlying hybrid assembly line, which harbors an epimerization domain in module 2, the *D*-configured leucine was assigned to C22. This also correlates with the structure of myxochromide SA_3 and identifies the condensation domain of module 3 originating from the B-type *mch* pathway as a ^DC_L domain.

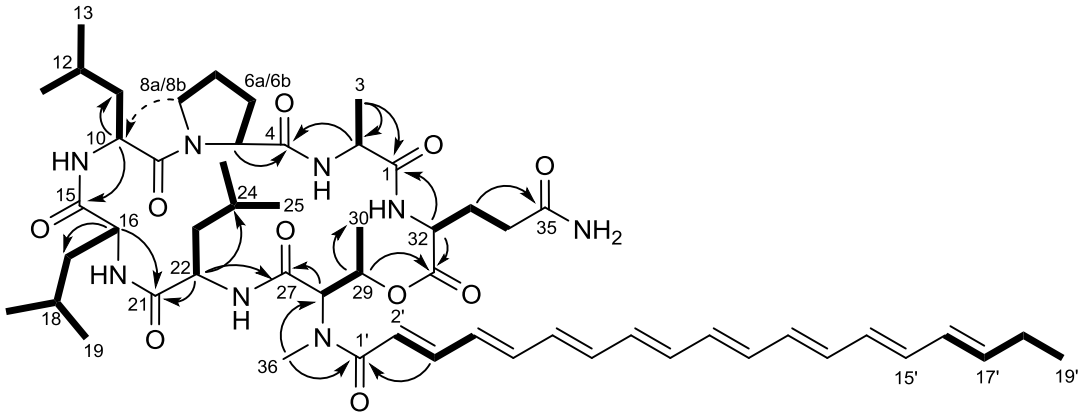

Fig. S20 Structure of myxochromide SB_4 showing selected COSY (bold line), ROESY (dashed arrow) and key HMBC (arrow) correlations.

Table S15 NMR spectroscopic data of myxochromide SB_4.

Moiety	Position	δ_C [a]	δ_H [b] (*J* in Hz)	HMBC [c]	ROESY [d, e]
L-Ala	1	174.5			
	2	50.3	4.26 *m*	1,3	
	3	15.5	1.42 *d* (7.4)	1,2	
L-Pro	4	174.0			
	5	63.6	4.11 *m*	4, 6a/b,7a/b	10
	6a	30.5	1.90 *m*	4,5,7a/b	
	6b	30.5	2.35 *m*	4, 5,7a/b	
	7a	25.9	2.05 *m*	5,6a/b,8a/b	
	7b	25.9	2.13 *m*	5,6a/b,8a/b	
	8a	48.3	3.68 *m*	6a/b,7a/b	10
	8b	48.3	3.85 *m*	6a/b,7a/b,9	10
L-Leu	9	174.0			
	10	49.6	4.95 *dd* [f]	9,11,12,15	8a/b, 5
	11a	41.3	1.51 *m*	10,12	
	11b	41.3	1.64 *m*	10,12	
	12	25.8	1.65 *m*	13,14	
	13	21.2	0.99 *m*	11,12,14	
	14	23.5	0.95 *m*	11,12,13	

L-Leu	15	174.4		
	16	54.5	4.27 *m*	15,17a/b,18,21
	17a	41.8	1.65 *m*	19,20
	17b	41.8	1.76 *m*	19,20
	18	25.9	1.74 *m*	
	19	21.1	0.91 *d* (6.1)	17a/b
	20	23.1	1.01 *m*	17a/b
D-Leu	21	174.1		
	22	52.6	4.68 *m*	21,23a/b,24
	23a	44.3	1.59 *m*	22,24,25,26
	23b	44.3	1.44 *m*	22,24,25,26
	24	25.7	1.52 *m*	
	25	22.8	0.94 *m*	23a/b,24,25
	26	22.8	0.94 *m*	23a/b,24,25
N-Me-*L*-Thr	27	168.6		
	28	61.0	5.57 *d* (3.5)	1´,27,29,36
	29	71.0	5.83 *m*	30,31
	30	16.2	1.09 *d* (6.6)	27,28,29
	36	35.5	3.23 *s*	1´,28
L-Gln	31	170.7		
	32	55.4	4.12 *m*	31,33,34
	33a	28.5	1.92 *m*	32,34,35
	33b	28.5	2.16 *m*	32,34,35
	34a	31.9	2.29 *m*	32,33a/b,35
	34b	31.9	2.53 *m*	32,33a/b,35
	35	177.4		
Side chain	1'	170.8		
	2'	120.0	6.69 *d* (14.9)	1´,3´
	3'	145.0	7.36 *dd* (14.5,11.2)	1´,2´,4´
	4'	138.4	6.55 *m*	5´
	5'	141.6	6.72 *m*	3´,4´
	6´-14´	*f*	*f*	
	15'	135.1	6.24 *m*	17´
	16'	130.9	6.12 *dd* (9.8,15.0)	17´
	17'	138.1	5.79 *m*	15´,18´,16´
	18'	26.5	2.14 *m*	16´,17´,
	19´	13.6	1.02 *t* (7.4)	18´,17´

[a] acquired at 125 MHz and assigned from 2D NMR spectra, referenced to solvent signal CD_3OD at δ 49.15 ppm.
[b] acquired at 500 MHz, referenced to solvent signal CD_3OD at δ 3.31 ppm.
[c] proton showing HMBC correlations to indicated carbons.
[d] proton showing ROESY correlations to indicated protons.
[e] acquired at 500 MHz, referenced to solvent signal CD_3OD at δ 3.31 ppm.
[f] overlapped signals.
[g] correlation obtained from HMBC spectra in $(CD_3)_2SO$ (data not shown).

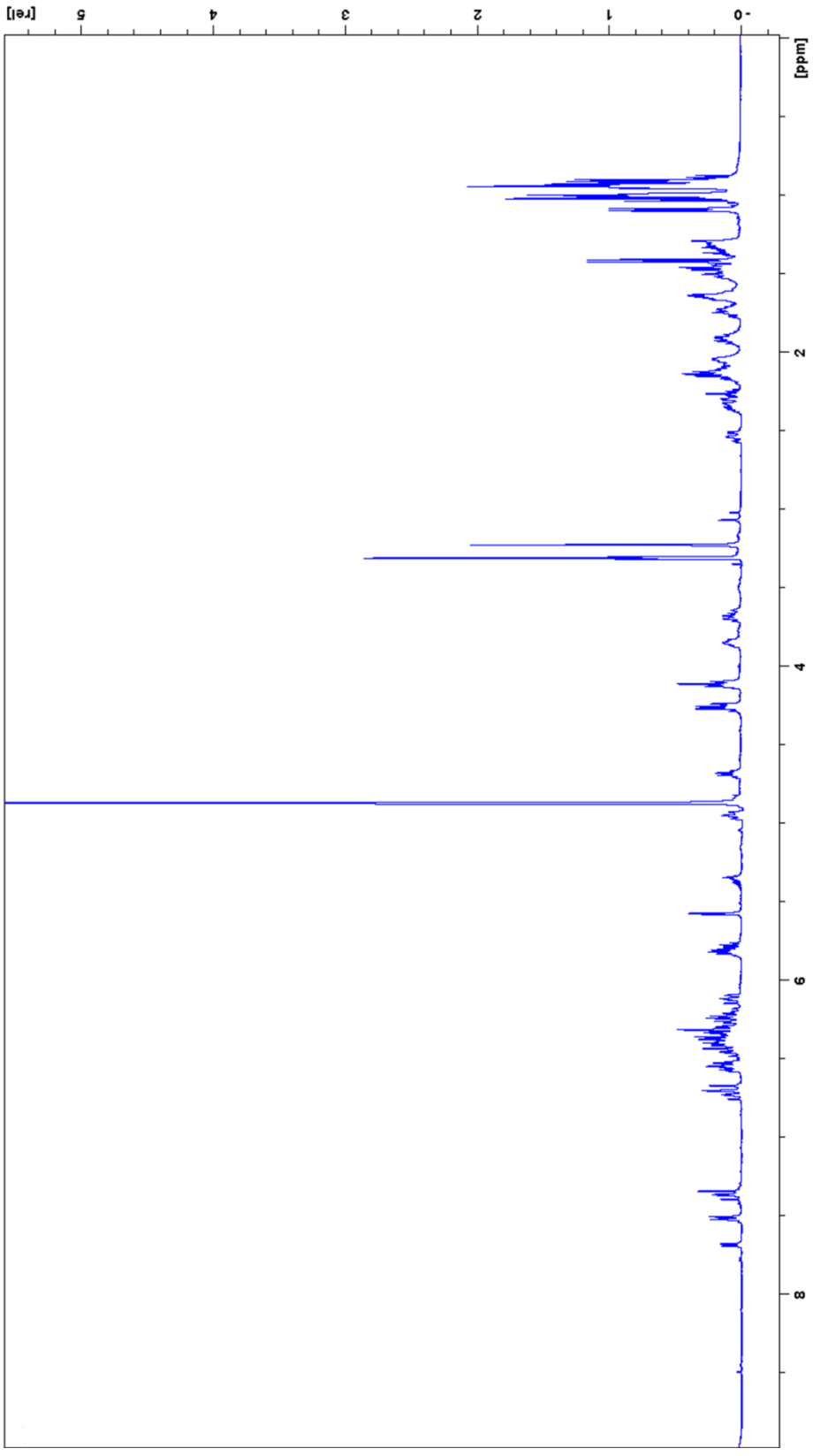

^{1}H-NMR spectrum of myxochromide SB_4 in CD_3OD (500 MHz)

Fig. S21 ***(continued on next page)***

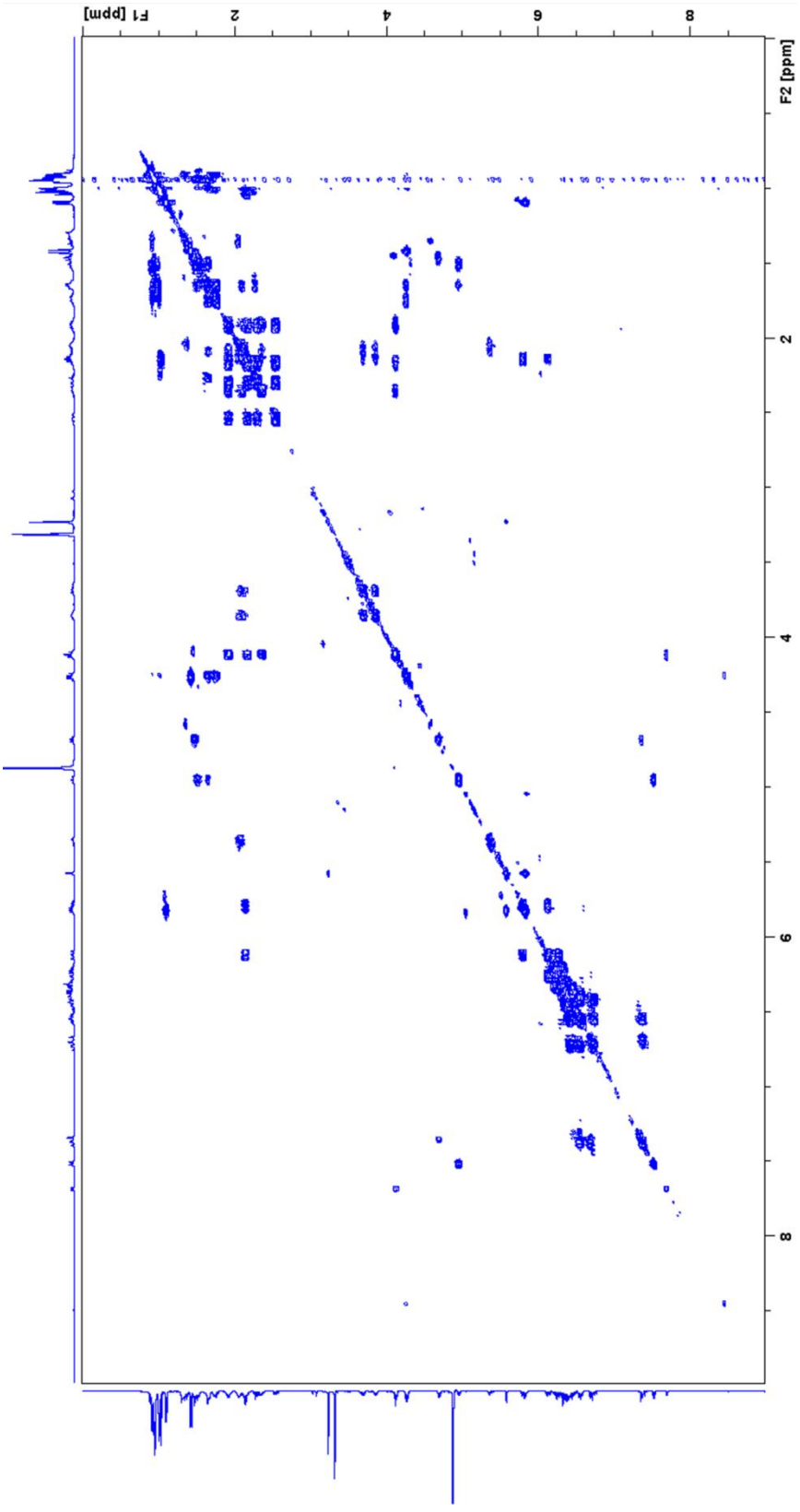

^{1}H-^{1}H COSY spectrum of myxochromide SB_4 in CD_3OD (500 MHz)

Fig. S21 ***(continued on next page)***

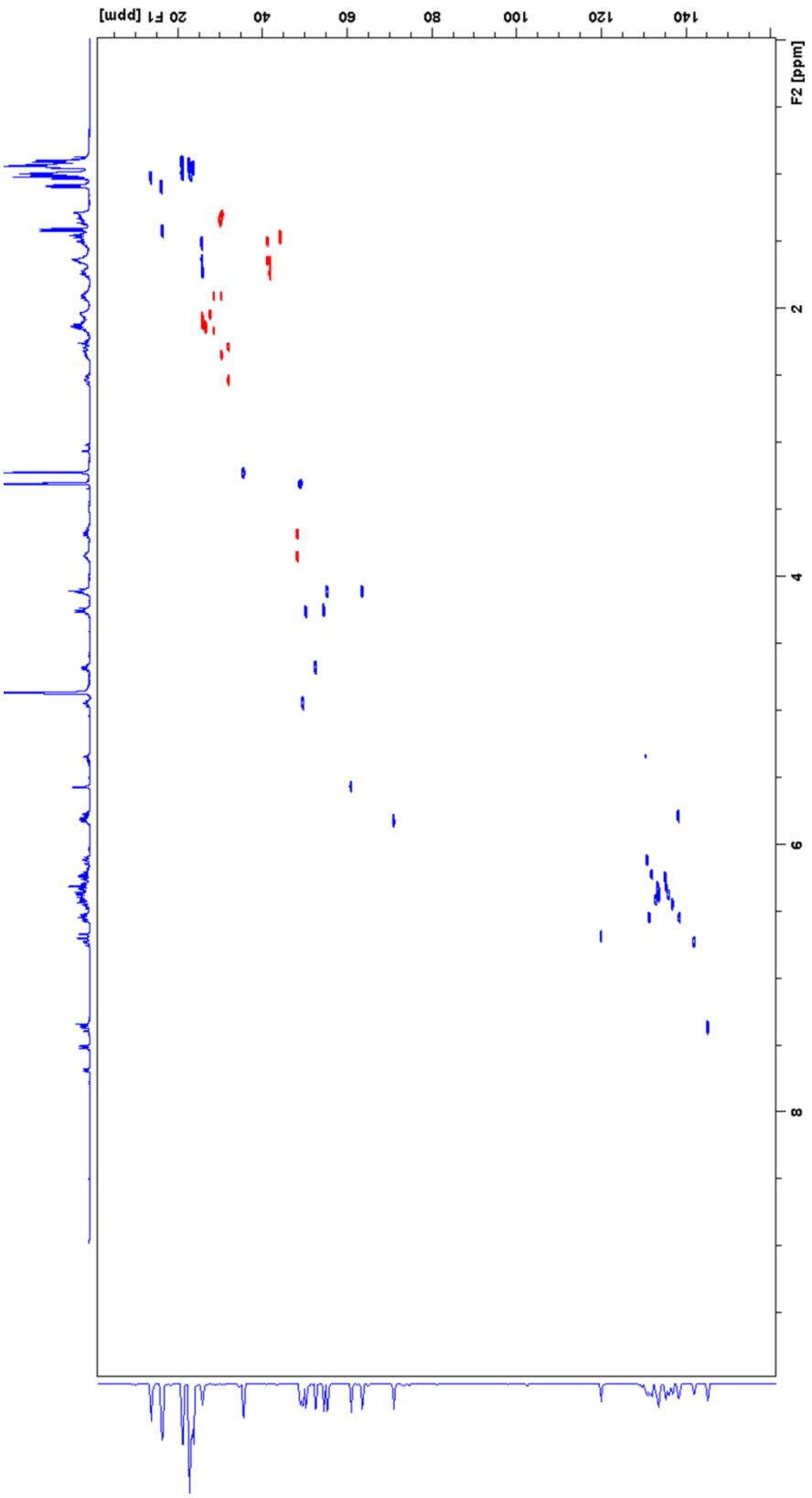

Fig. S21 ***(continued on next page)***

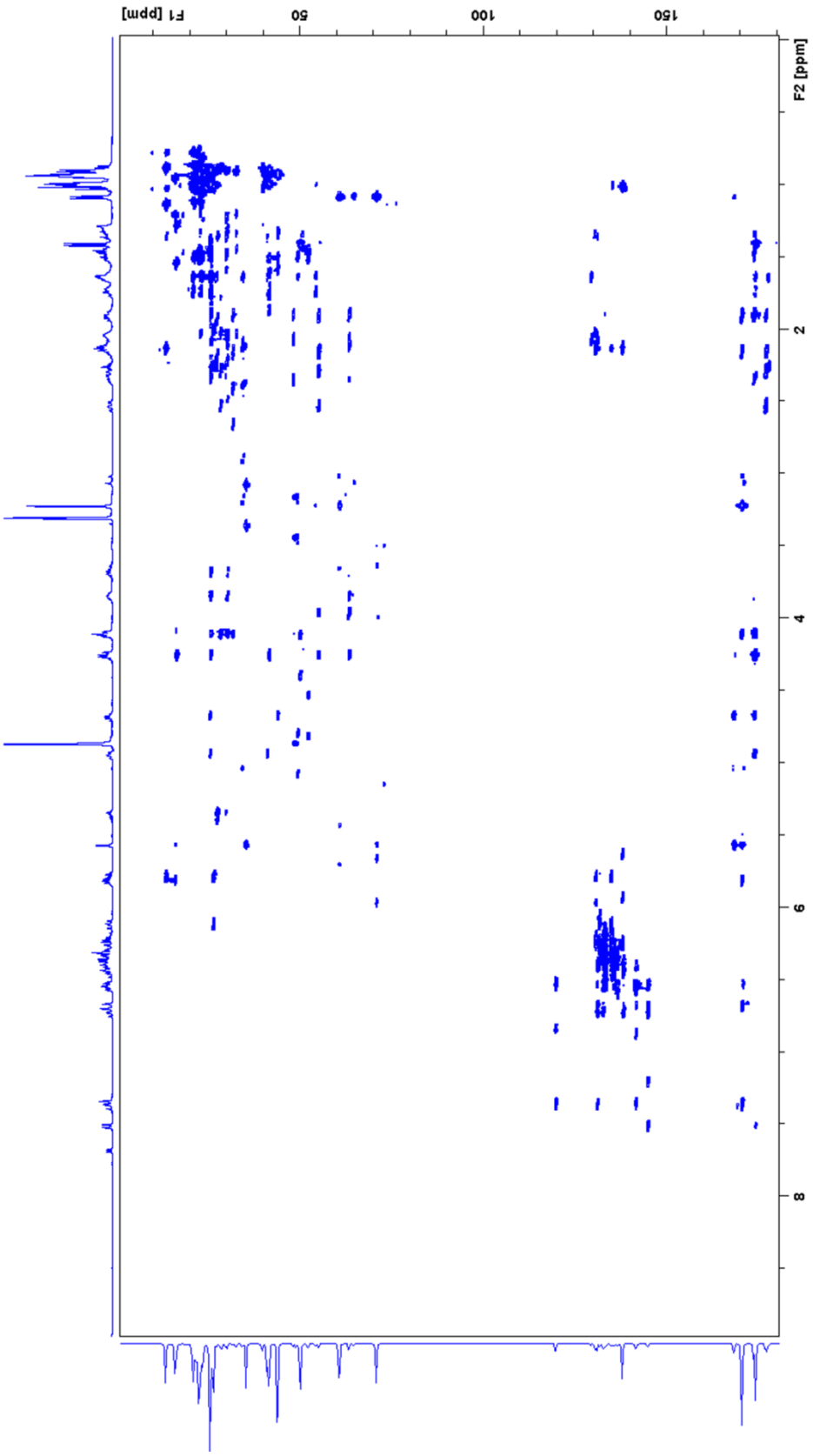

HMBC spectrum of myxochromide SB_4 in CD_3OD (500 MHz)

Fig. S21 ***(continued on next page)***

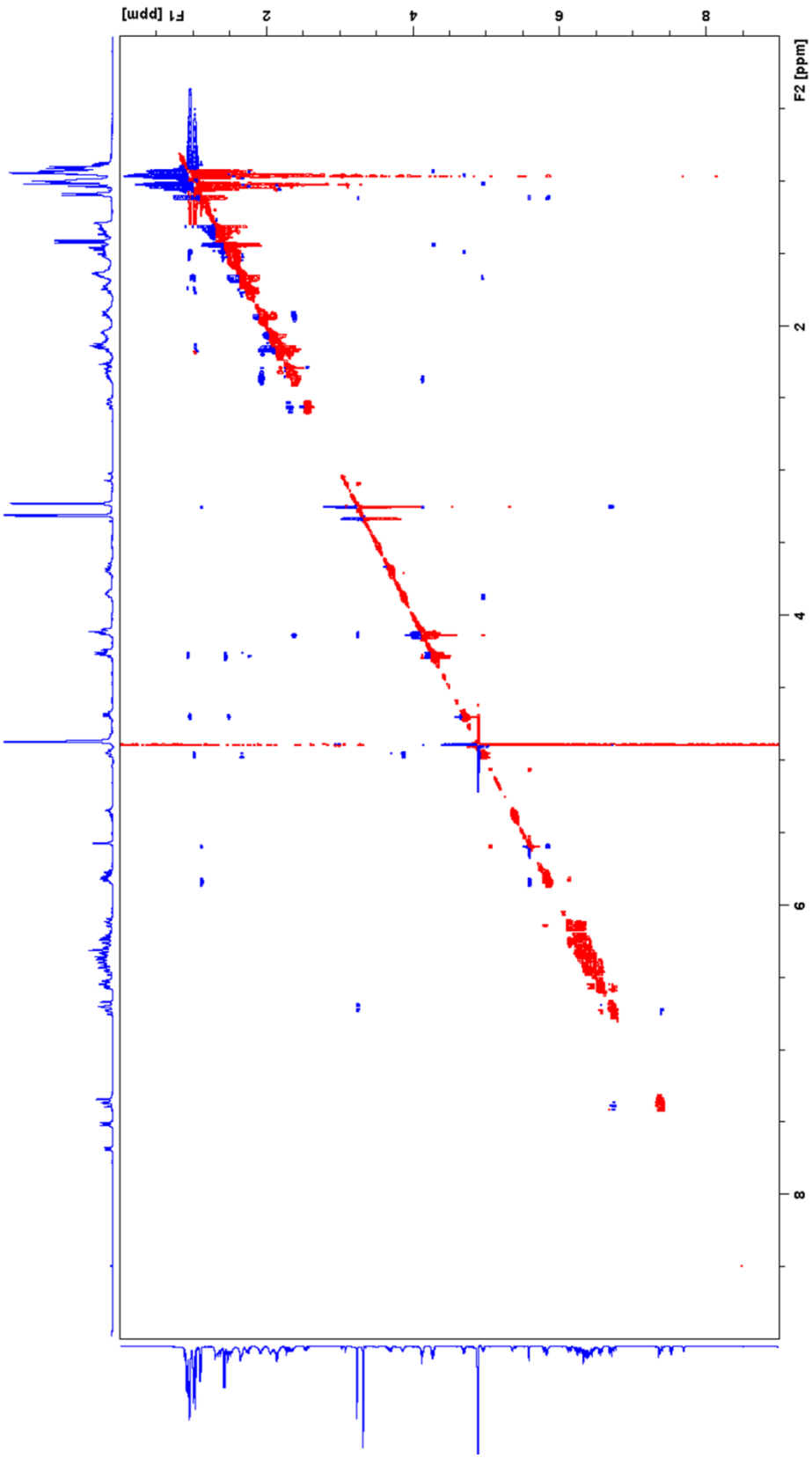

Fig. S21 NMR spectra of myxochromide SB_4.

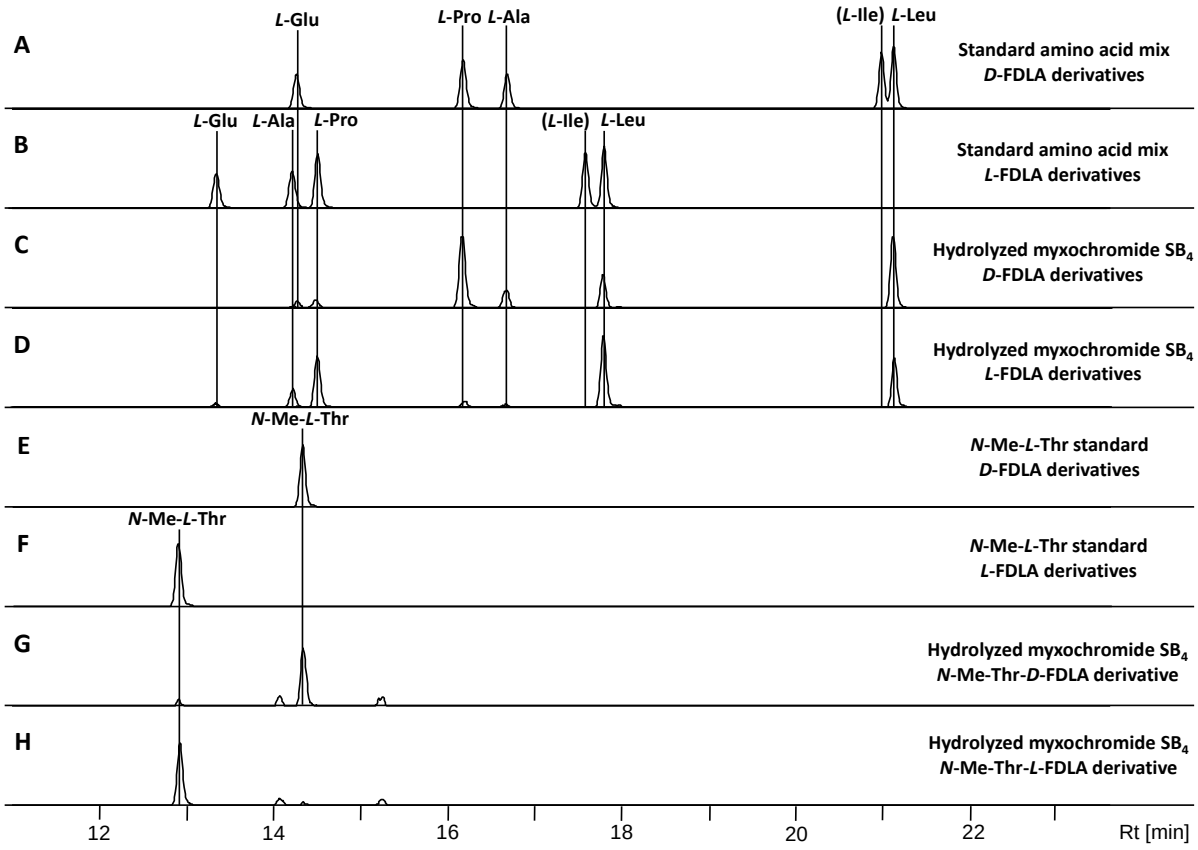

Fig. S22 Analysis of the absolute configuration of myxochromide SB_4. Extracted ion chromatograms (EIC) for ±0.05 *m/z* corresponding to the $[M+H]^+$ ions of derivatized amino acids, which are present in the peptide scaffold, are shown. **A**: Standard amino acid mix derivatized with *D*-FDLA reagent. **B**: Standard amino acid mix derivatized with *L*-FDLA reagent. **C**: Hydrolyzed myxochromide SB_4 derivatized with *D*-FDLA reagent. **D**: Hydrolyzed myxochromide SB_4 derivatized with *L*-FDLA reagent. **E**: Standard solution of *N*-Me-*L*-threonine derivatized with *D*-FDLA. **F**: Standard solution of *N*-Me-*L*-threonine derivatized with *L*-FDLA. **G**: Same sample as in **C** analyzed for the *N*-Me-*L*-threonine *D*-FDLA derivative. **H**: Same sample as in **D** analyzed for the *N*-Me-*L*-threonine *L*-FDLA derivative.

Table S16 Analytical data of detected amino acid derivatives and assignment of the absolute configuration of the amino acids in myxochromide SB_4.

aa-FDLA derivative	*L*-aa standards		Peptide hydrolysate		Assigned configuration
	t_R [min]	*m/z* $[M+H]^+$	t_R [min]	*m/z* $[M+H]^+$	
Glu-*D*-FDLA	14.3	442.1578	14.3	442.1572	**L**
Glu-*L*-FDLA	13.3	442.1579	13.3	442.1582	
Ala-*D*-FDLA	16.7	384.1520	16.7	384.1513	**L**
Ala-*L*-FDLA	14.3	384.1524	14.3	384.1525	
Pro-*D*-FDLA	16.2	410.1675	16.2	410.1672	**L**
Pro-*L*-FDLA	14.5	410.1675	14.5	410.1676	
Leu-*D*-FDLA	21.1	426.1989	21.1	426.1986	**L**
Leu-*L*-FDLA	17.8	426.1988	17.8	426.1985	
Leu-*D*-FDLA	21.1	426.1989	21.1	426.1986	**L**
Leu-*L*-FDLA	17.8	426.1988	17.8	426.1985	
Leu-*D*-FDLA	**21.1**	426.1989	**17.8**	426.1991	**D**
Leu-*L*-FDLA	**17.8**	426.1988	**21.1**	426.1988	
N-Me-Thr-*D*-FDLA	14.4	428.1782	14.4	428.1775	**L**
N-Me-Thr-*L*-FDLA	12.9	428.1786	12.9	428.1779	

5.2.4 Structure of myxochromide SC_4

Structure elucidation of myxochromide SC_4 was achieved using 1D ^1H and 2D ^1H-^1H COSY, HSQC, HMBC and ROESY spectra (Fig. S24). Carbon chemical shifts were extracted from 2D NMR data. NMR spectroscopic data are listed in Table S17. The COSY spectrum supported by HSQC and HMBC data showed presence of spin systems corresponding to *N*-Me-threonine, glutamine, proline and leucine residues as well as a polyene side chain. Amino acid sequence was established by means of key HMBC and ROESY correlations and final structure was elucidated as shown in Fig. S23. For the assignment of the absolute configuration of myxochromide SC_4, hydrolysis and Marfey analysis of the obtained amino acids,[7] was applied as described above.[7] The chromatograms obtained from HPLC-MS analysis are illustrated in Fig. S25 and stereochemical assignments are illustrated in Table S18. Comparison of the retention times and masses of derivatized standard amino acids and the hydrolyzed lipopeptide revealed that one of the two leucine residues (C7 and C13) from myxochromide SC_4 is *D*-configured. The second leucine residue as well as the amino acids proline (C2), *N*-Me-threonine (C19) and glutamine (C23), which was converted to glutamic acid during hydrolysis, were found to be *L*-configured. According to the domain organization of the underlying hybrid assembly line, which harbors an epimerization domain in module 2, the *D*-configured leucine was assigned to C13. This also correlates with the structures of myxochromide SA_3 myxochromide SB_4 and and identifies the condensation domain of module 3 originating from the C-type *mch* pathway as a ^DC_L domain.

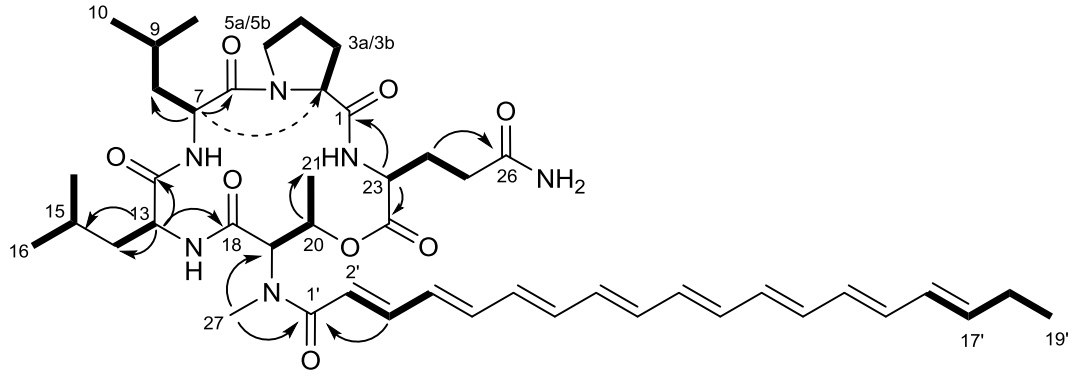

Fig. S23 Structure of myxochromide SC_4 showing selected COSY (bold line), ROESY (dashed arrow) and key HMBC (arrow) correlations.

Table S17 NMR spectroscopic data of myxochromide SC_4.

Moiety	Position	δ_C [a]	δ_H [b] (*J* in Hz)	HMBC [c]	ROESY [d,e,g]
L-Pro	1	174.2			
	2	63.0	4.34, *m*	1, 3, 7	7
	3a	32.6	2.18, *m*	4	
	3b		2.42, *m*	4	
	4	23.4	2.00, *m*		
	5a	47.7	3.59, *m*		
	5b		3.74, *m*		
L-Leu	6	173.9 [f]			
	7	49.7	4.66, *m*	6, 8, 9	2
	8a	42.5	1.55, *m*		
	8b		1.62, *m*		
	9	25.6	1.53, *m*		
	10	23.3	0.93, *m*	8, 9	

	11	23.3	0.93, *m*	8, 9
D-Leu	12	173.9 [f]		
	13	54.4	4.26, *m*	12, 14,15,18
	14a	40.8	1.39, *m*	12, 15
	14b		1.75, *m*	12, 15
	15	25.6	1.53, *m*	
	16	21.5	0.91, *m*	15
	17	21.5	0.91, *m*	15
N-Me-*L*-Thr	18	170.8		
	19	61.6	5.41, *m*	18
	20	72.1	5.97, *m*	
	21	16.8	1.24, *d* (6.5)	19, 20
	27	34.8	3.40, *m*	1', 19
L-Gln	22	171.1		
	23	54.4	4.42, *m*	1, 24, 25
	24a	28.8	2.03, *m*	26
	24b		2.11, *m*	26
	25a	31.7	2.22, *m*	26
	25b		2.22, *m*	26
	26	176.9		
Side chain	1'	170.8		
	2'	119.8	6.65, *d* (14.8)	
	3'	144.9	7.34, *dd* (14.8,11.7)	
	4'	141.8	6.54, *m*	
	5'-14'	[f]	[f]	
	15'	134.9	6.27, *m*	
	16'	130.7	6.12, *dd* (15.0, 10.0)	
	17'	138.1	5.79, *dt* (15.0, 6.7)	15'
	18'	26.6	2.14, *m*	17', 19'
	19'	13.6	1.02, *t* (7.4)	18'

[a] acquired at 175 MHz and assigned from 2D NMR spectra, referenced to solvent signal CD_3OD at δ 49.15 ppm.
[b] acquired at 700 MHz, referenced to solvent signal CD_3OD at δ 3.31 ppm.
[c] proton showing HMBC correlations to indicated carbons.
[d] proton showing ROESY correlations to indicated protons.
[e] acquired at 700 MHz, referenced to solvent signal CD_3OD at δ 3.31 ppm.
[f] overlapped signals.
[g] only relevant correlations listed

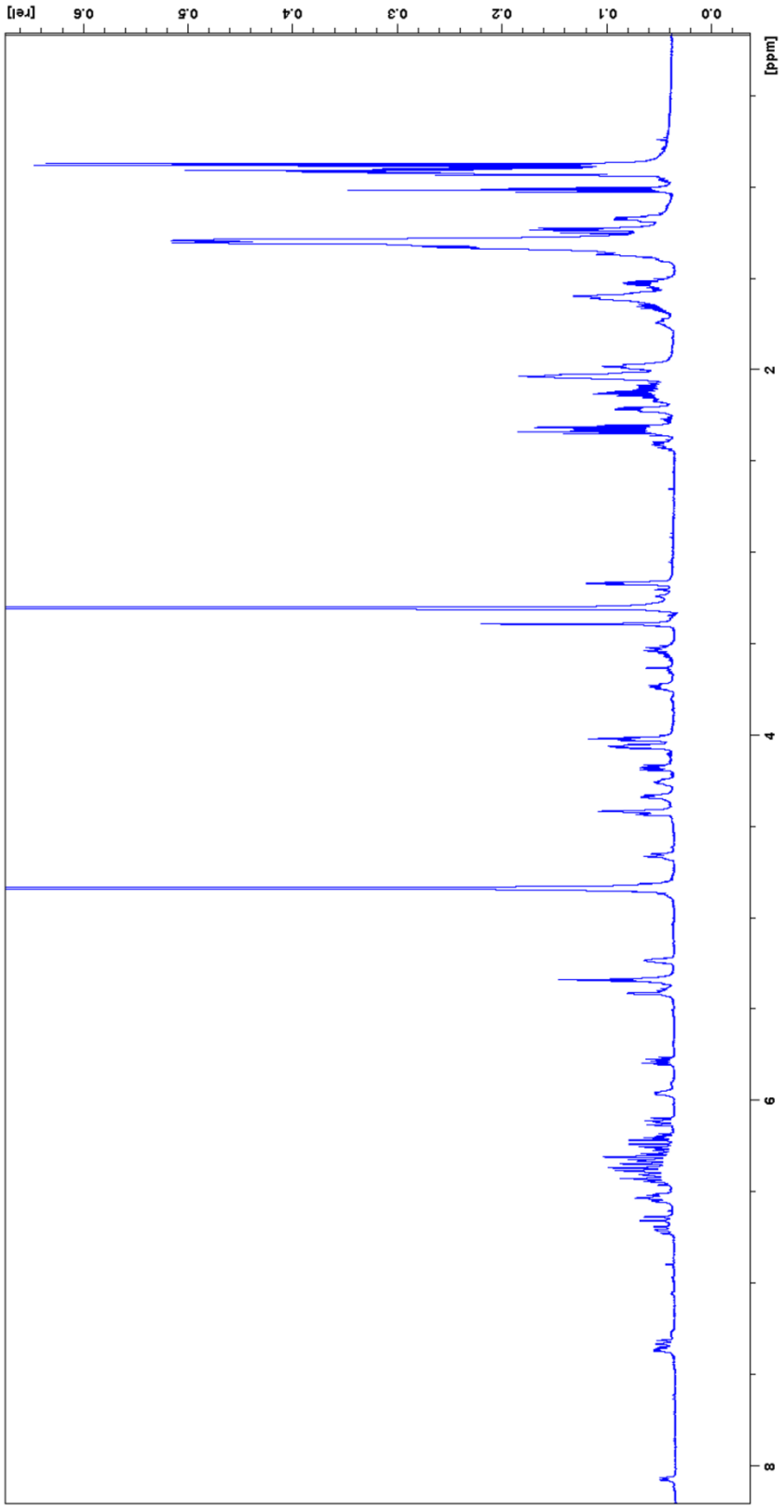

^{1}H-NMR spectrum of myxochromide SC_4 in CD_3OD (500 MHz)

Fig. S24 ***(continued on next page)***

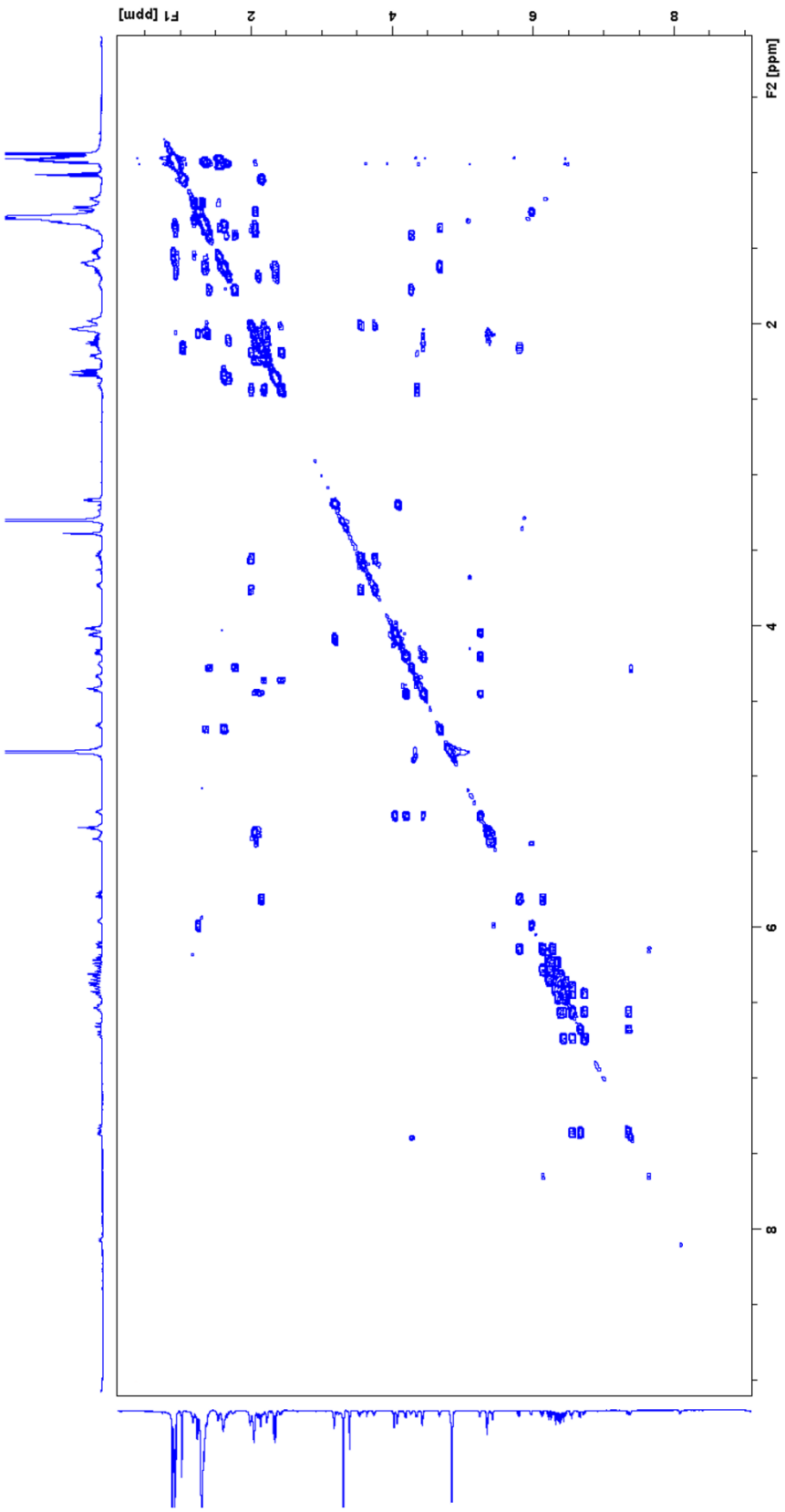

^{1}H-^{1}H COSY spectrum of myxochromide SC_4 in CD_3OD (500 MHz)

Fig. S24 ***(continued on next page)***

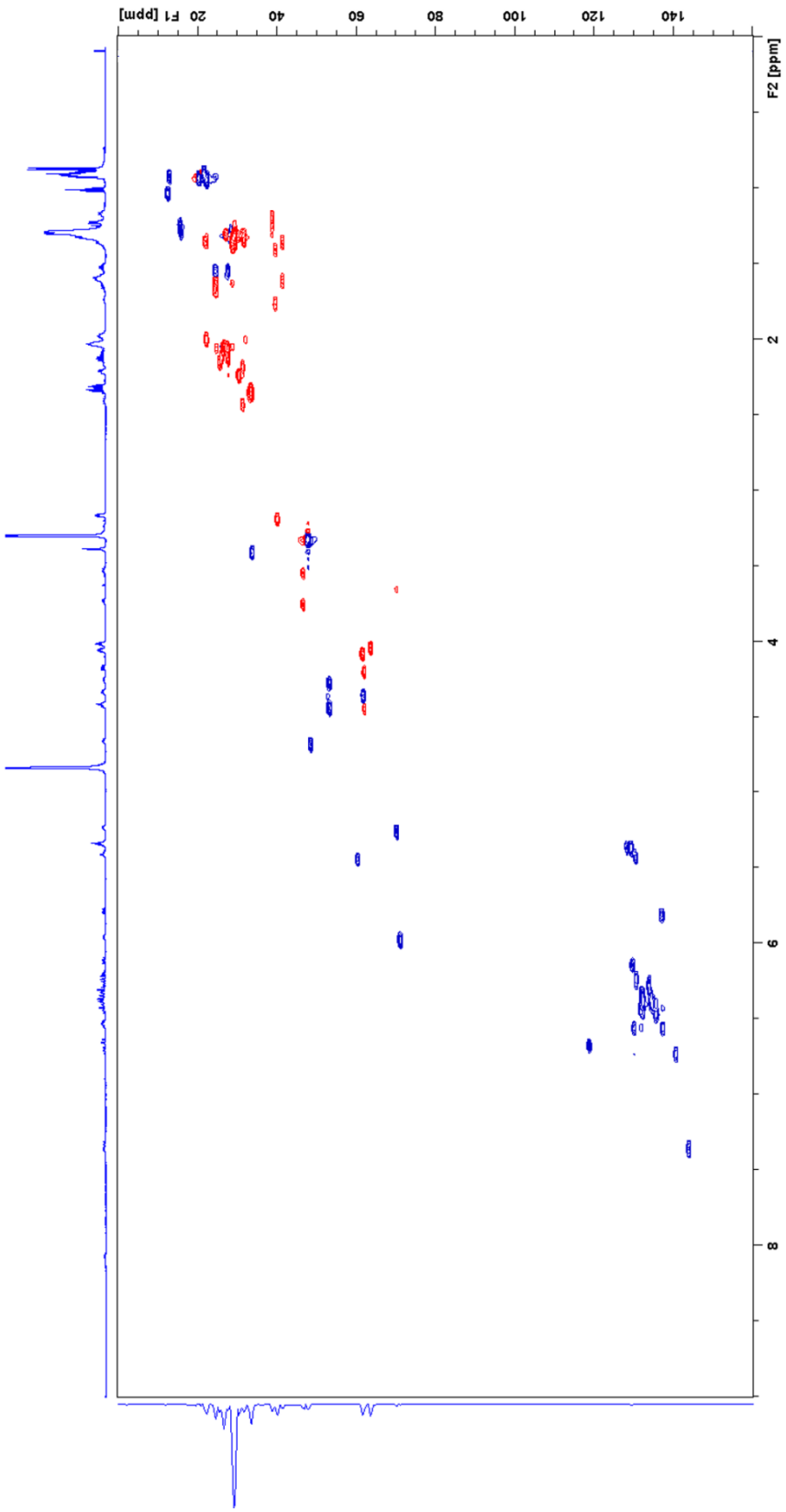

HSQC spectrum of myxochromide SC_4 in CD_3OD (500 MHz)

Fig. S24 ***(continued on next page)***

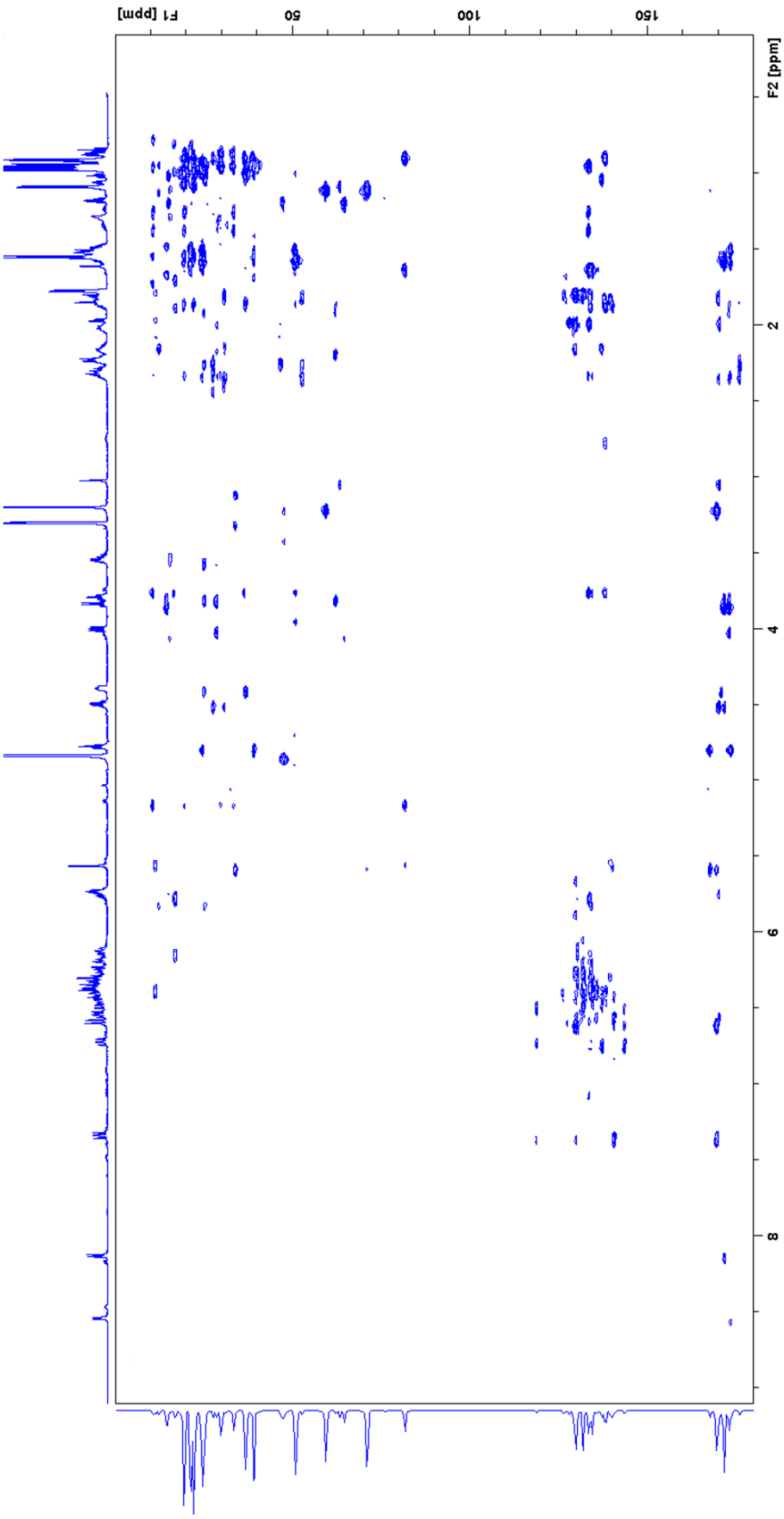

HMBC spectrum of myxochromide SC_4 in CD_3OD (500 MHz)

Fig. S24 ***(continued on next page)***

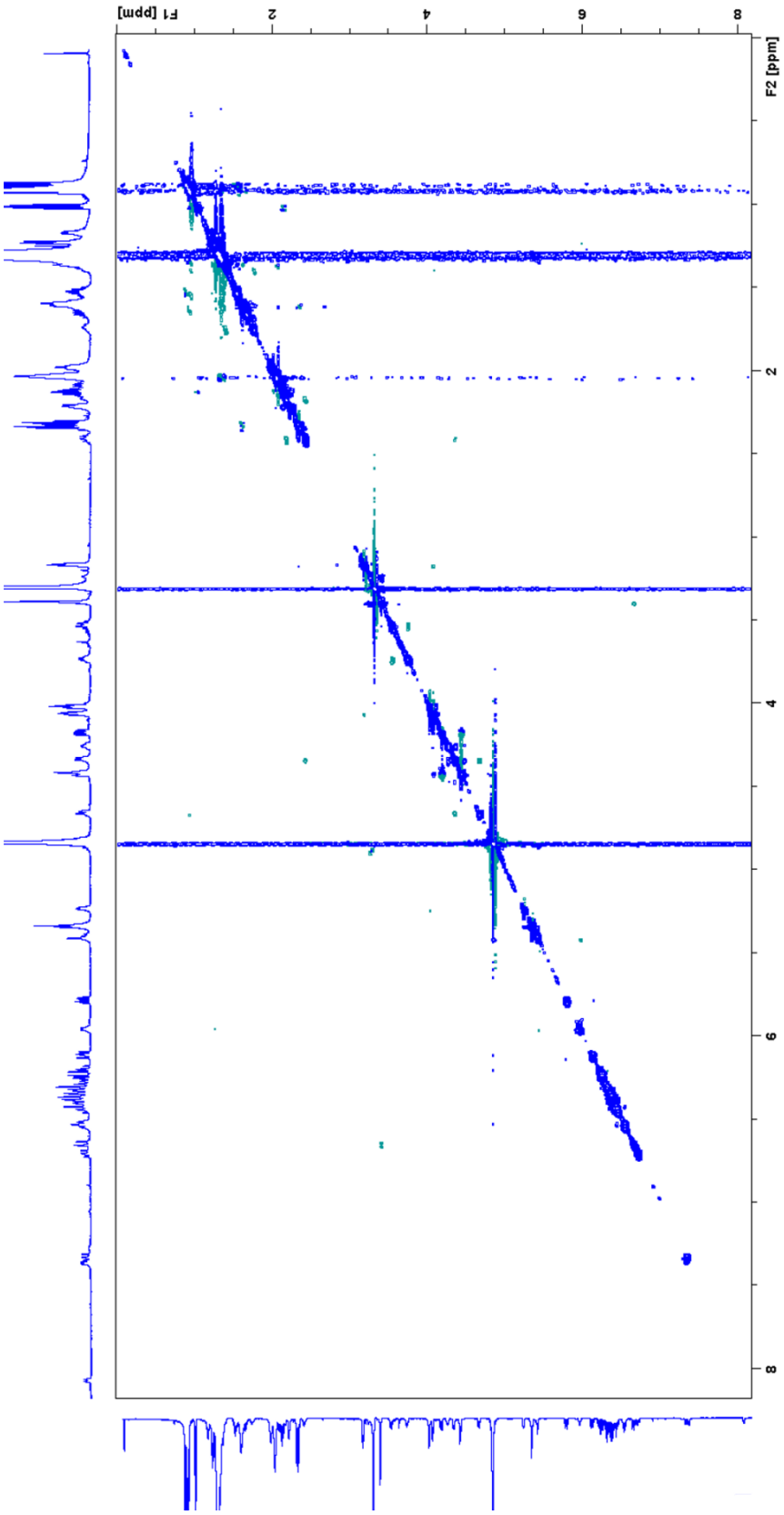

Fig. S24 NMR spectra of myxochromide SC_4.

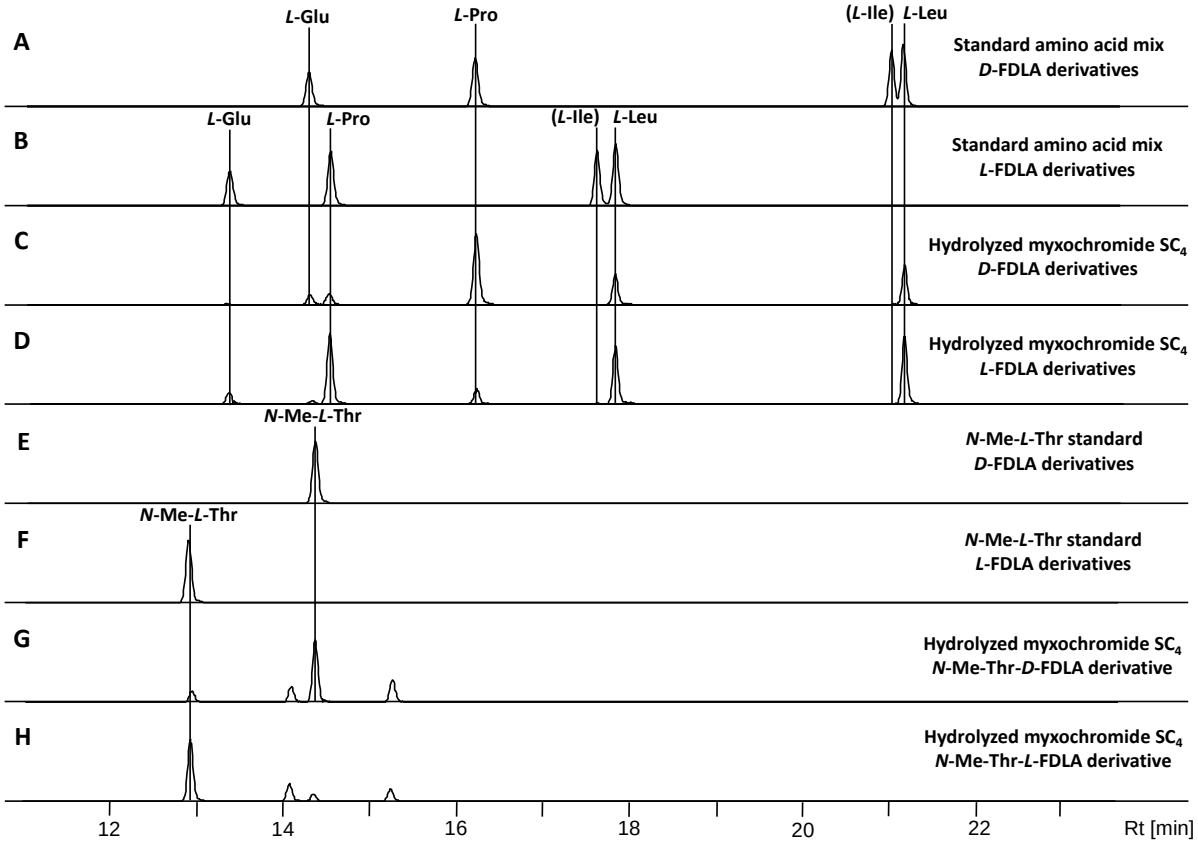

Fig. S25 Analysis of the absolute configuration of myxochromide SC_4. Extracted ion chromatograms (EIC) for ±0.05 *m/z* corresponding to the $[M+H]^+$ ions of derivatized amino acids, which are present in the peptide scaffold, are shown. **A**: Standard amino acid mix derivatized with *D*-FDLA reagent. **B**: Standard amino acid mix derivatized with *L*-FDLA reagent. **C**: Hydrolyzed myxochromide SC_4 derivatized with *D*-FDLA reagent. **D**: Hydrolyzed myxochromide SC_4 derivatized with *L*-FDLA reagent. **E**: Standard solution of *N*-Me-*L*-threonine derivatized with *D*-FDLA. **F**: Standard solution of *N*-Me-*L*-threonine derivatized with *L*-FDLA. **G**: Same sample as in **C** analyzed for the *N*-Me-*L*-threonine *D*-FDLA derivative. **H**: Same sample as in **D** analyzed for the *N*-Me-*L*-threonine *L*-FDLA derivative.

Table S18 Analytical data of detected amino acid derivatives and assignment of the absolute configuration of the amino acids in myxochromide SC_4.

aa-FDLA derivative	*L*-aa standards		Peptide hydrolysate		Assigned configuration
	t_R [min]	*m/z* $[M+H]^+$	t_R [min]	*m/z* $[M+H]^+$	
Glu-*D*-FDLA	14.3	442.1578	14.3	442.1572	**L**
Glu-*L*-FDLA	13.3	442.1579	13.3	442.1572	
Pro-*D*-FDLA	16.2	410.1675	16.2	410.1679	**L**
Pro-*L*-FDLA	14.5	410.1675	14.5	410.1668	
Leu-*D*-FDLA	21.1	426.1989	21.1	426.1990	**L**
Leu-*L*-FDLA	17.8	426.1988	17.8	426.1982	
Leu-*D*-FDLA	**21.1**	426.1989	**17.8**	426.1981	**D**
Leu-*L*-FDLA	**17.8**	426.1988	**21.1**	426.1980	
N-Me-Thr-*D*-FDLA	14.4	428.1782	14.4	428.1780	**L**
N-Me-Thr-*L*-FDLA	12.9	428.1786	12.9	428.1777	

5.2.5 Structure of myxochromide SD_3

Structure elucidation of myxochromide SD_3 was achieved using 1D ^1H and 2D ^1H-^1H COSY, HSQC and HMBC spectra (Fig. S27). Carbon chemical shifts were extracted from 2D NMR data. NMR spectroscopic data are listed in Table S19. The COSY spectrum supported by HSQC and HMBC data revealed the presence of *N*-Me-threonine, glutamine, alanine and leucine residues as well as and a polyene side chain. Amino acid sequence was established by means of key HMBC correlations and final structure was elucidated as shown in Fig. S26. For the assignment of the absolute configuration of myxochromide SD_3, hydrolysis and Marfey analysis of the obtained amino acids,[7] was applied as described above. The chromatograms obtained from HPLC-MS analysis are illustrated in Fig. S28 and stereochemical assignments are illustrated in Table S20. Comparison of the retention times and masses of derivatized standard amino acids and the hydrolyzed lipopeptide revealed that one of the two leucine residues (C5 and C11) from myxochromide SD_3 is *D*-configured. The second leucine residue as well as the amino acids alanine (C2), *N*-Me-threonine (C17) and glutamine (C21), which was converted to glutamic acid during hydrolysis, were found to be *L*-configured. This is in accordance with the absolute configurations observed in myxochromides SA_3, SB_4 and SC_4. According to the domain organization of the underlying hybrid assembly line, which harbors an epimerization domain in module 2, the *D*-configured leucine was assigned to C11. This also correlates with the structures of myxochromide SA_3 myxochromide SB_4 and and identifies the condensation domain of module 3 originating from the D-type *mch* pathway as a ^DC_L domain.

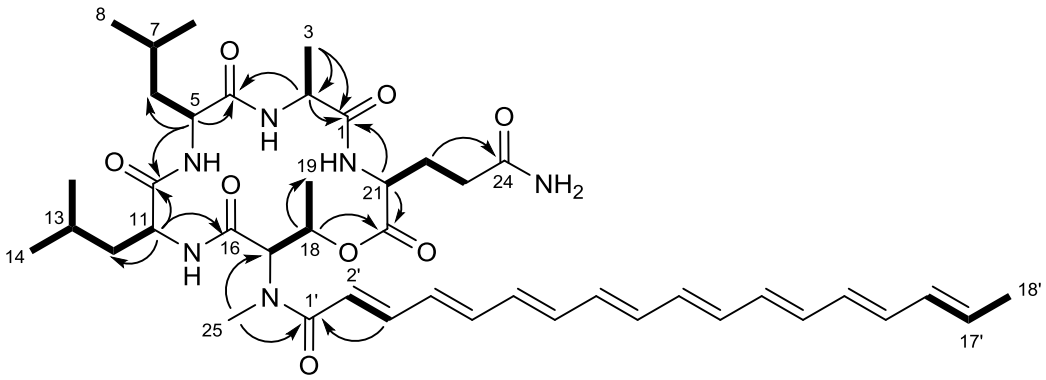

Fig. S26 Structure of myxochromide SD_3 showing selected COSY (bold line) and key HMBC (arrow) correlations.

Table S19 NMR spectroscopic data of myxochromide SD_3.

Moiety	Position	δ_C [a]	δ_H [b] (*J* in Hz)	HMBC [c]
L-Ala	1	172.7		
	2	50.6	4.21 *m*	1,3,4
	3	18.7	1.37 *d* (6.7)	1,3
L-Leu	4	174.7		
	5	54.2	4.19 *m*	4,6a/b,7, 10[e]
	6a	40.6	1.58 *m*	
	6b		1.65 *m*	
	7	25.9	1.71 *m*	
	8	23.2	0.99 *d* (6.3)	6,7,9
	9	21.1	0.91 *d* (6.5)	6,7,8
D-Leu	10	175.2		
	11	53.1	4.39 *m*	10,12,13,16
	12a	40.6	1.49 *m*	11

	12b	40.6	1.60 *m*	11
	13	25.7	1.56 *m*	
	14	22.6	0.92 *m*	12,13,15
	15	22.6	0.92 *m*	12,13,14
N-Me-*L*-Thr	16	169.8		
	17	59.5	5.43 *m*	16,18
	18	72.4	5.52 *m*	19,20
	19	17.2	1.15 *d* (6.9)	18,20
	25	35.1	3.02 *s*	1´,17
L-Gln	20	170.9		
	21	53.9	3.95 *m*	1,20,22a/b,23a/b
	22a	26.3	2.13 *m*	20,21,23a/b,24
	22b	26.3	2.25 *m*	20,21,23a/b,24
	23a	32.1	2.16 *m*	24
	23b	32.1	2.27 *m*	24
	24	177.7		
Side chain	1'	170.6		
	2'	120.1	6.59 *m*	1´,4´
	3'	144.9	7.35 *m*	1´
	4'	131.5	6.53 *m*	
	5´-15'	*dd*	*dd*	
	16'	133.1	6.15 *m*	
	17'	131.1	5.75 *m*	
	18'	18.3	1.78 *d* (7.1)	17´,16´

[a] acquired at 125 MHz and assigned from 2D NMR spectra, referenced to solvent signal CD_3OD at δ 49.15 ppm.
[b] acquired at 500 MHz, referenced to solvent signal CD_3OD at δ 3.31 ppm.
[c] proton showing HMBC correlations to indicated carbons.
[d] overlapped signals.
[e] HMBC acquired with 2k F1 resolution

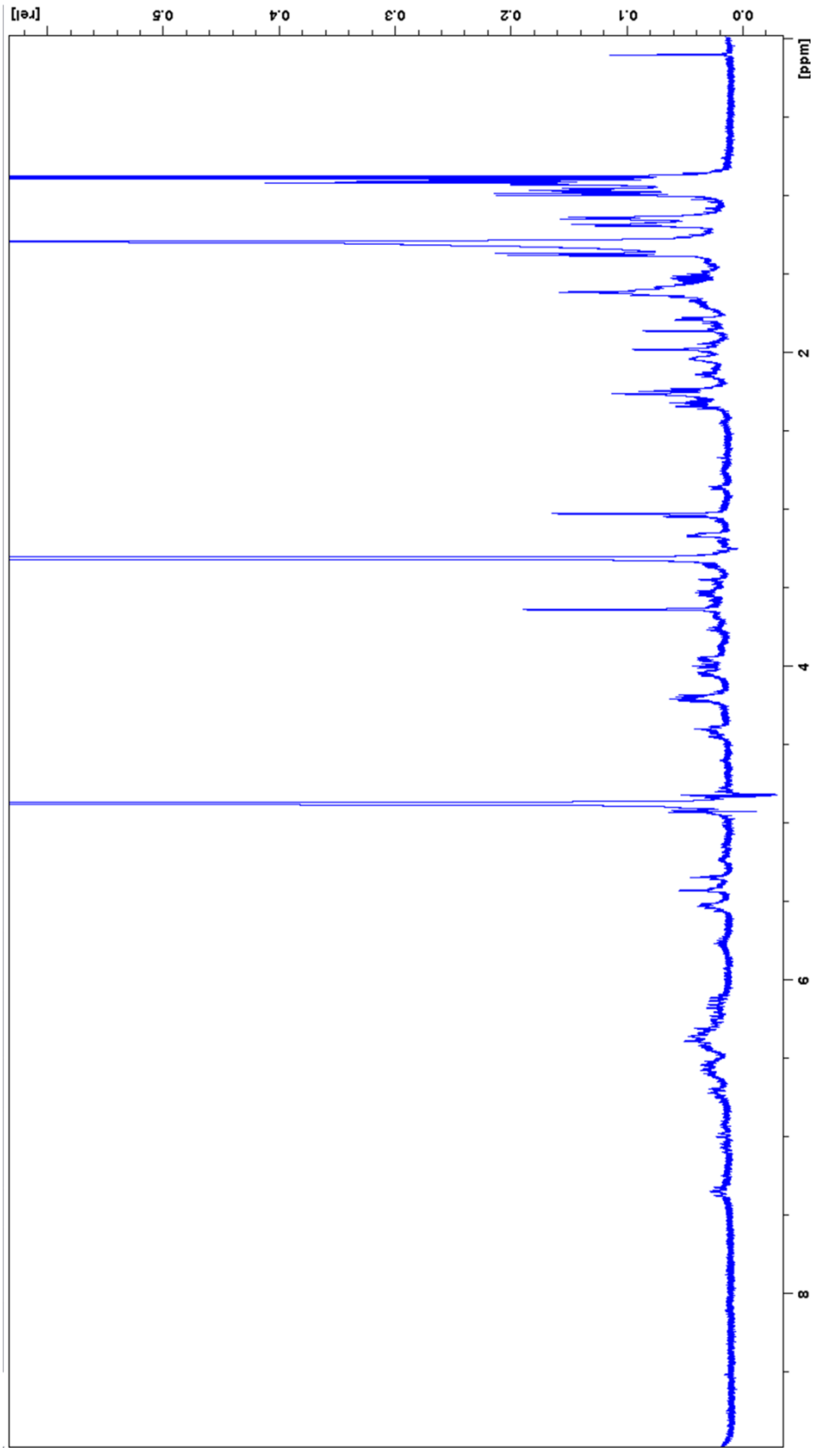

^{1}H-NMR spectrum of myxochromide SD_3 in CD_3OD (500 MHz)

Fig. S27 ***(continued on next page)***

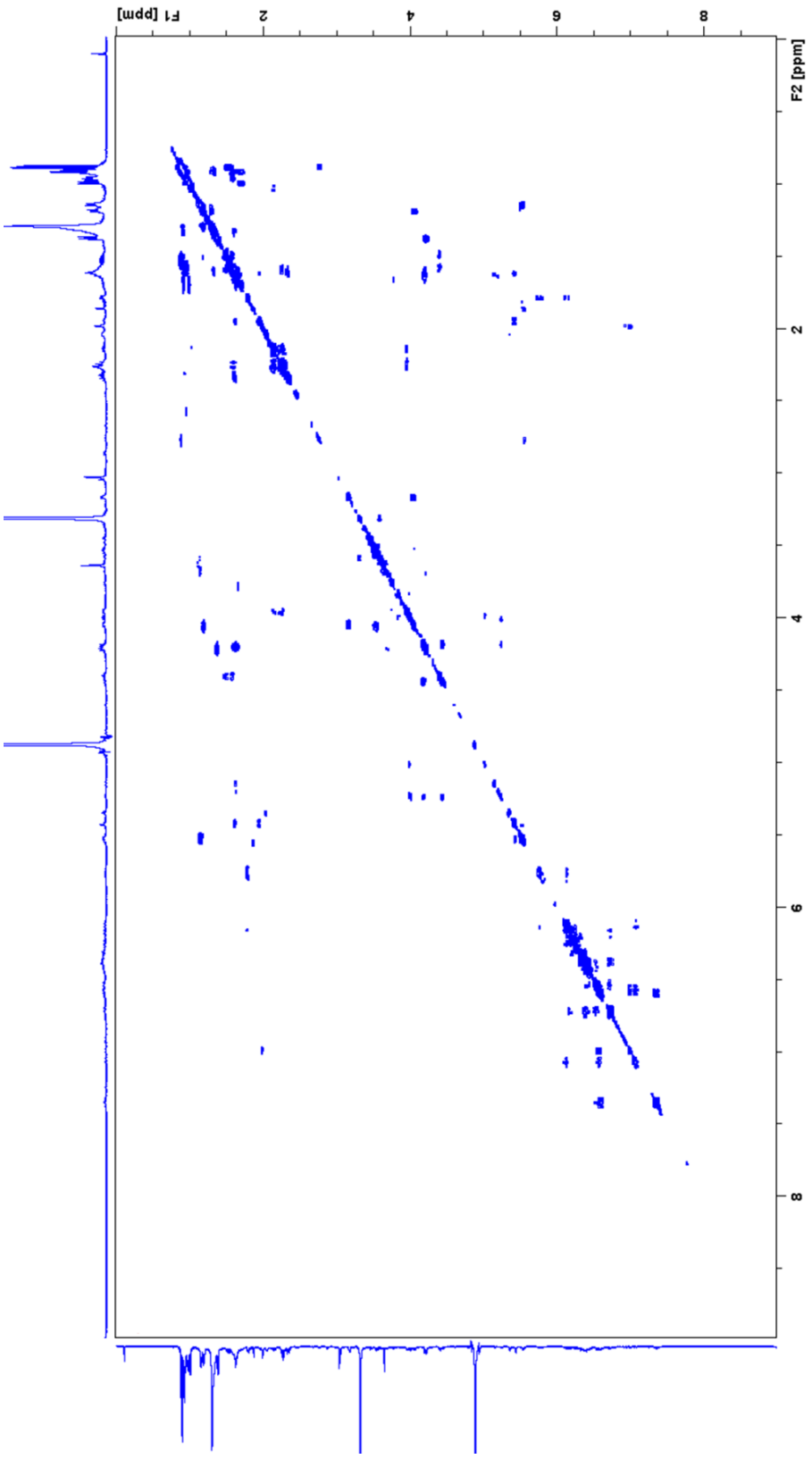

^{1}H-^{1}H COSY spectrum of myxochromide SD_3 in CD_3OD (500 MHz)

Fig. S27 ***(continued on next page)***

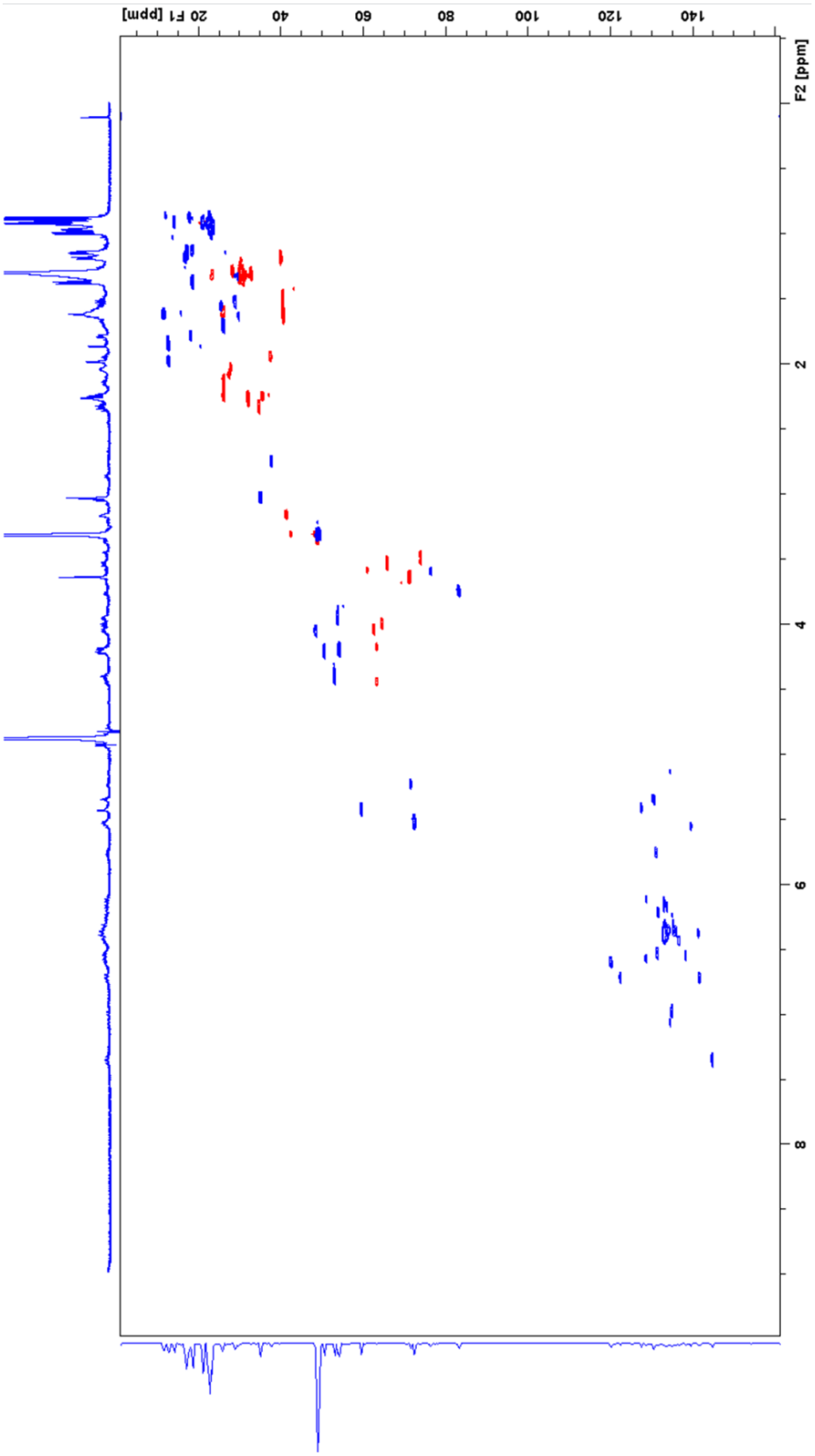

Fig. S27 ***(continued on next page)***

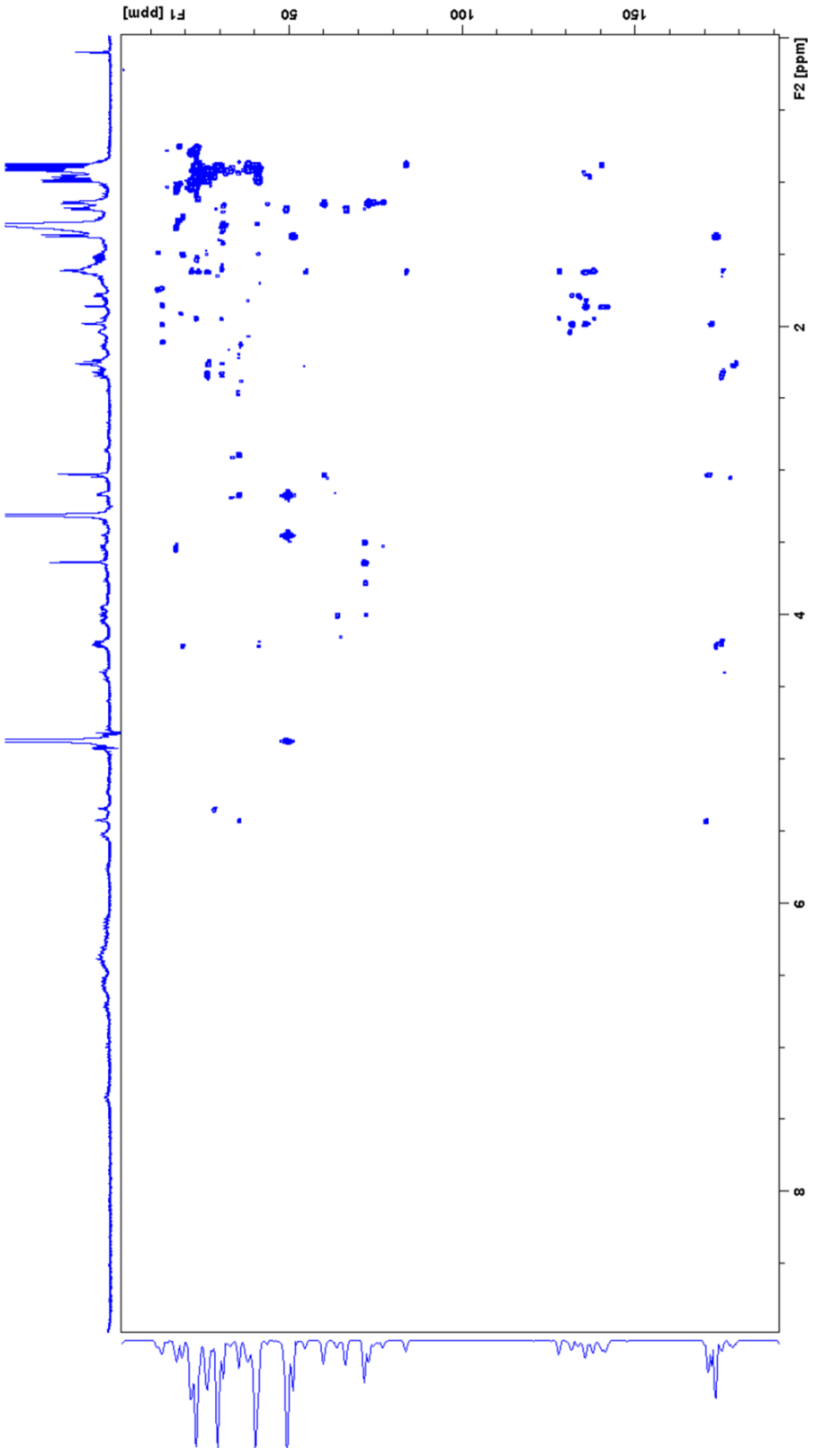

Fig. S27 NMR spectra of myxochromide SD_3.

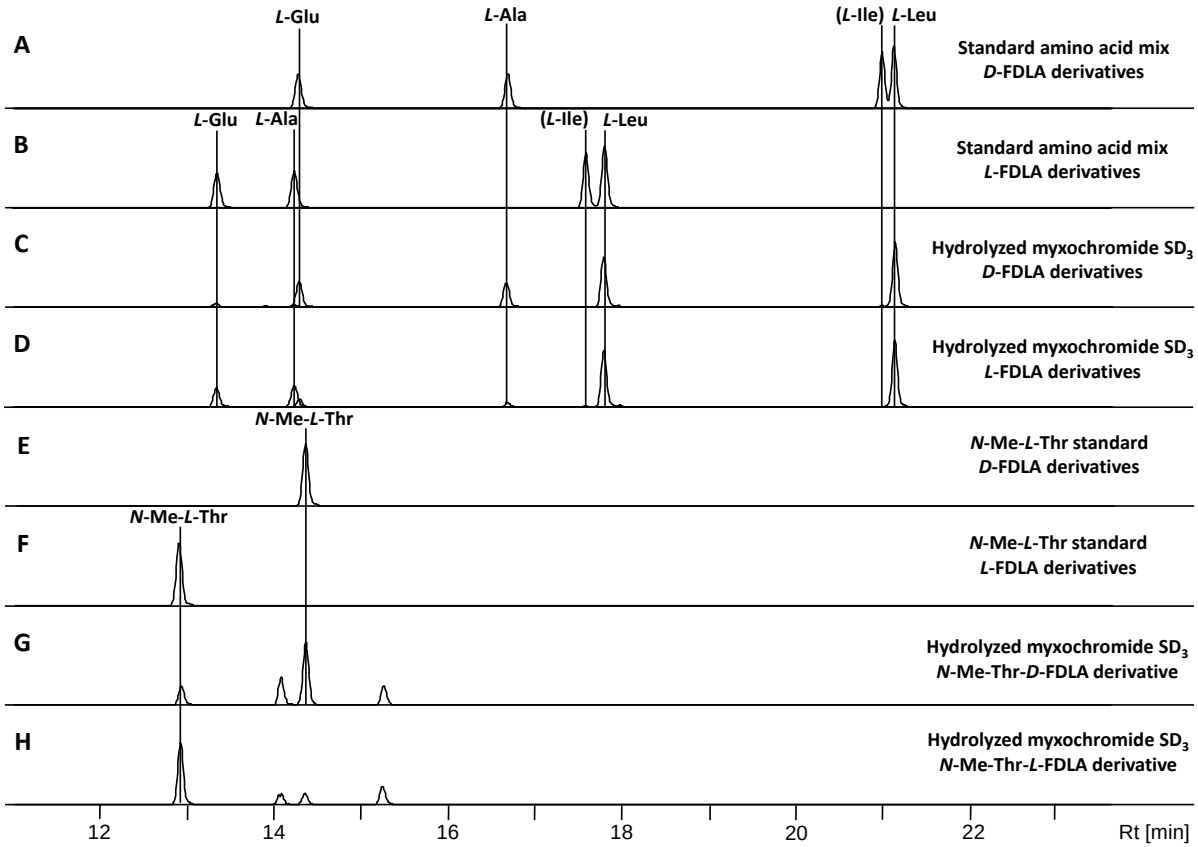

Fig. S28 Analysis of the absolute configuration of myxochromide SD_3. Extracted ion chromatograms (EIC) for ±0.05 *m/z* corresponding to the $[M+H]^+$ ions of derivatized amino acids, which are present in the peptide scaffold, are shown. **A**: Standard amino acid mix derivatized with *D*-FDLA reagent. **B**: Standard amino acid mix derivatized with *L*-FDLA reagent. **C**: Hydrolyzed myxochromide SD_3 derivatized with *D*-FDLA reagent. **D**: Hydrolyzed myxochromide SD_3 derivatized with *L*-FDLA reagent. **E**: Standard solution of *N*-Me-*L*-threonine derivatized with *D*-FDLA. **F**: Standard solution of *N*-Me-*L*-threonine derivatized with *L*-FDLA. **G**: Same sample as in **C** analyzed for the *N*-Me-*L*-threonine *D*-FDLA derivative. **H**: Same sample as in **D** analyzed for the *N*-Me-*L*-threonine *L*-FDLA derivative.

Table S20 Analytical data of detected amino acid derivatives and assignment of the absolute configuration of the amino acids in myxochromide SD_3.

aa-FDLA derivative	*L*-aa standards		Peptide hydrolysate		Assigned configuration
	t_R [min]	*m/z* $[M+H]^+$	t_R [min]	*m/z* $[M+H]^+$	
Glu-*D*-FDLA	14.3	442.1578	14.3	442.1575	**L**
Glu-*L*-FDLA	13.3	442.1579	13.3	442.1564	
Ala-*D*-FDLA	16.7	384.1520	16.7	384.1512	**L**
Ala-*L*-FDLA	14.3	384.1524	14.3	384.1519	
Leu-*D*-FDLA	21.1	426.1989	21.1	426.1986	**L**
Leu-*L*-FDLA	17.8	426.1988	17.8	426.1986	
Leu-*D*-FDLA	**21.1**	426.1989	**17.8**	426.1982	**D**
Leu-*L*-FDLA	**17.8**	426.1988	**21.1**	426.1984	
N-Me-Thr-*D*-FDLA	14.4	428.1782	14.4	428.1773	**L**
N-Me-Thr-*L*-FDLA	12.9	428.1786	12.9	428.1784	

6. References

1 S. C. Wenzel, B. Kunze, G. Höfle, B. Silakowski, M. Scharfe, H. Blöcker and R. Müller, *Chembiochem*, 2005, **6**, 375.

2 H. Sucipto, D. Pogorevc, E. Luxenburger, S. C. Wenzel and R. Müller, *Metab. Eng.*, 2017, **44**, 160.

3 C. Burgard, N. Zaburannyi, S. Nadmid, J. Maier, H. Jenke-Kodama, E. Luxenburger, H. S. Bernauer and S. C. Wenzel, *ACS Chem. Biol.*, 2017, **12**, 779.

4 R. Meyer, D. Figurski and D. Helinski, *Science (New York, N.Y.)*, 1975, **190**, 1226.

5 a) R. H. Durland, A. Toukdarian, F. Fang and D. R. Helinski, *J. Bacteriol.*, 1990, **172**, 3859; b) C. M. Thomas, R. Meyer and D. R. Helinski, *J. Bacteriol.*, 1980, **141**, 213; c) R. J. Meyer and D. R. Helinski, *Biochim. Biophys. Acta*, 1977, **478**, 109.

6 J. Fu, S. C. Wenzel, O. Perlova, J. Wang, F. Gross, Z. Tang, Y. Yin, A. F. Stewart, R. Müller and Y. Zhang, *Nucleic Acids Res.*, 2008, **36**, e113.

7 R. Bhushan and H. Bruckner, *Amino Acids*, 2004, **27**, 231.